

FUJI ELECTRIC REVIEW

2015
Vol.61 No.



Power Semiconductors Contributing in Energy Management



Power Semiconductors Contributing in Energy Management

High-efficiency energy usage has become an extremely important factor in achieving a low-carbon society. In particular, electric energy has become indispensable in numerous fields such as automobile, industrial machinery, social infrastructure and consumer electronics, and as such, there is much expectation that advances in power electronics technology will enable the high-efficiency usage of electric energy. Fuji Electric has been developing easy-to-use power semiconductors that are characterized by their high energy conversion efficiency and low noise as key devices in the field of power electronics technology.

In this special issue, we will introduce the latest technologies and products of Fuji Electric's power semiconductors.

Cover Photo (clockwise from the upper left):

3rd-generation direct liquid cooling power module for automotive applications, All-SiC module, 3,300-V withstand voltage SiC hybrid module



FUJI ELECTRIC REVIEW vol.61 no.4 2015

date of issue: December 30, 2015

editor-in-chief and publisher **EGUCHI Naoya**

Corporate R & D Headquarters
Fuji Electric Co., Ltd.
Gate City Ohsaki, East Tower,
11-2, Osaki 1-chome, Shinagawa-ku,
Tokyo 141-0032, Japan
<http://www.fujielectric.co.jp>

editorial office Fuji Electric Journal Editorial Office
c/o Fuji Office & Life Service Co., Ltd.
1, Fujimachi, Hino-shi, Tokyo 191-8502,
Japan

Fuji Electric Co., Ltd. reserves all rights concerning the republication and publication after translation into other languages of articles appearing herein.

All brand names and product names in this journal might be trademarks or registered trademarks of their respective companies.

Contents

Power Semiconductors Contributing in Energy Management	
All-SiC Module Packaging Technology	224
NAKAMURA, Hideyo NISHIZAWA, Tatsuo NASHIDA, Norihiro	
1,700-V Withstand Voltage SiC Hybrid Module	228
ONEZAWA, Takumi KITAMURA, Shoji ISO, Akira	
3,300-V Withstand Voltage SiC Hybrid Module Technology	232
KANEKO, Satoshi KANAI, Naoyuki TSUJI, Takashi	
7th-Generation “X Series” IGBT Module	237
KAWABATA, Junya MOMOSE, Fumihiko ONOZAWA, Yuichi	
2nd-Generation Small IPM	242
ARAKI, Ryu SHIRAKAWA, Toru KOGAWA, Hiroki	
HVIC Technologies for IPM	247
JONISHI, Akihiro AKAHANE, Masashi YAMAJI, Masaharu	
3rd-Generation Direct Liquid Cooling Power Module for Automotive Applications	252
ARAI, Hirohisa HIGUCHI, Keiichi KOYAMA, Takahiro	
Packaging Technology of 3rd-Generation Power Module for Automotive Applications	258
GOHARA, Hiromichi TAMAI, Yuta YAMADA, Takafumi	
RC-IGBT for Automotive Applications	263
YOSHIDA, Soichi NOGUCHI, Seiji MUKAI, Koji	
Relative Pressure Sensor for Automobile Fuel Tanks	267
KATO, Hirofumi ASHINO, Kimihiro SATO, Eisuke	
PWM Power Supply Control IC “FA8B00 Series” Capable of Handling Peak Loads	271
MATSUMOTO, Shinji YAMANE, Hiroki YABUZAKI, Jun	
2nd-Generation Low-Loss SJ-MOSFET “Super J MOS S2 Series”	276
WATANABE, Sota SAKATA, Toshiaki YAMASHITA, Chiho	
High-Speed Discrete IGBT “High-Speed W-Series”	280
HARA, Yukihito NAITO, Tatsuya KATO, Yoshiharu	
New Products	
Amorphous MOLTRA “FM-AT14”	285
Circuit Protector “CP30F Series”	288
7th-Generation “X Series” IGBT Module	291

All-SiC Module Packaging Technology

NAKAMURA, Hideyo* NISHIZAWA, Tatsuo* NASHIDA, Norihiro*

ABSTRACT

We applied the All-SiC (silicon carbide) module with new package structure to mega solar power conditioning sub-system (PCS), achieving 98.8% energy conversion efficiency and resulting in energy conservation. Key technologies are 3-dimensional wiring using Cu pins with power board instead of conventional Al wiring and full-mold structure using the thermosetting epoxy resin. These technologies lead to small package size, low inductance, and high reliability. We have optimized the package design to bring out the intrinsic performances of SiC device. Resin flow analysis and its visualization methods are carried out to design molding process, resulting in the full mold structure with free air void.

1. Introduction

Public interest in environmental issues such as global warming is increasing year by year, and worldwide society demands less greenhouse gas emissions representative of CO₂. Meeting such a need requires the active utilization of renewable energies and greater energy saving of power electronics equipment. In general, power semiconductors play a key role in the power conversion system of power electronics products. Silicon (Si) devices, which are the conventional mainstream, have undergone various breakthroughs and gradually approach its physical limit. Regarding this background, silicon carbide (SiC) devices, which are the next-generation semiconductors enabling even less power dissipation, are raising expectations for their contribution toward energy saving.

Fuji Electric has developed an All-SiC module using SiC metal-oxide-semiconductor field-effect transistors (SiC-MOSFETs) and SiC Schottky barrier diodes (SiC-SBDs) and using it to a power conditioning sub-system (PCS) for mega solar power plants. This paper describes the packaging technology of the All-SiC module.

2. Features of New Package

In order to achieve more efficient power conversion of high-capacity photovoltaic power generation as mega solar power plants, Fuji Electric started mass production of mega solar PCSs that employ All-SiC modules in 2014. Figure 1 shows the external appearance of the mega solar PCS, its built-in power unit and the All-SiC module. It uses the All-SiC module in voltage boosting circuit and achieves a high efficiency of

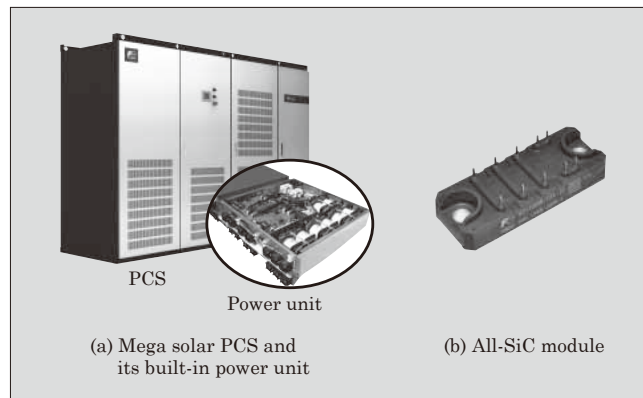


Fig. 1 Mega solar PCS and All-SiC module

98.8% to save energy. Further efforts have been made to reduce the size and weight of the equipment⁽¹⁾.

Figure 2 shows cross-sectional structures of the new package used in the All-SiC module and the conventional package used in a silicon insulated-gate bipolar transistor (Si-IGBT) module. Table 1 shows the comparison of the typical characteristics of these modules. The new package contains small size SiC chips connected in parallel. In order to flow large current through wiring on the chip, we applied 3-dimensional wiring with Cu pins and a power substrates instead of aluminum wires. For the size advantage, the footprint is reduced to approximately 40% compared with the conventional module. This miniaturization achieved by 3-dimensional wiring effectively reduces the inductance less than a quarter of the conventional one. Additionally, thermal resistance is decreased approximately a half of conventional module by using a ceramics insulating substrate consisting of a high-thermal-conductive ceramics substrate (Si₃N₄) bonded with thick copper plates and by adopting a structure without metal base⁽²⁾⁽³⁾. Furthermore, the use of

* Corporate R&D Headquarters, Fuji Electric Co., Ltd.

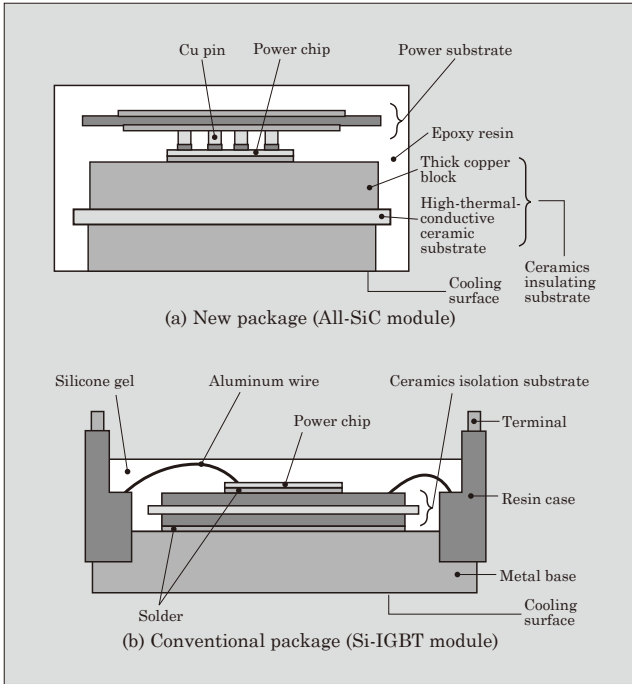


Fig. 2 Cross-sectional package structure

Table 1 Comparison of typical characteristics between the new and conventional packages (Relative comparison at 1,200-V/100-A rating)

Package characteristics	Conventional package	New package
Thermal resistance (K/W)	0.469	0.209
Inductance (nH)	52	12
Footprint	1	0.42

epoxy resin for the molding resin improves reliability. Molding technology ensures the isolation of the chips and ceramics substrate and also suppresses the distortion of joint area between the chips and Cu pins. Adopting transfer mold forming for this epoxy resin molding eliminates the need for a conventional resin case, leading to miniaturization and productivity improvement. In the new package structure, the epoxy resin is the key component that determines the performance of the module.

3. Package Structure Design

3.1 Internal wiring structure

The SiC-MOSFET allows faster switching compared with the conventional Si-IGBT. To bring out advantage of the ability, it is necessary to reduce surge voltage that increases in proportion to the switching speed and this make it crucial to reduce the inductance of internal wiring.

The new package has achieved miniaturization by adopting 3-dimensional wiring that uses Cu pins and a power substrate as shown in Fig. 2(a). This decreases the wiring distance and reduces self-inductance. Furthermore, we attempted to reduce the inductance

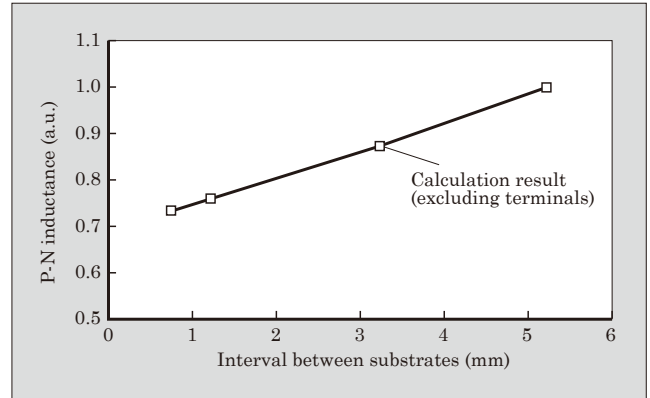


Fig. 3 Relationship between the substrate interval and inductance

further by arranging the power substrate and ceramics insulating substrate in parallel and by connecting the wiring to make the change in the current (di/dt) occur in the opposite directions⁽⁴⁾. In this structure, the closer the 2 substrates are positioned, the more the inductance decreases as shown in Fig. 3. Consequently, we set the interval as narrow as possible on the condition that it does not affect the insulation performance or assembly work. As a result, the P-N inductance of the new package is less than 25% (approx. 12nH) compared with the conventional package.

Since a mega solar PCS handles large current, multiple All-SiC modules are connected in parallel. In this case, the inductance is inversely proportional to the number of modules. This is more advantageous for high-speed switching than the conventional case where a smaller number of large-capacity modules were used.

3.2 Molding structure

A full-mold structure with thermosetting epoxy resin can relief the stress inside the module. In the view of reliability, stress is occurred at joint areas of the chip. Molding can cover surrounding of the chip and other joint areas, and distortion is eased⁽⁵⁾. This effect improves the power cycle capability at $\Delta T_j = 150^\circ\text{C}$ by 20 times or more compared with the conventional package⁽⁶⁾.

However, the issue with the full-mold structure is caused by the fact that materials with different linear expansion coefficients are molded together. When the package cured under elevated temperature is returned to normal temperature, internal stress is generated and warpage occurs in the entire module. It is necessary to keep the warpage as low as possible because it may increase stress or thermal resistance when the product is mounted on a cooling fin or cause a pump-out phenomenon*1 of the compound due to the temperature change during operation.

Figure 4 shows the results of the finite element method (FEM) analysis and actual measurement to examine the relationship between the warpage and the thickness of the main body (thickness of resin) of

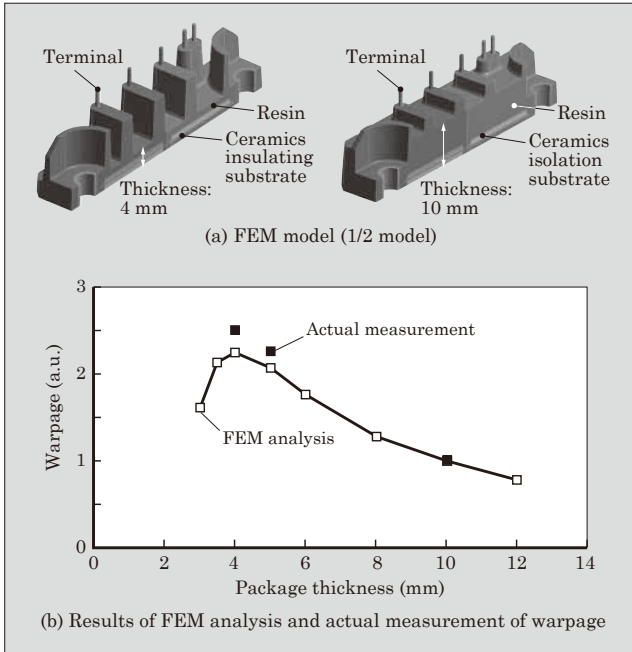


Fig. 4 FEM model of the new package and results of analysis and actual measurement of warpage

the new package excluding protrusions. The results indicate that the warpage becomes smaller when the package is either thicker or thinner than a certain thickness. This is probably caused by the fact that, in the region where the package is thin and dominated by the rigidity of the ceramics insulating substrate, the stress on the ceramics insulating substrate decreases with the decrease of the resin thickness, resulting in smaller warpage. On the other hand, in the region where the package is thick and is dominated by the rigidity of the resin, the rigidity of the resin increases further with the increase in the resin thickness so that the package is less affected by the ceramics insulating substrate, resulting in smaller warpage. In real-world situations, however, when the thickness of the ceramics insulating substrate, chip thickness and power substrate lamination are considered, the module would be manufactured in the region where the rigidity of the resin dominates. Consequently, it is effective to produce the All-SiC module with thicker epoxy resin to obtain low warpage module. In this case, it is important to optimize the resin thickness and inductance value because a thicker resin part requires a longer terminal to be extended outside, causing an increase in inductance. The insulation distance between the terminal and ground (creepage/clearance distance) must also be considered.

As a result, the internal structure of the module is

*1: Pump-out phenomenon: Phenomenon where the compound between the module and cooling fin is pushed out of the space due to repeated deformations of the package caused by temperature changes during operation, resulting in an increase of thermal resistance

designed to arrange most components on the cooling surface side. This is done to reduce inductance by arranging the power substrate and ceramics insulating substrate at a narrower interval and to suppress warpage by making the module thicker. When transfer mold forming is used for this high concentrated structure, the resin hardly flows smoothly and evenly inside the module. Therefore, it requires a mold process design based on an accurate recognition of the resin flow.

4. Mold Process Design

4.1 Simulation techniques and mold design

One of the concerns of the transfer mold forming of the new package is scattered voids (trapped air) and welds (sections where resin flows meet together) inside the module. These are caused by the deterrence of the flow. The chips, Cu pins and other internal components are rationale. The volatile filling speed at the narrow space and that at the other space can also generate voids and welds (resin flow junction part).

To understand this phenomenon, simulation of the resin flow was done. Figure 5 shows the simulation model and result of the resin flow. As a result of this, welding position, air trap and/or bubbles in the flowing resin was clarified by changing molding conditions. This result is reflected to the mold design.

4.2 Resin flow visualization

In order to improve mass production quality and productivity, it needs to optimize the mold design and process conditions. This modulation needs to consider factors of the air vent operation and the flow and elimination behavior of bubbles that cannot be calculated by

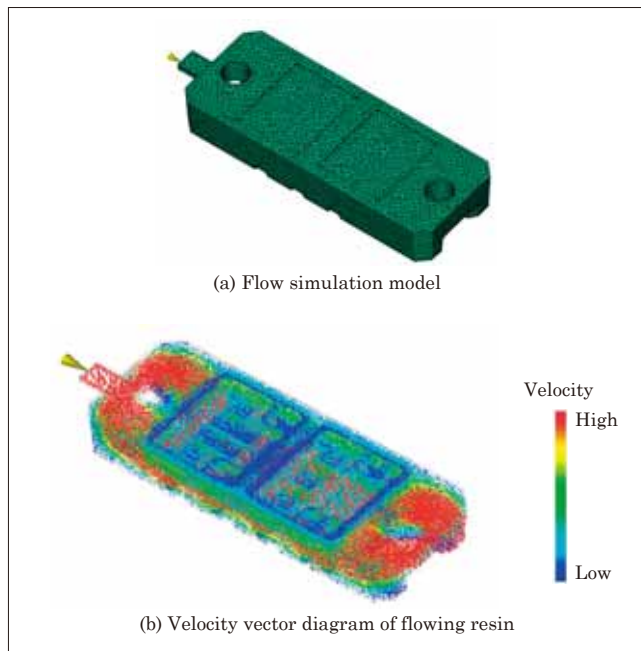


Fig. 5 Resin flow simulation

simulation.

Therefore, molding visualization is done by using experimental glass plate as shown in Fig. 6. As a result of this, it is successful to avoid the air trap and welds by arranging an air vent, optimizing the gate shape and modulating the flow conditions including speed, temperature and pressure. For example, Fig. 6(b) illustrates the process in which the void generated by the air trapped near the mounting hole is pushed down to the inside of the ring and disappears. It is hard to understand the resin flow behavior by simulation.

As described above, both of the simulation and practical visualization of the resin flow are important for accurately understanding the mechanism of the void. These technologies are used to develop mold pro-

cess design techniques that are applied to the mold design and molding conditions. At the result, it is able to achieve the All-SiC module in a full-mold structure.

5. Postscript

This paper describes the packaging technology of the All-SiC module. For the design of the All-SiC package, not only structure design but also mold process design using simulation and practical visualization of resin flow are important.

We continue to contribute to developing the power electronics technologies and realizing a low carbon society through developing small- to large-capacity modules and broadening their application to various power electronics.

References

- (1) Nashida, N. et al. All-SiC Module for Mega-Solar Power Conditioner. FUJI ELECTRIC REVIEW. 2014, vol.60, no.4, p.214-218.
- (2) Horio, M. et al. "New Power Module Structure with Low Thermal Impedance and High Reliability for SiC Devices". Proceedings of PCIM, 2011, p.229-234.
- (3) Ikeda, Y. et al. "Investigation on Wirebond-less Power Module Structure with High-density Packaging and High Reliability". Proceedings of ISPSD. 2011, p.272-275.
- (4) Horio, M. et al. "Ultra Compact and High Reliable SiC MOSFET Power Module with 200°C Operating Capability". Proceedings of ISPSD. 2012, p.81-84.
- (5) Hinata, Y. et al. "Full SiC Power Module with Advanced Structure and its Solar Inverter Application". Proceedings of APEC. 2013, p.604-607.
- (6) Nashida, N. et al. "All-SiC Power Module for Photovoltaic Power Conditioner System". Proceedings of ISPSD. 2014, p.342-345.

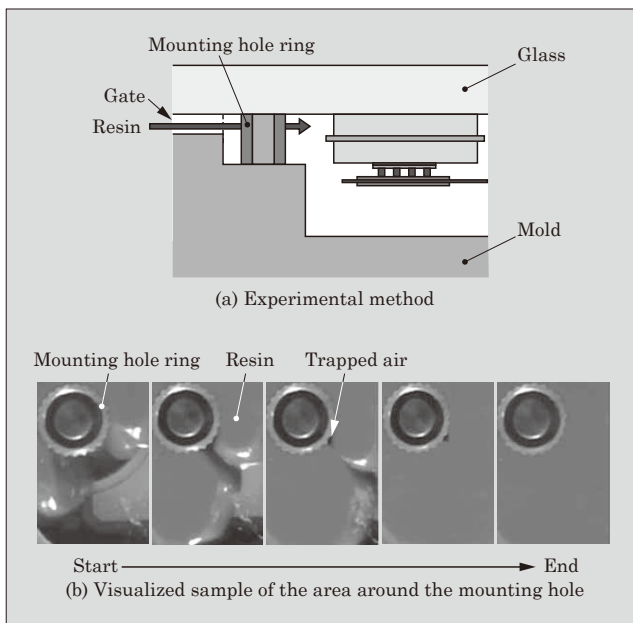


Fig. 6 Experiment of resin flow visualization



1,700-V Withstand Voltage SiC Hybrid Module

ONEZAWA, Takumi* KITAMURA, Shoji* ISO, Akira*

ABSTRACT

Fuji Electric has developed a SiC hybrid module with a 1,700-V withstand voltage. It is designed for use in the traction market as a power device that can be utilized in inverters that contribute to energy savings. This module is equipped with 6th-generation IGBT chips and applies SiC-SBD chips to its FWDs. It has a product rating of 1,700 V/1,200 A (2 in 1) and has 2 specifications: standard specifications that make much of power dissipation, and low $V_{CE(sat)}$ specifications suitable for low switching frequencies. The standard specifications reduce loss by 18% compared with conventional Si modules. Furthermore, the low $V_{CE(sat)}$ specifications achieve 6% loss reduction compared with the standard specifications at low switching frequency condition.

1. Introduction

In recent years, reduction of emissions of CO₂ and other greenhouse gases has been demanded for restraining the progress of global warming. Power electronics including power conversion devices are not exempt from the demand and further energy saving is required for more reduction of emissions of greenhouse gases. Power conversion devices have become widespread in the entire society including those for social infrastructure such as electric railways and those for consumers such as air conditioners and energy saving can make significant contributions to the reduction of greenhouse gases. Energy saving of inverters, which are mounted on power conversion devices, can be realized by technological innovation of their components such as power devices, circuits and control. For power devices, continuing to achieve further reduction of power dissipation is an important mission.

At present, the mainstream of power devices is insulated-gate bipolar transistor (IGBT) modules that use silicon (Si) IGBT and free wheeling diode (FWD) chips. However, performance of Si devices is approaching its theoretical limit based on physical properties and significant reduction of power dissipation cannot be expected. Silicon carbide (SiC) devices, which are characterized by high heat resistance and high breakdown field tolerance, have achieved a dramatic reduction of power dissipation that is difficult to realize with Si devices and opened up the potential for realizing efficiency improvement and size reduction of inverters.

Fuji Electric has commercialized SiC hybrid modules, which combine the 600-V, 1,200-V and 1,700-V withstand voltage SiC-Schottky barrier diode (SiC-SBD) chips developed and Si-IGBT chips. Above all,

we have focused our attention on the development of 1,700-V withstand voltage SiC hybrid module products intended for main power supply of electric railways to expand the product line. This application essentially requires enhancement of the blocking voltage and capacity and we have developed SiC hybrid modules by applying the high-power IGBT module technology accumulated up to now^{(1) to (3)}.

This paper describes SiC hybrid modules with a rating of 1,700 V/1,200 A (2 in 1).

2. Overview

Figure 1 shows the external appearance of the 1,700-V withstand voltage SiC hybrid module. It has a high-reliability package that uses AlSiC, a composite material of aluminum and silicon carbide, for the base material and aluminum nitride (AlN) featuring high thermal conductivity for the insulating substrate material. AlSiC has a linear expansion coefficient of $7.5 \times 10^{-6}/^{\circ}\text{C}$, which is close to $4.5 \times 10^{-6}/^{\circ}\text{C}$ of an AlN substrate, and offers improved heat cycle life and power cycle life as compared with a copper (Cu) base.

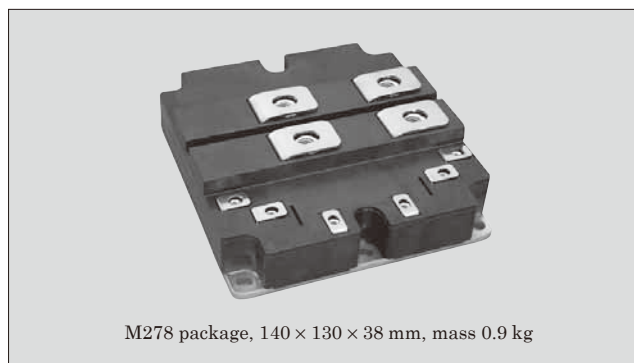


Fig. 1 1,700-V withstand voltage SiC hybrid module

* Electronic Devices Business Group, Fuji Electric Co., Ltd.

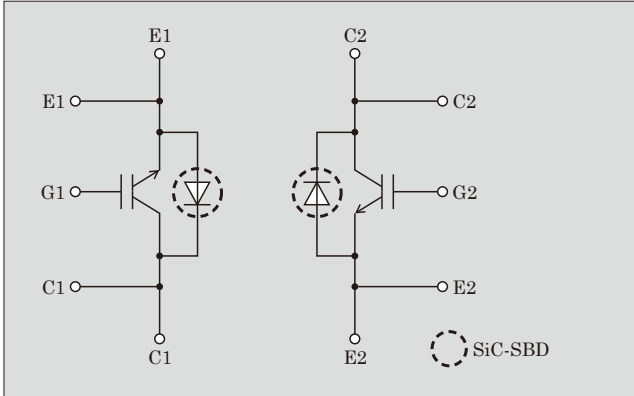


Fig. 2 Equivalent circuit of 1,700-V withstand voltage SiC hybrid module

Figure 2 shows an equivalent circuit. This module integrates the 6th-generation IGBT chips and applies 1,700-V withstand voltage SiC-SBD chips to its FWDs.

In electric railway traction applications, operation is mostly at a low switching frequency of up to approximately 0.5 kHz in carrier frequency and steady-state loss is dominant. Accordingly, low saturation voltage $V_{CE(sat)}$ characteristic is preferable. In the main circuit of high capacity inverters, the main circuit inductance L_s is larger than those of low to medium capacity inverters. As shown in Equation 1, the effect of L_s and gradient of the turn-off current di/dt causes the turn-off surge voltage V_{sp} generated to increase and low V_{sp} is preferable. However, decreasing the turn-off speed to suppress this V_{sp} causes increased loss, which poses a problem. From this perspective, in order to satisfy the low $V_{CE(sat)}$ and low V_{sp} requirements, we have added to the product line the low $V_{CE(sat)}$ specifications with the priority on the steady-state loss and V_{sp} on top of the standard specifications with the priority on the switching loss. By optimizing the thickness of the IGBT chips mounted, we have improved the E_{off} - $V_{CE(sat)}$ trade-off and realized the minimization of the total loss by adjusting the amount of carriers injected from the collector.

$$V_{sp} = V_{cc} + L_s \frac{di_c}{dt} \dots \dots \dots (1)$$

- V_{sp} : Turn-off surge voltage (V)
- V_{cc} : Circuit voltage (V)
- L_s : Main circuit inductance (H)
- I_c : Collector current (A)

3. Characteristics

3.1 1,700-V withstand voltage SiC hybrid module with standard specifications

(1) FWD output characteristics

Figure 3 shows the forward current (I_F) versus forward voltage (V_F) characteristics of the 1,700-V withstand voltage SiC-SBD used for the SiC hybrid module. If a current that is about to flow into one of the chips connected in parallel is larger than that into other

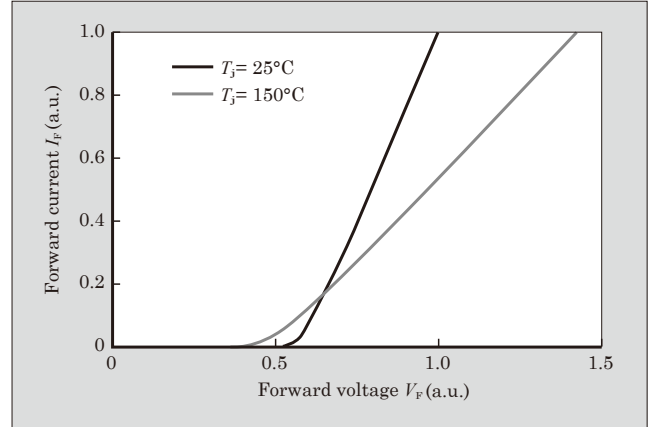


Fig. 3 V_F - I_F characteristics

chips, the resistance increases because of the strong positive temperature characteristics of the SiC-SBD, which prompts self-adjustment to restrain the current increase, making current imbalance less likely to occur. For that reason, the characteristics are effective in high-power IGBT modules with many parallel connections of chips.

(2) Switching characteristics

Figure 4 compares the reverse recovery waveforms of the SiC hybrid and Si modules. With the SiC hybrid module, the reverse recovery current peak value I_{rp} is significantly lower. This is because that the SiC-SBD is a unipolar device and minority carrier injection and sweep-out do not take place. Figure 5 shows a comparison of turn-on waveforms between the SiC hybrid

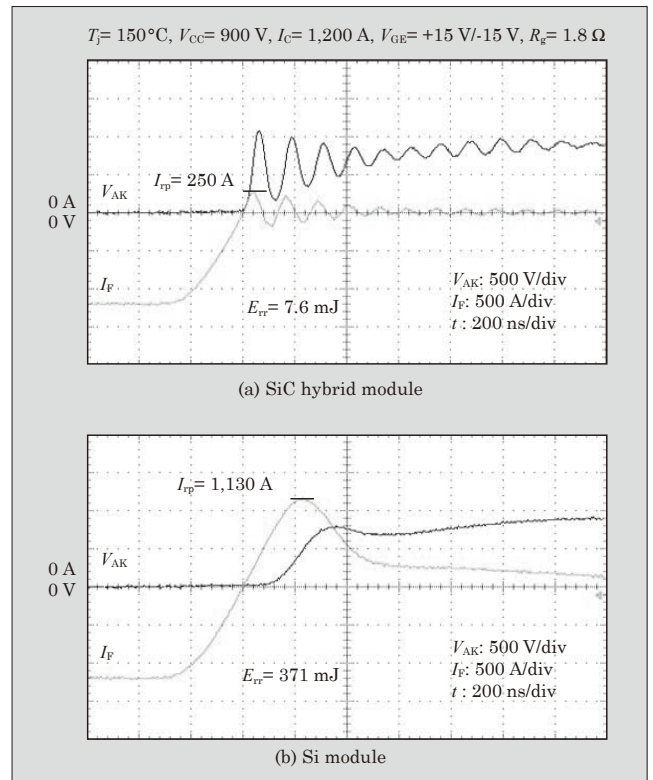


Fig. 4 Reverse recovery waveforms

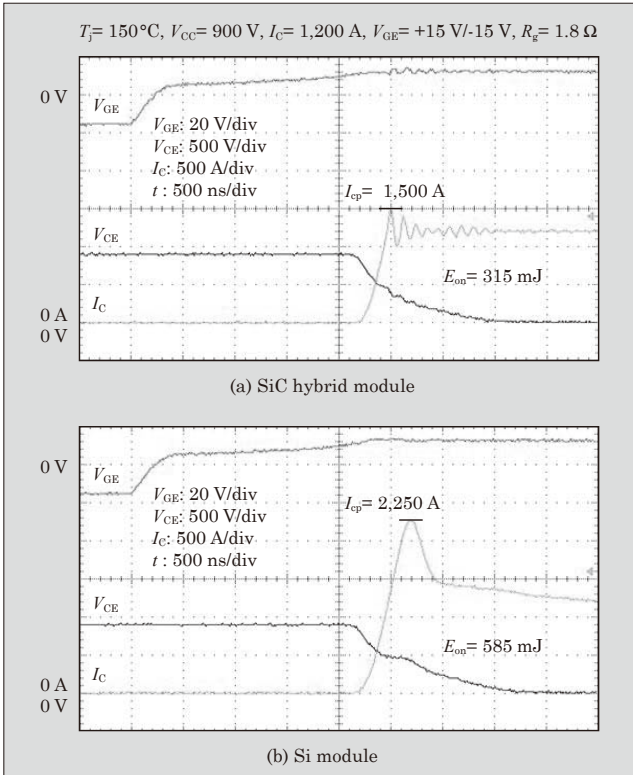


Fig. 5 Turn-on waveforms

and Si modules. The SiC hybrid module allows a significant reduction in the reverse recovery current as described above and the turn-on current peak value I_{cp} , which reflects it, can be significantly reduced as well.

In this way, while the Si module has the E_{rr} of 371 mJ, it is 7.6 mJ with the SiC hybrid module, which is a reduction of approximately 98%. In addition, as compared with the E_{on} of 585 mJ with the Si module, it is 315 mJ with the SiC hybrid module, a reduction of approximately 46%.

(3) Generated loss of module in inverter

Figure 6 shows the results of simulation of generated loss in an inverter. It indicates that the generated loss of the SiC hybrid module can be reduced as

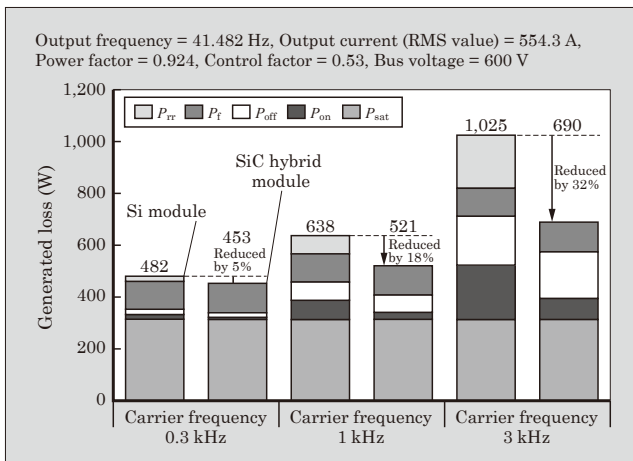


Fig. 6 Simulation of generated loss in inverter

compared with the Si module by 5%, 18% and 32% for the carrier frequency of 0.3 kHz, 1 kHz and 3 kHz respectively. In this way, increasing the carrier frequency increases the loss reduction rate, which raises expectations for application of the SiC hybrid module in high-frequency operation.

3.2 1,700-V withstand voltage SiC hybrid module with low $V_{CE(sat)}$ specifications

(1) IGBT output characteristics

Figure 7 shows the $V_{CE(sat)}$ - I_C characteristics. The standard and low $V_{CE(sat)}$ specifications both have a positive temperature characteristic and current imbalance is unlikely to occur, which allows easy parallel connection. The low $V_{CE(sat)}$ specifications offer a reduction of 0.20 V at $T_j = 25^\circ\text{C}$ and 0.22 V at $T_j = 150^\circ\text{C}$ from the standard specifications.

(2) Switching characteristics

Figure 8 compares turn-off waveforms. While V_{sp} is 1,420 V with the standard specifications, it is 1,260 V with the low $V_{CE(sat)}$ specifications, a reduction of 160 V. Figure 9 shows the V_{sp} - I_C characteristics. It indicates a reduction of approximately 10% at the rated current of 1,200 A. Figure 10 shows the turn-off loss E_{off} - I_C characteristics. With the low $V_{CE(sat)}$ specifications, E_{off} is shown to increase by approximately 70% at the rated current as compared with the standard specifications. This is because that, with the low $V_{CE(sat)}$ specifications, the tail current is increased by optimization of the amount of carriers injected from the collector in order to suppress the surge voltage.

(3) Generated loss of module in inverter

Figure 11 shows the results of simulation of generated loss in an inverter. With the low $V_{CE(sat)}$ specifications, P_{off} increases when the carrier frequency is 0.3 kHz but the generated loss is reduced by 11% as compared with the Si module and by 6% as compared with the standard specifications. Accordingly, in a region with a small carrier frequency, the low $V_{CE(sat)}$ specifications offer a reduction not only of V_{sp} but also of the generated loss as compared with the standard specifications.

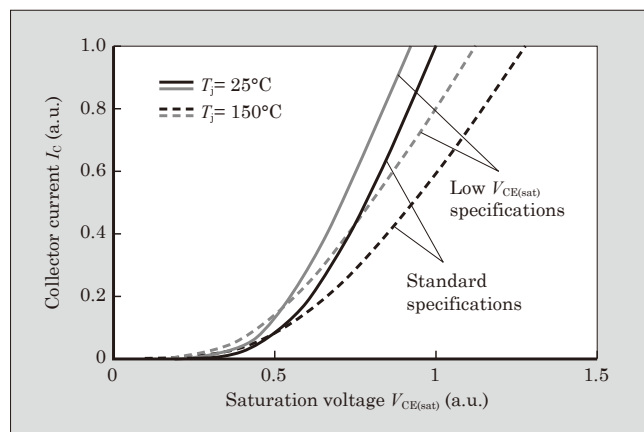


Fig. 7 $V_{CE(sat)}$ - I_C characteristics

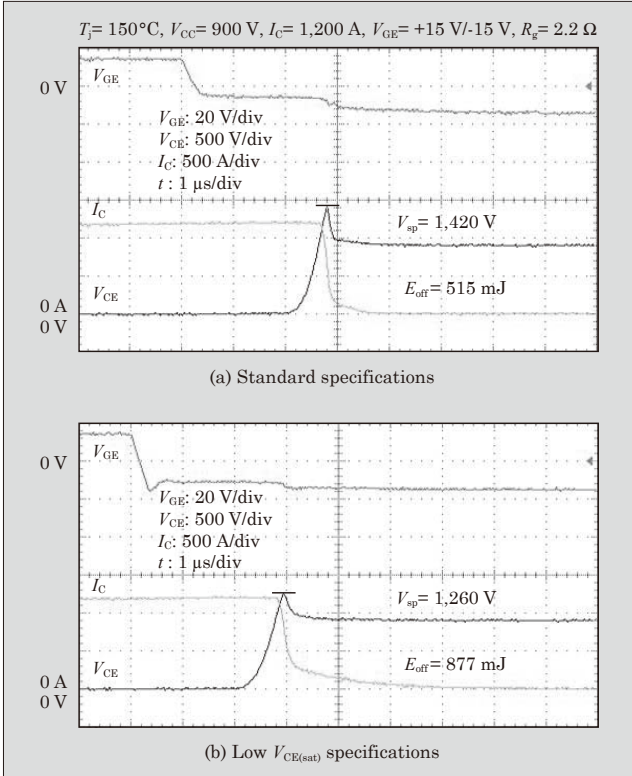


Fig. 8 Turn-off waveforms

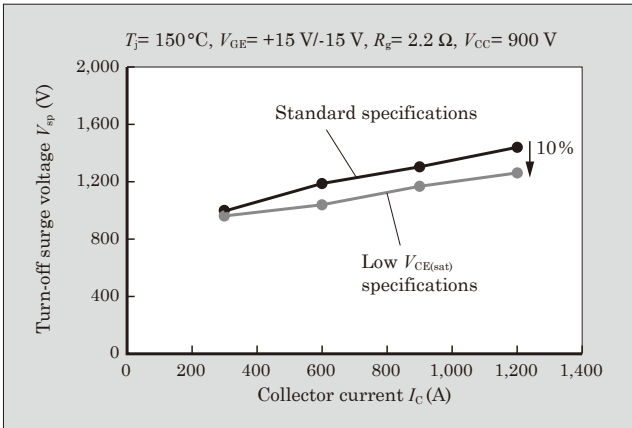


Fig. 9 V_{sp} - I_C characteristics

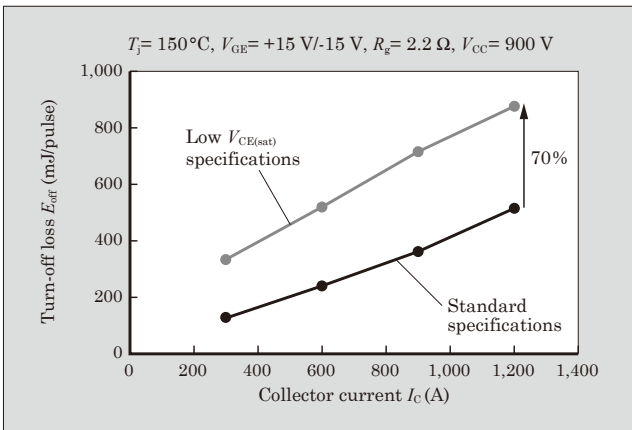


Fig. 10 E_{off} - I_C characteristics

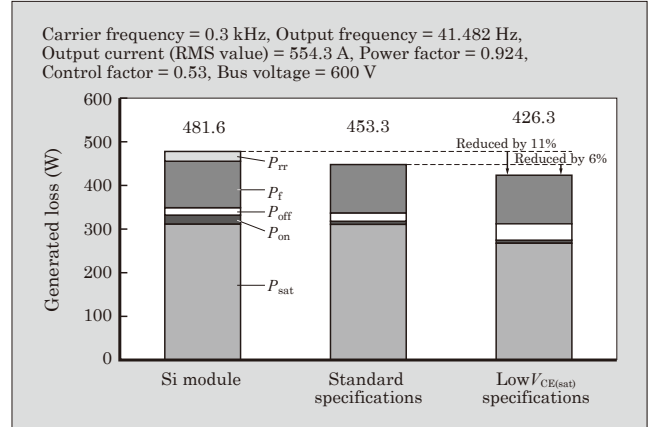


Fig. 11 Results of simulation of generated loss in inverter

4. Postscript

This paper describes a 1,700-V withstand voltage SiC hybrid module. This product, which has realized a significant reduction of power dissipation of the device itself, is expected to make substantial contributions to efficiency improvement and size reduction of inverters. In the future, we intend to promote further product line enhancement of SiC hybrid modules and work on the building of a product line of All-SiC modules, which use SiC-MOSFET chips instead of IGBTs and SiC-SBD chips instead of FWDs, to contribute to energy savings.

References

- (1) Nakazawa, M. et al. Hybrid Si-IGBT and SiC-SBD Modules. FUJI ELECTRIC REVIEW. 2014, vol.60, no.4, p.70-74.
- (2) Kobayashi, K. et al. 1,700 V Withstand Voltage SiC Hybrid Module. FUJI ELECTRIC REVIEW. 2013, vol.59, no.4, p.218-220.
- (3) Kobayashi, K. et al. 1,200 V Withstand Voltage SiC Hybrid Module. FUJI ELECTRIC REVIEW. 2014, vol.60, no.4, p.210-213.

3,300-V Withstand Voltage SiC Hybrid Module Technology

KANEKO, Satoshi* KANAI, Naoyuki* TSUJI, Takashi*

ABSTRACT

There has been increasing demand for electronics to achieve not only energy savings, but also be more compact, lightweight and improved performance such as high output. Fuji Electric is seeking to meet these demands by pursuing the development of a SiC hybrid module with a 3,300-V withstand voltage. By adopting the SiC-SBDs that we developed in partnership with the joint research body Tsukuba Power-Electronics Constellation (TPEC), we have been able to reduce generated loss by 24% compared with current Si modules. In addition, we have also utilized Sn-Sb solder to ensure high reliability and have been able to improve continuous operation temperature by 25 °C. Moreover, we made use of the reducing effect of generated loss to achieve improvements in power density while also reducing the footprint size by approximately 30%.

1. Introduction

With increasing amounts of natural resources and energy being consumed in the world, environmental pollution and resource depletion are posing major problems and the improvement of energy efficiency is strongly desired. According to this background, power electronics equipment, characterized by power saving in transmission, conversion, control and supply of electric power, is attracting attention.

Demands placed on power electronics equipment encompass a wide range from those of society for mitigating environmental load by saving energy to those relating to performance improvements such as high reliability, controllability, size and weight reduction, and high output. In order to meet these demands, it is essential to make technological improvements to power devices, circuits and control that constitute power electronics equipment. In particular, for power devices, which are key components, compact and low-loss power modules are desired.

At present, representative power modules are composed of insulated-gate bipolar transistors (IGBTs), which generally integrate silicon (Si) IGBT and free wheeling diode (FWD) chips. However, the performance of Si chips is approaching the theoretical limit based on physical properties and the dramatic characteristic improvements of the past can no longer be expected. Accordingly, wide band gap semiconductors, which have higher performance than Si, are drawing attention. Silicon carbide (SiC), one such semiconductor, not only features a higher withstand voltage and lower loss than conventional Si but is also capable of high-temperature and high-frequency operation. It allows power modules to increase the power density,

achieving the size reduction.

This paper describes the technology used for the 1,200-A SiC hybrid module with a 3,300-V withstand voltage that integrates this SiC chip.

2. Configuration of SiC Hybrid Module

Fuji Electric has commercialized SiC hybrid modules integrating SiC Schottky barrier diodes (SiC-SBDs) and Si-IGBTs with a withstand voltage of

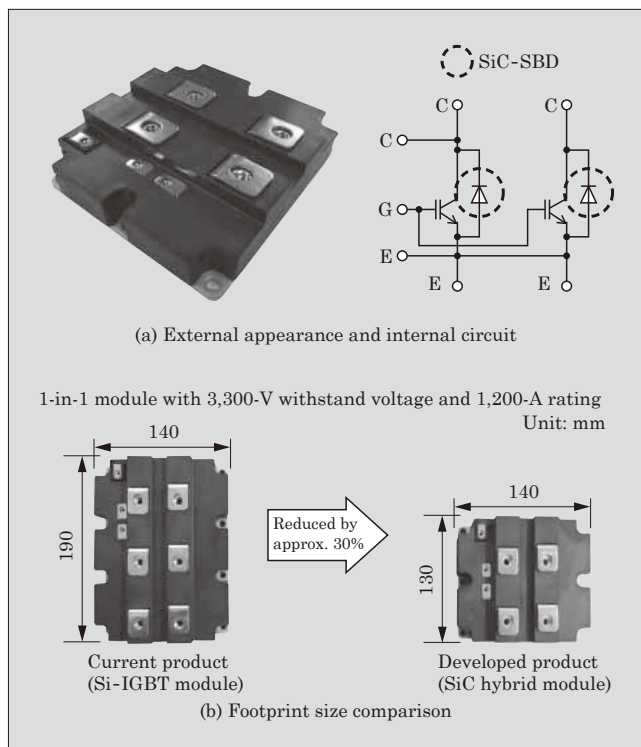


Fig.1 Overview of 3,300-V withstand voltage SiC hybrid module

* Corporate R&D Headquarters, Fuji Electric Co., Ltd.

600 V, 1,200 V and 1,700 V. We have now developed an SiC hybrid module with a 3,300-V withstand voltage in order to meet the demand for even higher withstand voltages.

Figure 1 shows the external appearance and internal circuit of the 3,300-V withstand voltage SiC hybrid module and a footprint size comparison with a Si-IGBT module. As the FWD, we have used the SiC-SBD developed in partnership with the joint research project of the Tsukuba Power-Electronics Constellations (TPEC). Its generated loss is significantly reduced compared to that of present Si-IGBT. We have employed Sn-Sb solder under the chip, which is one of the packaging technologies used for the 7th-generation “X Series” IGBT modules, to ensure high reliability. We have thereby successfully improved the continuous operating temperature from 125°C of the current Si-IGBT to 150°C⁽¹⁾⁽²⁾. The reduction in generated loss and improvement of operating temperature have enabled us to achieve a power density increase, and the footprint size of the module has been reduced by approximately 30% as compared with the current product as shown in Fig. 1(b).

3. Packaging Technology Challenges Arising from Hybridization

3.1 Issue with and study of multi-parallel connection structure

In order to achieve a 1,200-A rating in hybridization, it is necessary to connect a number of chips in parallel due to the chip rated current limitation. Package structures with this multi-parallel connection are susceptible to a current imbalance due to variations in chip characteristics, leading to the degradation of long-term reliability. To deal with this issue, we conducted thermal analysis in a simulation to verify the conditions of temperature and thermal stress of the individual chips. Based on the results of this verification, we have determined that the effect of variations in chip characteristics on variations of chip temperature can be simulated. We have made use of this analysis to reflect the results in the package structure of the developed product for improving its reliability.

3.2. Improvement of power cycle capability

To achieve miniaturization by hybridization, a package structure that accommodates chip temperature increase is essential. An increase in the chip temperature increases not only the thermal stress on the constituent materials but also temperature variations due to starting and stopping, which requires the product to assure its performance for high thermal fatigue. Accordingly, to improve the ΔT_j power cycle capability, which serves as a guideline for this assurance, we have employed Sn-Sb solder under the chips, a packaging technology for the 7th-generation X Series IGBT modules. Sn-Sb solder offers high strength and has an

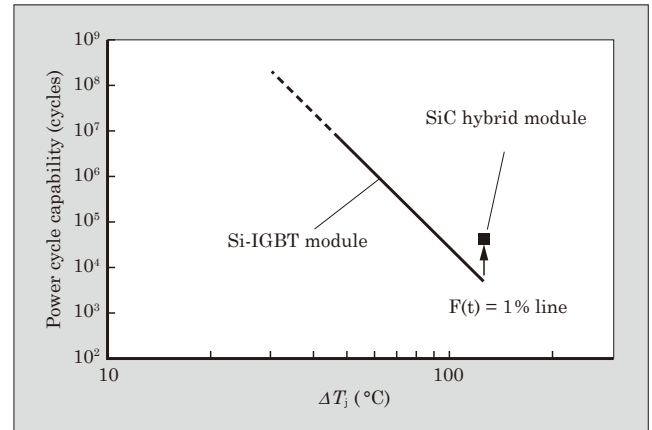


Fig.2 ΔT_j power cycle test results

effect of restraining the progress of cracking resulting from thermal fatigue⁽¹⁾⁽²⁾.

Figure 2 shows ΔT_j power cycle test results of a SiC hybrid module and Si-IGBT module. As compared with the Si-IGBT module, the SiC hybrid module has been shown to have a power cycle capability about 5 times higher when $\Delta T_j = 125^\circ\text{C}$.

4. Characteristics⁽³⁾⁽⁴⁾

4.1 Forward characteristics

Figure 3 shows the forward characteristics of SiC hybrid and Si-IGBT modules, and Fig. 4 the temperature dependence of forward voltage V_F at the 1,200-A rating. As shown in Fig. 4, V_F of the SiC hybrid module is smaller by about 29% than that of the Si-IGBT module at 25°C, which is reversed at 150°C to be larger by about 30%. However, while the Si-IGBT module has negative temperature characteristics, in which V_F decreases as the chip junction temperature T_j increases, the SiC hybrid module has positive temperature characteristics. When chips with negative temperature characteristics are connected in parallel, the internal resistance decreases as T_j increases. This allows the current to flow more easily, leading to a susceptibility to a current imbalance caused by a concentration of

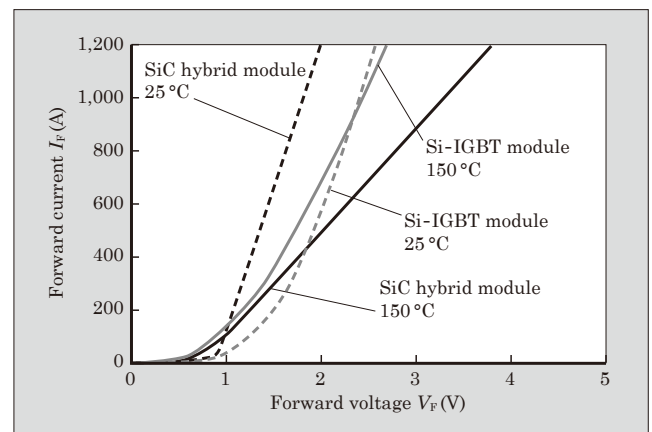


Fig.3 Forward characteristics

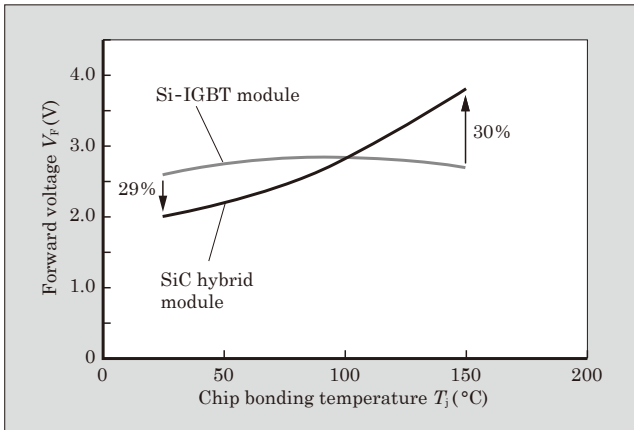


Fig.4 Temperature dependence of forward voltage

current in some of the chips.

Meanwhile, positive temperature characteristics cause the internal resistance to increase as T_j increases, which results in equal sharing of the current by chips connected in parallel. Accordingly, SiC hybrid modules are advantageous in multi-parallel connections.

4.2 Leakage current characteristics

Figure 5 shows the leakage current characteristics

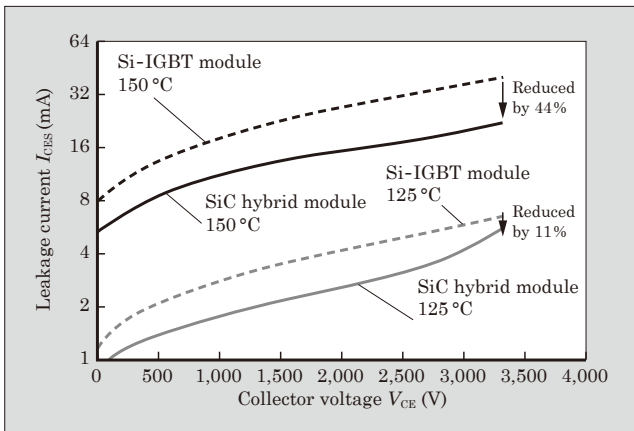


Fig.5 Leakage current characteristics

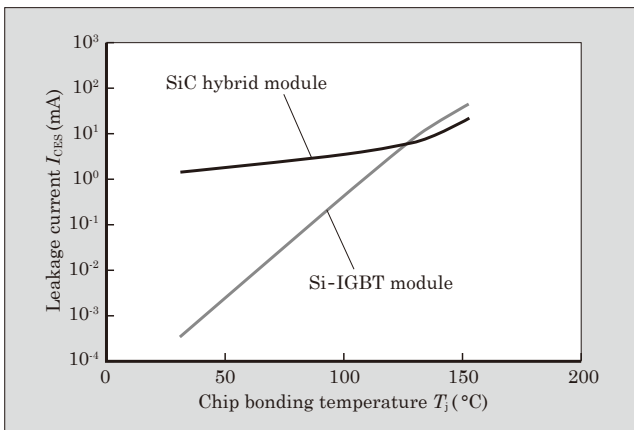


Fig.6 Temperature dependence of leakage current

of SiC hybrid and Si-IGBT modules, and Fig. 6 the temperature dependence of leakage current. At a temperature of 125 °C and collector voltage of 3,300 V, the leakage current of the SiC hybrid module I_{CES} is smaller by about 11% than that of the Si-IGBT module. At 150 °C, the difference becomes even larger, and reaches 44%. As shown in Fig. 6, I_{CES} of the Si-IGBT module shows a great change according to the temperature. On the other hand, the leakage current of the SiC hybrid module is nearly constant, which shows that its temperature dependence is small. This is because its band gap is about 3 times as large as that of Si and the excitation of the carriers due to the increase of T_j is small. Accordingly, the SiC hybrid module is capable of operating at higher temperatures than the Si-IGBT module.

4.3 Switching characteristics

(1) Reverse recovery characteristics

Figure 7 compares reverse recovery waveforms of

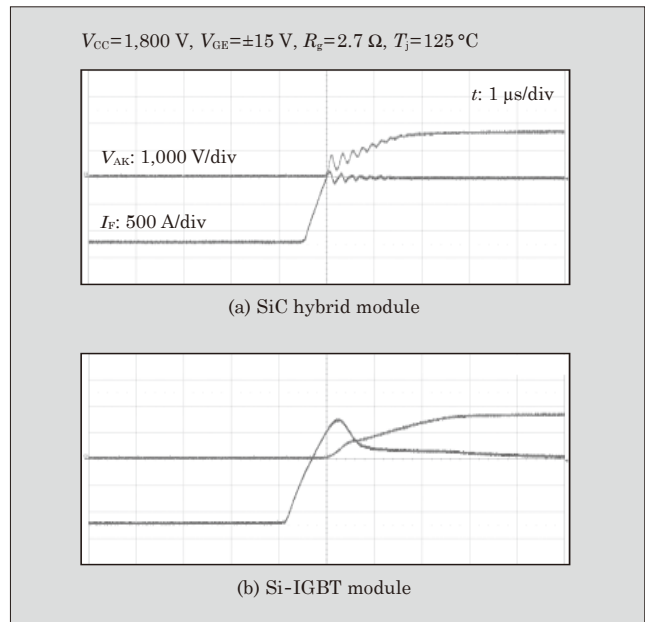


Fig.7 Reverse recovery waveforms

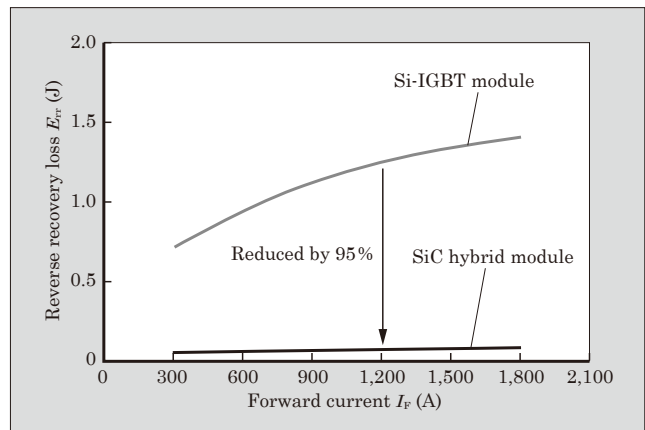


Fig.8 Current dependence of reverse recovery loss

the SiC hybrid and Si-IGBT modules. As compared with the Si-IGBT module, the SiC hybrid module exhibits a much lower reverse recovery peak current. This is because the SiC-SBD is a unipolar device and there is no storage effect caused by minority carriers. Figure 8 shows the current dependence of reverse recovery loss E_{rr} . For E_{rr} , at the 1,200-A rating, the generated loss can be reduced by 95% as compared with the Si-IGBT module. At 300 A or 1,800 A, the generated loss can also be reduced to the same level. Thus, the generated loss can be reduced in a wide range from low- to high-current regions.

(2) Turn-on characteristics

Figure 9 shows a comparison of turn-on waveforms between the SiC hybrid and Si-IGBT modules. The reverse recovery peak current of the SiC-SBD is reflected in the IGBT turn-on current in the opposite arm, and the turn-on peak current can be significantly reduced as well. As shown in Fig. 10, the turn-on loss E_{on} at the 1,200-A rating can be reduced by 28% as compared

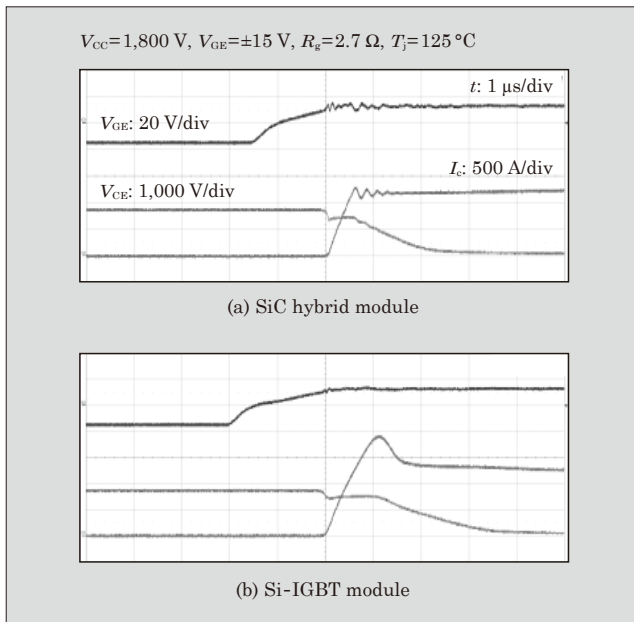


Fig.9 Turn-on waveforms

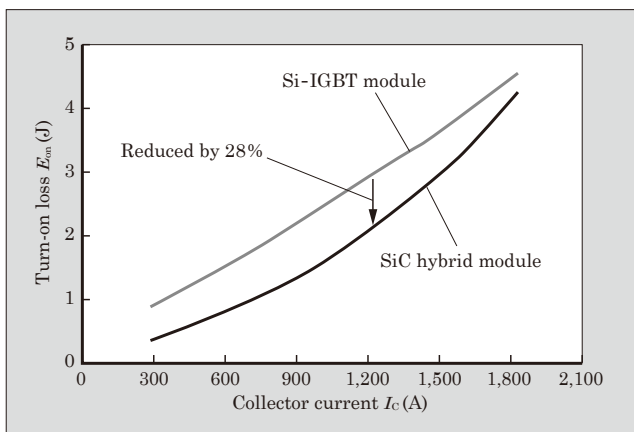


Fig.10 Current dependence of turn-on loss

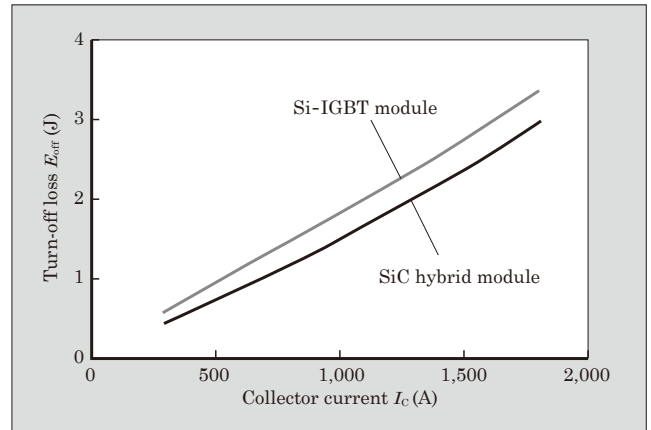


Fig.11 Current dependence of turn-off loss

with the Si-IGBT module.

(3) Turn-off characteristics

Figure 11 shows the current dependence of the turn-off loss E_{off} of the SiC hybrid and Si-IGBT modules. The surge peak voltage generated at turn-off can be generally defined by Equation (1). When the current changing rate dI_C/dt of the IGBT and the main circuit inductance L_s of the evaluation circuit are equivalent, the value of the transient on-state voltages of the diode appears as the difference in the surge peak voltage. The SiC-SBD has a drift layer with a lower resistance than that of the Si-FWD, resulting in the low transient on-state voltage. Accordingly, the turn-off surge peak voltage can be kept low with the SiC hybrid module, and E_{off} can also be reduced.

$$V_{sp} = V_{cc} + L_s \frac{dI_C}{dt} + V_{fr} \dots\dots\dots(1)$$

- V_{sp} : Surge peak voltage (V)
- V_{cc} : Applied voltage (V)
- L_s : Main circuit inductance (H)
- I_C : Collector current (A)
- V_{fr} : Transient on-state voltage (V)

4.4 Inverter power loss

Figure 12 shows the calculated results of inverter power loss in the SiC hybrid and Si-IGBT modules. At

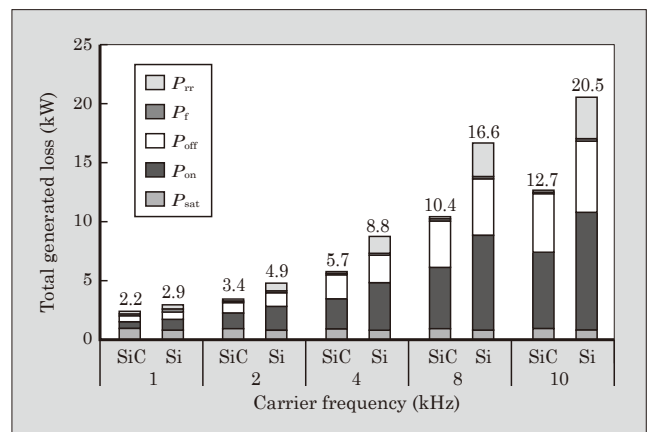


Fig.12 Results of calculating inverter power loss

a carrier frequency of 1 kHz, the total power loss of the SiC hybrid module can be reduced by 24% as compared with the Si-IGBT module. In addition, with a higher carrier frequency, the reduction rate of the total power loss is increased and the reduction can be as large as 38% at a carrier frequency of 10 kHz. This means that the SiC hybrid module can raise expectations for application to products that require high-frequency operation.

We have developed a traction converter for propulsion system (inverter, converter) that integrates the developed product for Central Japan Railway Company, which is mounted on Shinkansen trains (bullet train) and is currently undergoing running test.

5. Postscript

This paper has described the technology of the 3,300-V withstand voltage SiC hybrid module. The technology has been used for the 3,300-V withstand voltage SiC hybrid module that employs the SiC-SBD developed jointly with the cooperative research body Tsukuba Power-Electronics Constellations and Fuji Electric's Si-IGBT. The developed product adopts SiC-SBDs and Sn-Sb solder, thereby realizing an increase in power density and making significant contribu-

tions to efficiency improvement and miniaturization of power electronics equipment. In the future, we intend to proceed with study on developing all products with SiC to achieve a further performance improvement and promote energy saving.

We would like to extend our sincere gratitude to the people involved from the joint research body Tsukuba Power-Electronics Constellations who have offered their cooperation to the development of the SiC-SBD.

References

- (1) Momose, F. et al. New Assembly Technologies for $T_{jmax}=175^{\circ}C$ Continuous Operation Guaranty of IGBT Module. FUJI ELECTRIC REVIEW. 2013 vol.59, no.4, p.226-229.
- (2) Gohara, H. et al. Packaging Technology of 2nd-Generation Aluminum Direct Liquid Cooling Module for Hybrid Vehicles. FUJI ELECTRIC REVIEW. 2014, vol.60, no.4, p.228-232.
- (3) Nakazawa, M. et al. Hybrid Si-IGBT and SiC-SBD Modules. FUJI ELECTRIC REVIEW. 2014, vol.60, no.4, p.70-74.
- (4) Kobayashi, K. et al. 1,700 V Withstand Voltage SiC Hybrid Module. FUJI ELECTRIC REVIEW. 2013, vol.59, no.4, p.218-220.



7th-Generation “X Series” IGBT Module

KAWABATA, Junya* MOMOSE, Fumihiko‡ ONOZAWA, Yuichi*

ABSTRACT

In recent years, the IGBT module market has been seeing increasing demand for compact modules with low loss and high reliability. In order to meet these demands, we have developed the 7th-Generation “X Series” IGBT Module. By significantly reducing the loss of IGBT and FWD chips and developing a package characterized by its high heat dissipation, high heat resistance and high reliability, we have reduced the module’s footprint by approximately 36% and power loss by approximately 10% and achieved long-term reliability. Furthermore, by enhancing its withstanding and characteristics during high-temperature operation, we increased the maximum temperature for continuous operation to 175°C, from the conventional temperature of 150°C. These enhancements have enabled the module to significantly increase output current, and this further increase the power density and miniaturizes the size of power converters.

1. Introduction

In recent years, there has been increasing demand to improve energy efficiency and reduce CO₂ emissions as measures for preventing the depletion of fossil fuels and mitigating global warming. As a result, the use of power conversion equipment that utilize power semiconductors has been spreading to a wide variety of fields, and the market for these devices has been expanding rapidly. Insulated-gate bipolar transistor (IGBT) modules are commonly being used as power semiconductor devices in a wide range of fields such as the industrial, consumer, automotive and renewable energy sectors. Since the introduction of IGBT modules to the market, there have been many technological innovations that have facilitated significant advances in miniaturization and reduced power dissipation⁽¹⁾. These developments have contributed to the miniaturization (reduced cost) and increased efficiency of power conversion equipment. However, the miniaturization of IGBT modules has caused a rise in chip junction temperature T_j due to increased power density, as well as degradation in reliability. Therefore, further miniaturization of IGBT modules in the future will require not only improvements in the characteristics of IGBT and free wheeling diode (FWD) chips, but also improvements in exothermicity and reliability through packaging technology innovation.

Fuji Electric has newly developed a 7th-generation “X Series” IGBT module that adopts 7th-generation chip technology and packaging technology in order to achieve further miniaturization, reduced power dissipation and increased reliability for IGBT modules. The X Series IGBT module not only achieves minia-

turization, but also makes continuous operation at $T_j=175^\circ\text{C}$ possible by improving chip characteristics and the long-term reliability of packaging. As a result, operation at even greater output currents is now possible when compared with the previous 6th-generation “V Series” IGBT modules, which supported continuous operation up to 150°C.

2. 7th-Generation Chip Technology

By significantly reducing the loss for the IGBT and FWD, the X Series IGBT module simultaneously achieves reduced power dissipation and chip size miniaturization. Furthermore, the module secures sufficient capability in the various areas that tend to be problematic at high temperature operation, thus enabling it to support continuous operation at $T_j=175^\circ\text{C}$.

2.1 7th-generation IGBT chip technology

Figure 1 shows the cross sectional structure of the IGBT. The basic structure of the 7th-generation IGBT is the same as the 6th-generation IGBT, having a trench-gate structure for the front surface structure. It also adopts a thin wafer IGBT that uses a field stop (FS) layer for the back side. Compared with the 6th-generation IGBT, the reduction in the thickness of the drift layer has enabled it to achieve a reduced on-state voltage (collector-emitter voltage). Moreover, by refining the design and optimizing the trench-gate structure of the front surface, it is able to suppress the hole pull-out from the p-channel at the time of conduction, while also increasing the injection enhanced (IE) effect by raising the carrier concentration on the front surface side, as well as significantly improving the trade-off relation between the on-voltage and turn-off loss. Generally, a thinner drift layer would create concern regarding voltage oscillation and degradation in with-

* Electronic Devices Business Group, Fuji Electric Co., Ltd.

‡ Corporate R&D Headquarters, Fuji Electric Co., Ltd.

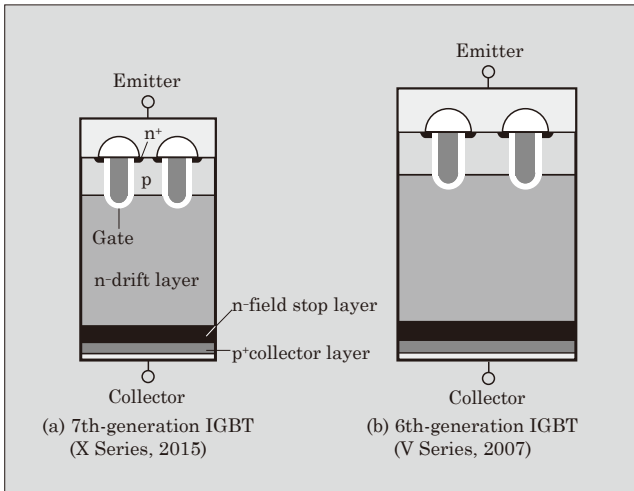


Fig.1 IGBT cross sectional structure

stand voltage at the time of turn-off, but by optimizing the FS layer, we have been able to suppress voltage oscillation and secure a sufficient withstand voltage.

Figure 2 shows the output characteristics of the 7th-generation IGBT. Comparing its rated current density with the 6th-generation IGBT, it has a lower on-state voltage of approximately 0.5 V at $T_j=150^\circ\text{C}$. Furthermore, even when operating at 175°C , it has an on-voltage of approximately 0.45 V lower than that of the 6th-generation IGBT at 150°C .

In general, it is well known that a trade-off relation between IGBT on-state voltage and turn-off loss exists. Figure 3 shows the trade-off characteristics of the 7th-generation IGBT on-state voltage and the turn-off loss. As mentioned earlier, the 7th-generation IGBT significantly reduces on-voltage, and it also greatly reduces tail current during turn-off by thinning its drift layer. It thereby decreases turn-off loss by 10%. As a result, compared with the 6th-generation IGBT, it achieves a significant improvement in the trade-off characteristics of turn-off loss and on-state voltage.

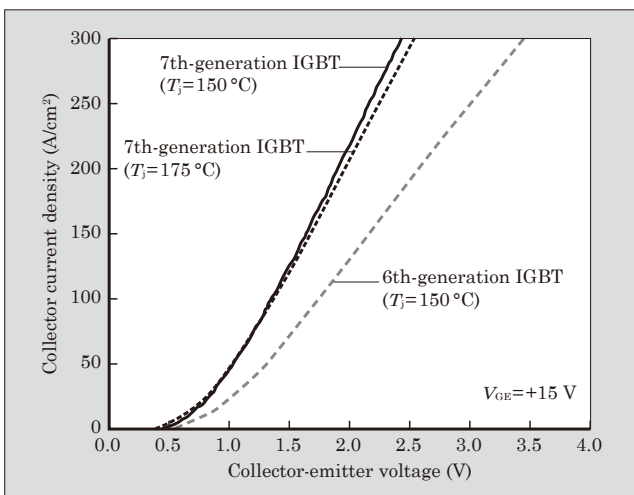


Fig.2 7th-generation IGBT output characteristics

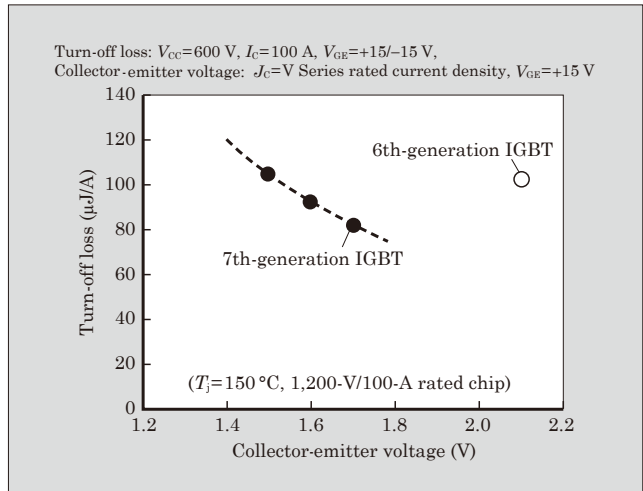


Fig.3 7th-generation IGBT trade-off characteristics

2.2 7th-generation FWD chip technology

By reducing the thickness of the drift layer, the 7th-generation FWD reduces forward voltage, and as shown in Fig. 4, it achieves smooth reverse recovery waveforms compared with the 6th-generation FWD through optimization of local lifetime control. In addition, it significantly reduces reverse recovery loss by reducing reverse recovery peak current and tail current. Figure 5 shows the trade-off characteristics of reverse recovery loss and forward voltage. When compared with the 6th-generation FWD at the same forward voltage, it achieves a reverse recovery loss reduction by approximately 30%.

On the other hand, reverse recovery surge voltage and voltage oscillation during reverse recovery can become problematic since a thinner drift layer generally makes it easier for the depletion region to reach the surface of the reverse side during reverse recovery⁽²⁾. The 7th-generation FWD has optimized the reverse surface structure to suppress stretching of the depletion region during reverse recovery operation, and by preventing the depletion layer from reaching the reverse surface side, it is able to reduce reverse recovery voltage oscillation and reverse recovery surge voltage

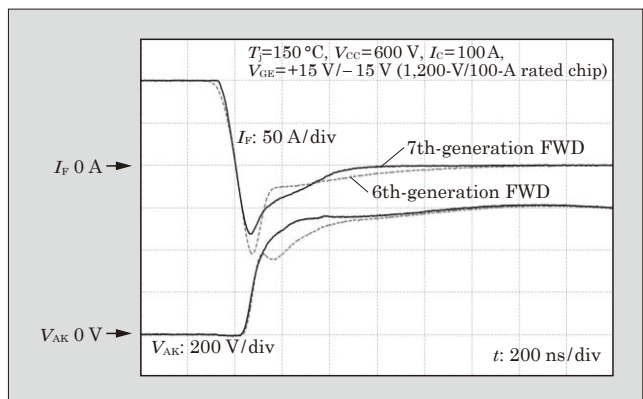


Fig.4 7th-generation FWD reverse recovery waveforms

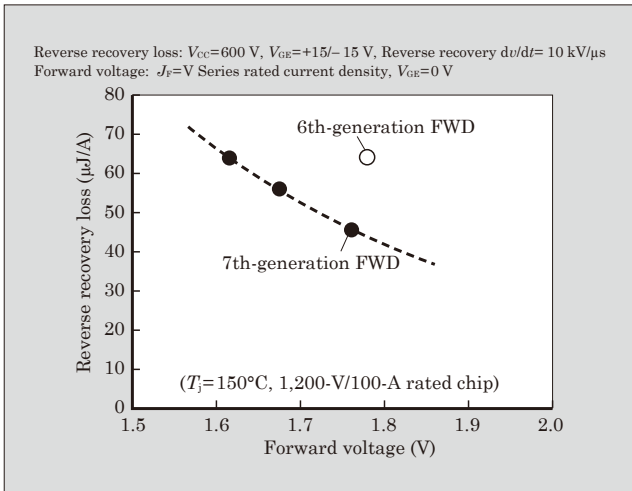


Fig.5 Reverse recovery loss and forward voltage trade-off characteristics

to not more than those of the 6th-generation FWD.

3. 7th-Generation Packaging Technology

In order to miniaturize IGBT modules, it is necessary to miniaturize the IGBT and FWD. However, miniaturization of the chip results in increased power density, and this causes degraded reliability due to a rise in chip temperature. To solve the issue, the X Series IGBT module makes use of a development in high heat-dissipating packaging technology to further suppress the rise in chip temperature, as well as high-reliability and high heat-resistant packaging technology to achieve continuous operation at 175 °C.

3.1 New AlN isolation substrate

In order to improve the exothermicity of the chip in the X Series IGBT module, we improved the thermal resistance of the isolation substrate, which occupies the largest portion among thermal resisting components from the chip to the cooling fins. Materials such as Al₂O₃ (alumina) and the highly thermal conductive AlN (aluminum nitride) are often used as materials for isolation substrates. In order to improve thermal resistance, it would be suitable if we could make use of an AlN isolation substrate, but since general AlN isolation substrates utilize a thick ceramic substrate, they are highly rigid, and thus reliability degradation becomes a concern due to higher thermal stress being applied to the solder located below the substrate when the molded case temperature rises. As a countermeasure, it is necessary to reduce the stress generated in the solder. Therefore, we tested methods for decreasing the rigidity of AlN isolation substrates by reducing the thickness of the ceramic substrate, as well as for alleviating the thermal stress that is applied to the solder located below the substrate. Conventionally, developing a thinner AlN isolation substrate has not been practical because there are concerns regarding

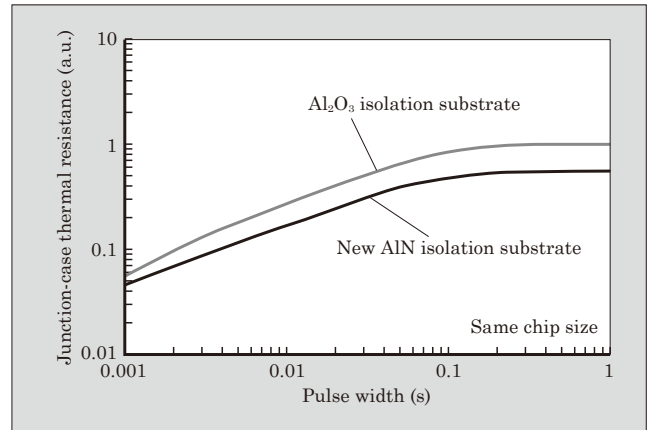


Fig.6 Junction-case thermal resistance

the degradation of the dielectric strength of the module products and possible cracking in the ceramic substrate during the mounting processes of customers. Therefore, we have developed a new thin type AlN isolation substrate that is characterized by its enhanced strength achieved by optimizing ceramic sintering conditions, distributed thermal stress via an innovative substrate circuit pattern design, and optimized isolation design achieved by revising creepage distance⁽³⁾.

By thus utilizing this new thin type AlN isolation substrate that achieves high heat dissipation and high reliability, we have ensured long-term reliability for the IGBT module, while also significantly reducing thermal resistance. Figure 6 shows the thermal resistance between the junction and case of an IGBT module that utilizes the new AlN isolation substrate. Thermal resistance has been reduced by approximately 45% on a chip that is the same size as the Al₂O₃ isolation substrates that are currently in widespread use. By using the new AlN isolation substrate for products that are particularly susceptible to increases in power density and rises in chip temperature, it is possible to overcome the temperature rise problems that IGBT module miniaturization has brought about.

3.2 Improvement of ΔT_j power cycle capability

There has been strong demand for long-term reliability in IGBT modules in order to lengthen the service life of power conversion equipment. In particular, capability against repetitive thermal stress (ΔT_j power cycle capability) is a major issue. In order to achieve operation at an even greater output current for the X Series IGBT module, the feasible region for continuous operation has been improved from the previous $T_j=150^\circ\text{C}$ to 175°C . In general, when T_j rises, the materials around the chip deteriorate quicker, and this, in turn, degrades ΔT_j power cycle capability⁽⁴⁾. ΔT_j power cycle capability is largely influenced by degradation in the product lifespan because wire bonding contact points on the chip and solder below the chip receive the greatest amount of thermal stress. To ensure that the X Series IGBT module has a sufficient ΔT_j power cycle

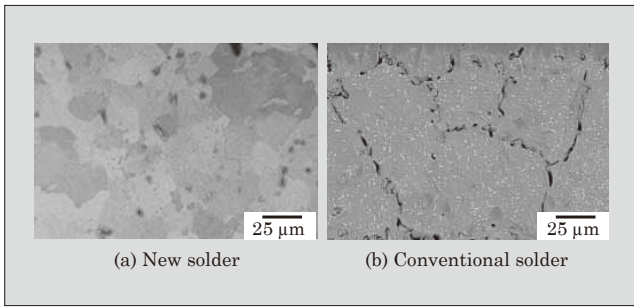


Fig.7 Cross section of solder below chip after a ΔT_j power cycle capability test

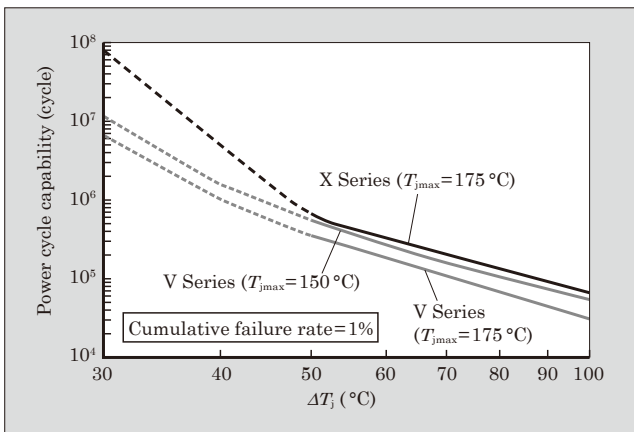


Fig.8 ΔT_j power cycle capability

capability even at $T_j=175^\circ\text{C}$, we optimized the design of the wire bonding and also applied our newly developed high strength solder.

Figure 7 shows the results of cross-section observation of the solder below the chip after a ΔT_j power cycle capability test following the same cycle. Although cracks were observed in the conventionally used solder, we verified that cracking was suppressed in the new solder. Figure 8 shows the ΔT_j power cycle capability. The X Series IGBT module achieves approximately twice as much capability as the V Series IGBT module ($T_{j\text{max}}=175^\circ\text{C}$, $\Delta T_j=50^\circ\text{C}$). Therefore, long-term reliability has been ensured with a ΔT_j power cycle capability equivalent to or better than conventional modules even when operating at $T_{j\text{max}}=175^\circ\text{C}$.

3.3 High heat-resistant silicone gel

To ensure the long-term reliability of the IGBT module, we were still faced with the issue of deteriorating silicone gel at high-temperature operation. In general, silicone gel hardens in proportion with temperature rise, and this causes a concern regarding cracking in the hardened gel. The cracks fracture the isolation sheath of the gel, and this degrades isolation performance. Therefore, in order to achieve continuous operation at 175°C , we newly developed a high heat-resistant silicone gel. The high heat-resistant silicone gel makes use of an optimized material composition for suppressing hardening at high temperatures. We

performed a high-temperature shelf test (215°C , 2,000 hours) and verified that there was no cracking in the high heat-resistant silicone gel, although cracking did occur in the conventional silicone gel as a result of the hardening.

Figure 9 shows the relation between the environmental temperature and the lifespan of the silicone gel. The lifespan of the high heat-resistant silicone gel at 175°C is greatly improved over that of conventional silicone gel, while it also has the same lifespan that the conventional silicone gel has at 150°C . As a result, isolation performance equivalent to that of the conventional module at 150°C has been ensured even during continuous operation at 175°C .

Furthermore, the relation between the environmental temperature and the coefficient of elasticity of the silicone gel is shown in Fig. 10. While the conventional silicone gel is characterized by rapid hardening

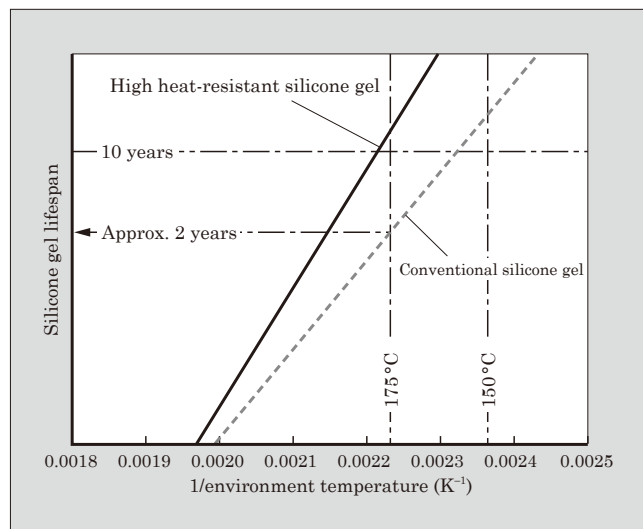


Fig.9 Relation between environment temperature and lifespan of silicone gel

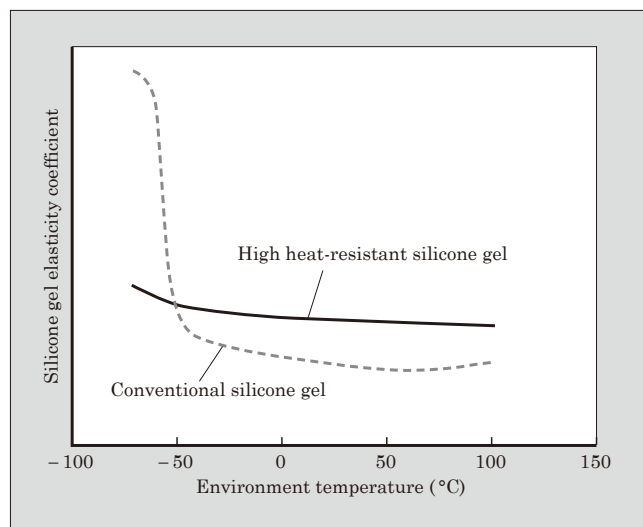


Fig.10 Relation between environment temperature and coefficient of elasticity of silicone gel

at temperatures of -50°C or below, the high heat-resistant silicone gel suppresses rise in the coefficient of elasticity even at low temperatures, thus enabling it to achieve an improvement in isolation in low temperature environments. By using the high heat-resistant silicone gel, IGBT modules can be used in various installation environments, and they are expected to be utilized in a wide range of applications.

4. IGBT Module Miniaturization

Significant improvement in loss characteristics via the application of 7th-generation IGBT and FWD, as well as large-scale improvement in exothermicity and reliability through the adoption of innovative packaging technology have made it possible for the X Series IGBT module to achieve further miniaturization and greater power density than conventional modules. As an example, for the V Series IGBT module in a EP2 package with a rated capacity of 1,200 V, the maximum current rating was 50 A, whereas the X Series IGBT module is able to achieve a new rating of 75 A. In addition, it is possible to reduce the footprint by approximately 36% when migrating from the conventional V Series IGBT module EP3 package with a rating of 75 A.

The X Series IGBT module not only has a more compact size and greater power density, but it also dissipates less power at the same time. Figure 11 shows the calculated results of power loss and IGBT junction temperature during normal operation in an X Series IGBT module EP2 package with a rated current capacity of 75 A. Compared with a V Series IGBT module EP3 package with a rated product capacity of 75 A, it successfully reduces power loss by approximately 10%, while also reducing the IGBT junction temperature by approximately 10°C ($f_c=8\text{ kHz}$).

As described above, the improvements in ΔT_j power

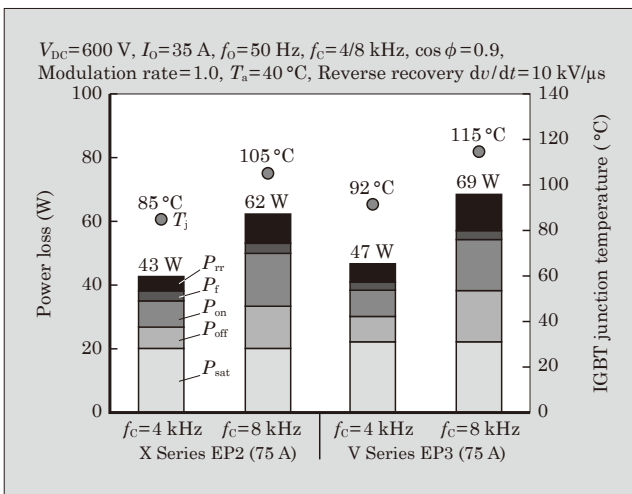


Fig.11 Power loss and IGBT junction temperature during normal operation

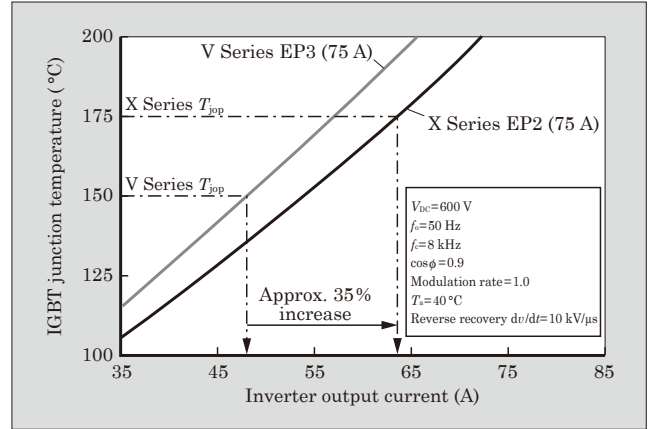


Fig.12 Inverter output current and IGBT junction temperature

cycle capability and silicone gel heat resistance have made continuous operation at 175°C possible for the X Series IGBT module. As a result, it has become possible to further improve power density in power conversion equipment, and as shown in Fig. 12, it is also possible to increase output current by approximately 35% compared with V Series IGBT module EP3 packages with a rated current capacity of 75 A.

5. Postscript

The 7th-generation “X Series” IGBT module is capable of simultaneously achieving miniaturization, reduced power dissipation and higher reliability by significantly reducing loss for IGBT and FWD, and by taking advantage of the development of high-reliability and high heat-dissipating packaging technology. Since migrating from conventional products to the 7th-generation IGBT module makes it possible to miniaturize the size of power conversion equipment and reduce costs, it is expected that power conversion equipment will become more widely utilized and efficient in the future, thus enabling them to contribute greatly to solving the world’s energy issues.

References

- (1) Kobayashi, Y. et al. “The New IGBT-PIM with the 6th generation V-IGBT chip technology”. Proceeding of PCIM Europe 2007.
- (2) Onozawa, Y. et al. “Development of the 1200 V FZDiode with Soft Recovery Characteristics by the New Local Lifetime Control Technique”. Proceeding of ISPSD 2008, p.80-83.
- (3) Momose, F. et al. “The New High Power Density Package Technology for the 7th Generation IGBT Module”. PCIM Europe 2015.
- (4) Saito, T. et al. “New assembly technologies for $T_{jmax}=175^{\circ}\text{C}$ continuous operation guaranty of IGBT module”. Proceeding of PCIM Europe 2013, p.455-461.

2nd-Generation Small IPM

ARAKI, Ryu* SHIRAKAWA, Toru* KOGAWA, Hiroki*

ABSTRACT

Fuji Electric has been developing small intelligent power modules (IPMs) that integrate into a single package the power devices and control IC needed in the system construction of motor drives. We have now developed a 2nd-generation small IPM based on 7th-generation IGBT technology to achieve even more energy savings. The module reduces the loss by 10% or more in the intermediate load region, such as in the case of a 5.6-kW air conditioner, and by 20% or more in the rated and maximum load region compared with the 1st-generation module. In addition, temperature rise in the soldering on the circuit board has also been reduced by approximately 20°C compared with the 1st-generation module. Overall, the module achieves enhanced energy savings, expands output current, and increase reliability during circuit board mounting and a greater degree of freedom during system design.

1. Introduction

As there is a growing interest in global environmental issues, there is increasing demand to save on the energy consumed by consumer electronics such as air conditioners and washing machines and industrial motor drive systems.

For consumer electronics, energy-saving regulations based on the annual performance factor (APF), which indicates energy consumption efficiency close to the actual use, have been tightened globally. The focus is, thus, given not only to improving efficiency under the rated and maximum load conditions but also to reducing loss in the intermediate load condition, which is closer to the actual use. In the Japanese and Chinese markets, in particular, significant improvement of energy saving performance is required for popular models, which form the main range, in addition to high-end models.

In addition, with inverters and servos for industrial use, there is increasing demand for chassis downsized by improving power density.

In order to meet these demands, Fuji Electric has commercialized small intelligent power modules (IPMs) that integrate into a single package the power devices and control IC needed in the system construction of motor drives⁽¹⁾. Small IPMs, which integrate a 3-phase inverter bridge circuit with control and protection circuits, have been making contributions to size reduction and energy saving of inverters.

To achieve further energy saving in each application, we have developed the 2nd-generation small IPM by inheriting the 1st-generation small IPM and using the basis of a 7th-generation insulated-gate bipolar transistor (IGBT) technology⁽²⁾, which combines wafer

thinning and miniaturization.

2. Product Overview

Figure 1 shows the external appearance of the 2nd-generation small IPM and Table 1 the product lineup and major characteristics. The 2nd-generation small IPM has a compatible package structure with the same external size and pin assignment as those of the 1st-generation products. The product line includes the 600-V/10- to 30-A ratings. New addition of the 10-A rating has been made for air conditioner compressors with an input power of 1.5 kVA and for small-capacity industrial inverters and servos with 0.1- to 0.2-kW outputs. The module provides 2 types of temperature protection function: with analog temperature output only and with overheat protection added.

Figure 2 shows the configuration of internal equivalent circuit of the small IPM. The small IPM integrates a 3-phase inverter bridge circuit composed of low-loss IGBTs and high-speed free wheeling diodes (FWDs) on an insulating metal substrate. It has a low voltage integrated circuit (LVIC) chip for driving

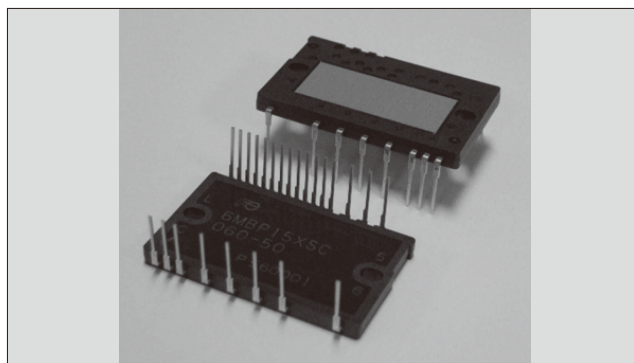


Fig. 1 2nd-generation small IPM

* Electronic Devices Business Group, Fuji Electric Co., Ltd.

Table 1 Product lineup and major characteristics

Voltage	Type	I_C	I_{CP}	$V_{CE(sat)}$ (typ.)	V_F (typ.)	Temperature protection function
600 V	6MBP10XSA060-50	10 A	30 A	1.40 V	1.40 V	Temperature sensor output
	6MBP10XSC060-50					Temperature sensor output and overheat protection
	6MBP15XSA060-50	15 A	45 A	1.40 V	1.40 V	Temperature sensor output
	6MBP15XSC060-50					Temperature sensor output and overheat protection
	6MBP20XSA060-50	20 A	60 A	1.40 V	1.55 V	Temperature sensor output
	6MBP20XSC060-50					Temperature sensor output and overheat protection
	6MBP30XSA060-50	30 A	90 A	1.40 V	1.45 V	Temperature sensor output
	6MBP30XSC060-50					Temperature sensor output and overheat protection

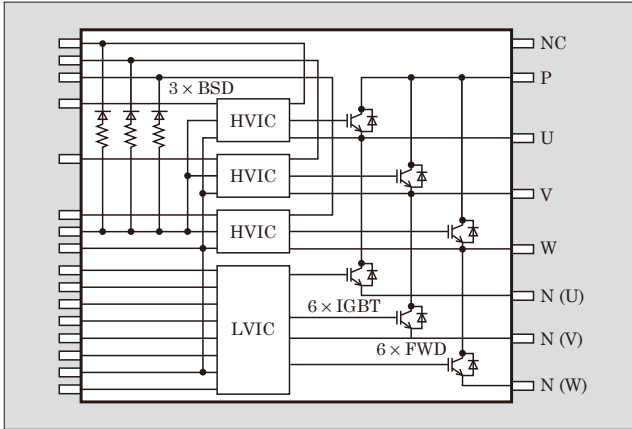


Fig. 2 Configuration of internal equivalent circuit

the IGBTs on the low side and high voltage integrated circuit (HVIC) chips for driving the IGBTs on the high side of this 3-phase inverter bridge circuit. By providing boot strap diodes (BSDs) with built-in a current limiting resistor for the drive circuit on the high side, insulated power supply can be constructed with a small number of external parts.

The 2nd-generation small IPM has not only achieved a significant reduction of loss from the 1st-generation but also the guaranteed operating temperature range has expanded from 125 °C to 150 °C. In addition, it has realized a greater degree of design freedom and expanded the operating range of inverters by optimizing the overheat detection level and improving the overcurrent detection accuracy.

3. Features

Table 2 shows the characteristics of the 2nd-generation small IPM. The following describes the features.

(1) Improvement of APF by loss reduction

Using the low-loss device based on the 7th-generation IGBT technology and optimizing the drive performance allow for a significant reduction of loss and improvement of the APF.

(2) Improvement of degree of design freedom and expansion of operating range of inverters

Increasing the guaranteed operating temperature $T_{j(ope)}$ increases the allowable current, which allows the operating range to be expanded. In addition, expand-

Table 2 Characteristics of 2nd-generation small IPM

Item	2nd generation	1st generation
Type	6MBP15XSC060-50	6MBP15VSC060-50
V_{CE}	600 V	600 V
I_C	15 A	15 A
I_C (pulse)	45 A	30 A
$T_{j(ope)}$	-40 °C to +150 °C	-40 °C to +125 °C
$V_{CE(sat)}$ (typ.)	1.40 V	1.80 V
E_{off} (typ.)	0.26 mJ	0.56 mJ
V_F (typ.)	1.40 V	1.65 V
Short-circuit protection detection accuracy	480 ± 25 mV	480 ± 50 mV
Temperature protection	Temperature sensor output and overheat protection (143 °C ± 7 °C)	Temperature sensor output and overheat protection (125 °C ± 10 °C)

ing the peak collector current rating and improving the accuracy of short circuit detection allow the overload operating range, where a large current flows instantaneously at startup, to be expanded. This makes it possible for the same rating to accommodate a motor capacity of one level higher.

(3) Reduction of thermal resistance

A high-heat-dissipation aluminum insulating substrate with the thermal conductivity improved by approximately 1.5 times from the 1st-generation small IPM has been employed to reduce the thermal resistance. This has successfully suppressed the increase in junction temperature, which, together with the loss reduction, has increased the allowable current.

3.1 Features in device design

(1) Low-loss power device design

Figure 3 shows a comparison of the IGBT cross-section structure. The 7th-generation IGBT device is based on the field stop (FS) structure that we have developed up to now and combines further wafer thinning and miniaturization technology.

For the 2nd-generation small IPM, the specific resistance and thickness of the drift layer have been optimized based on the 7th-generation IGBT technology. In addition, the FS layer profile and the surface channel density and layout have been optimized, thereby improving the trade-off between the $V_{CE(sat)}$ and E_{off}

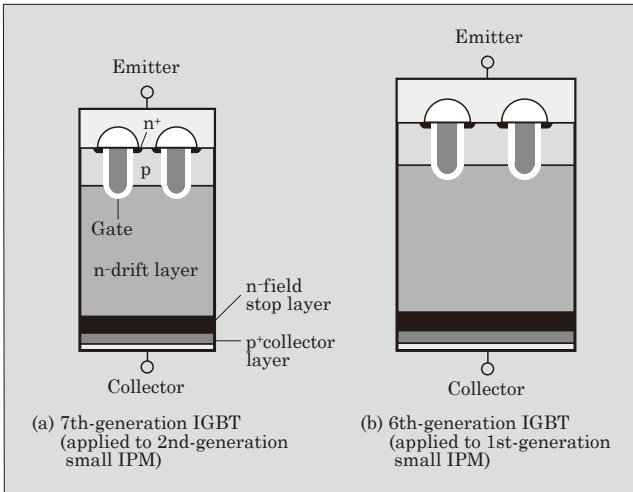


Fig. 3 IGBT cross-section structure

characteristics.

Figure 4 compares the trade-off between the $V_{CE(sat)}$ and E_{off} characteristics with that of the 1st-generation small IPM and Fig. 5 compares the turn-off waveforms. The trade-off between the $V_{CE(sat)}$ and E_{off} characteristics shows an improvement from the 1st generation by approximately 25% in terms of $V_{CE(sat)}$ and approximately 50% in terms of E_{off} due to the tail current reduction through wafer thinning. In this way, we

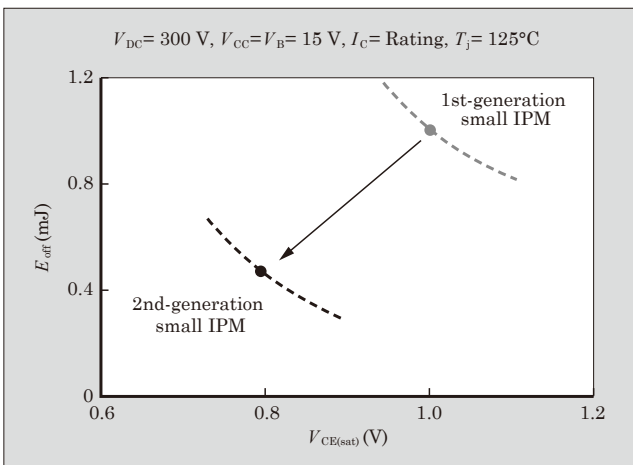


Fig. 4 Trade-off between $V_{CE(sat)}$ and E_{off} characteristics

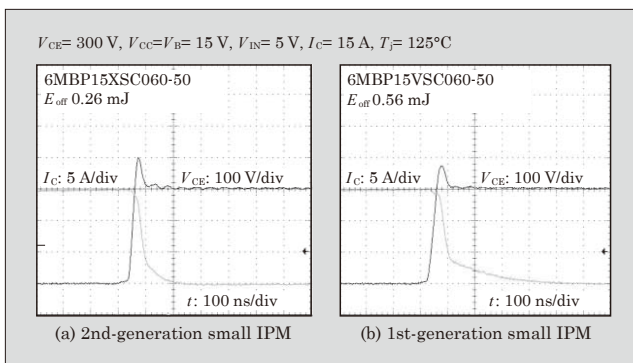


Fig. 5 Turn-off waveforms

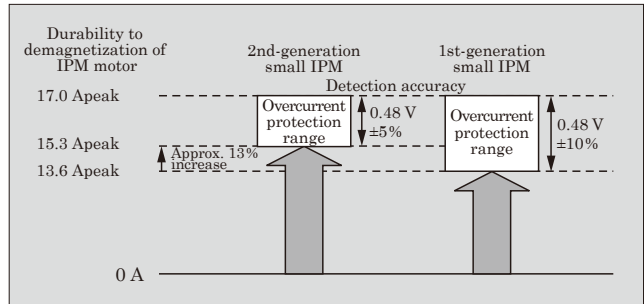


Fig. 6 Comparison of overcurrent protection level

have improved the APF, which is an index of energy saving, by reducing loss under the intermediate load conditions and increased the allowable current by significantly reducing the loss under the maximum load conditions.

(2) Improvement of overcurrent detection accuracy

Figure 6 shows a comparison of the overcurrent protection level of interior permanent magnet (IPM) motors in two generations. For IPM motors used for compressors of air conditioners, the motor's demagnetization capability in high output conditions must be ensured. Therefore, overcurrent protection in the overload region is important. To expand the operating range, the detection accuracy for overcurrent protection makes a major contribution.

With the 2nd-generation small IPM, the range of detection accuracy for overcurrent protection can be reduced by half from 10% of the 1st generation to 5%. This brings out the motor characteristics close to the limits, thereby increasing the current under the maximum load conditions by approximately 13%.

3.2 Features in package design

(1) High-temperature operation guarantee

To increase the guaranteed operating temperature $T_{j(ope)}$ described above, it is necessary to improve reliability including the power cycle capability in view of actual use.

For that purpose, the 2nd-generation small IPM has the thermal fatigue of the wire bonds reduced so as to improve the power cycle capability. In this way, the thermal stress of the package components in high-temperature operation can be reduced. This has enabled the device to satisfy the level of 15 keycycles or more in the power cycle test assuming $T_{j(ope)} = 150^\circ\text{C}$ ($\Delta T_j = 100^\circ\text{C}$).

(2) Reduction of temperature rise

In order to increase the allowable current along with the expansion of the operating range, it is necessary to reduce the thermal resistance of the package to restrain the temperature rise of the power device.

Figure 7 shows the cross-section structure of the package. The structure of the small IPM employs a high-heat-dissipation aluminum insulating substrate for the terminal case, and the efficiency has been improved. The issue is to both reduce the thermal resis-

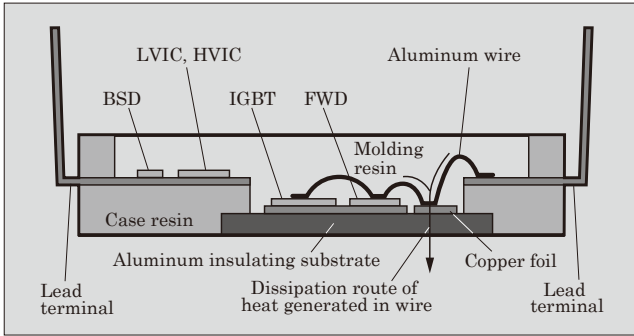


Fig. 7 Package cross-section structure

tance and ensure a sufficient withstand voltage of the aluminum insulating substrate. To do this, we have focused on and optimized the trade-off between the thickness of the insulating layer in the aluminum insulating substrate, which is a major factor that determines the package thermal resistance characteristics, and the withstand voltage.

To increase the allowable current, it is necessary to reduce the temperature rise in the soldering part on the circuit board. Accordingly, the 2nd-generation small IPM is built with a structure that dissipates the heat generated in the wire to the aluminum insulating substrate side in order to reduce the temperature rise in the soldering part. Temperature rise is reduced by dissipating the Joule heat, which is generated in the wire when a current is flowed, to the aluminum insulating substrate side.

4. Effect of Application

Figure 8 shows the results of a trial calculation of the loss under the 150% overload conditions assuming a 0.75-kW industrial inverter. Comparing with the 1st generation, the 2nd-generation small IPM has achieved a loss reduction of approximately 20%. This means the device can also be applied to inverters of 1.0 kW, one level higher capacity.

Figure 9 shows the results of trial calculation of

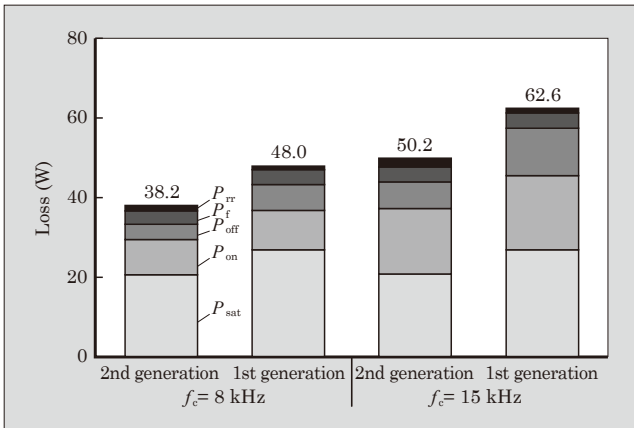


Fig. 8 Trial calculation results of loss for 0.75-kW industrial inverter

loss in the individual operation mode assuming an air conditioner of 5.6-kW output that uses a 600-V/15-A IPM. The 2nd-generation small IPM shows lower loss than the 1st-generation in all load ranges. In the intermediate load region, which has an impact on the APF performance in particular, the loss is lower by more than 10%.

The loss is also lower in the rated and maximum load ranges by more than 20%, which allows the device to be applied to an air conditioner of 7.2 kW, a one level higher capacity, with the 15-A rating.

Figure 10 shows the results of evaluating the temperature rise during PWM operation, which corresponds to steady-state operation of an air conditioner. The 2nd-generation small IPM has achieved an approximately 25% increase of the allowable output current from the 1st generation by increasing the guaranteed operating temperature ($T_{j(ope)} = 150^\circ\text{C}$) along with loss reduction and reduction of temperature rise.

In addition, temperature rise in the soldering part on the circuit board has also been reduced by about 20°C compared with the 1st-generation module. With the 2nd-generation module, the output current has

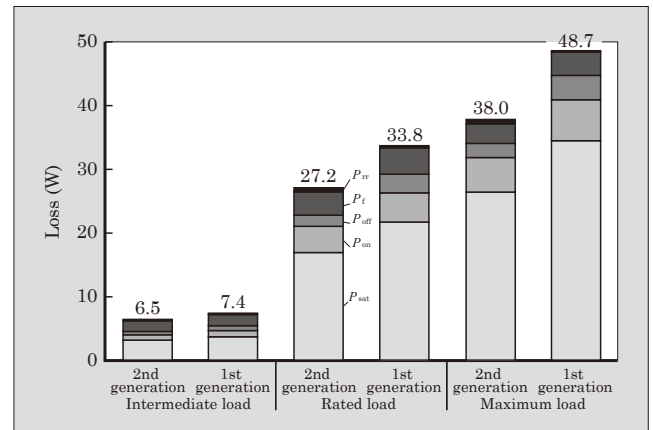


Fig. 9 Trial calculation results of loss for 5.6-kW air conditioner

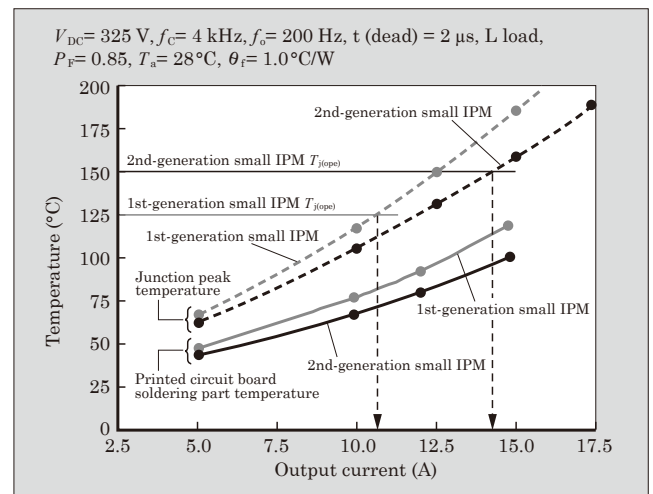


Fig. 10 Evaluation results of temperature rise during PWM operation

been increased and reliability when it is mounted on the circuit board is improved, which provides improved degree of design freedom as well.

Figure 11 shows the result of evaluating the conduction noise with the module mounted on a 5.6-kW output air conditioner. In the frequency region from 500 kHz to 30 MHz, the tolerance of the quasi peak (QP) value of the CISPR14-1 standard is satisfied and, together with the loss reduction described above, low noise has also been confirmed.

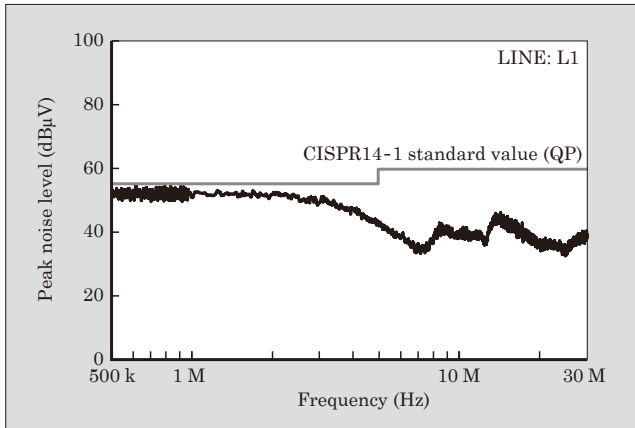


Fig. 11 Evaluation results of conduction noise for 5.6-kW air conditioner

5. Postscript

This paper has described the features of the 2nd-generation small IPM. By applying the optimized IGBT device based on the 7th-generation IGBT technology, the 2nd-generation small IPM achieves a significant loss reduction and contributes towards energy saving of various systems. In addition, the allowable current has been increased by raising the guaranteed operating temperature and reducing the thermal resistance. In this way, the product helps to expand the applicable motor capacity and improves the degree of design freedom of systems.

We intend to continue developing products capable of realizing energy saving in overall systems with an even wider product lineup.

References

- (1) Yamada, T. et al. "Novel Small Intelligent Power Module For RAC". proc. 2012 PCIM Asia.
- (2) T. Heinzl. et al. "The New High Power Density 7th Generation IGBT module for Compact Power Conversion Systems". Proceeding of PCIM Europe 2015, p.359-367.

HVIC Technologies for IPM

JONISHI, Akihiro* AKAHANE, Masashi* YAMAJI, Masaharu*

ABSTRACT

A high voltage integrated circuit (HVIC), which is a gate driver IC with a high breakdown voltage, is one of the key devices required in enhancing the functionality of intelligent power modules (IPMs). Fuji Electric has developed HVIC technology characterized by its advanced functionality, compactness, high reliability, and guaranteed industrial use at 600 V/1,200 V for small- and medium-capacity IPM. By reducing the circuit area and adopting high breakdown voltage technology and enhanced noise resistant level-shift circuit technology, we have reduced the chip size by 20% while improving the breakdown voltage and reliability. In addition, we have achieved over-current and over-heat protection circuit technology for upper-arm IGBT, as well as level-down functionality for alarm signals.

1. Introduction

An intelligent power module (IPM) is a power semiconductor module that integrates into one package a driver IC with the gate drive and protective functions together with insulated-gate bipolar transistors (IGBTs) or other power switching devices and free wheeling diodes (FWDs). IPMs help reduce the number of parts and size and simplify the design of systems and are used in wide-ranging applications including industrial machines, consumer electronics such as air conditioners and power supply equipment for servers.

Fuji Electric developed the world's first IPM using bipolar transistors in 1986. Ever since then, we have been actively developing products that help to improve the reliability and reduce the size of systems. One such product was the world's first IPM equipped with an IGBT chip overheat protection function that we released in 1997⁽¹⁾. In 2012, we commercialized a small-capacity IPM for inverter air conditioners. It eliminates the need for an external insulation circuit or level-shift circuit by employing a high-voltage integrated circuit (HVIC), which is a high breakdown voltage gate driver IC. Furthermore, we are working on ways to incorporate HVICs in medium-capacity IPMs for industrial use.

HVICs to be mounted on IPMs are required to withstand 600 V and 1,200 V according to the breakdown voltage class of the IPM. In addition, they must also offer high reliability to withstand the noise caused by IGBT switching, integrate various protection circuits and have a small chip size.

Based on the 800-V breakdown voltage guaranteed HVIC technology⁽²⁾ developed in 2010, Fuji Electric has developed new industrial 600-V/1,200-V breakdown

voltage guaranteed HVIC technology. It features high functionality, compactness and high reliability and is intended for small- and medium-capacity IPMs of up to the 1,200-V/100-A class. Of the new technology, this paper describes the device-process technology and circuit component technology.

2. Features of HVIC for IPMs

Figure 1 shows the 1,200-V breakdown voltage guaranteed HVIC chip prototyped for medium-capacity IPMs and Fig. 2 a block diagram of its circuit and peripheral circuit. One feature of the HVIC is that it integrates 3 circuits into one chip: a low-side circuit operated based on the ground potential, high-side circuit operated based on the source potential of the upper-arm IGBT to provide the gate drive function, and level-shift circuit responsible for the level-up function for control signals. The source potential of the upper-arm IGBT may vary from about -100 to over +1,000 V along with switching and a high isolation breakdown voltage is provided between the high-side and low-side

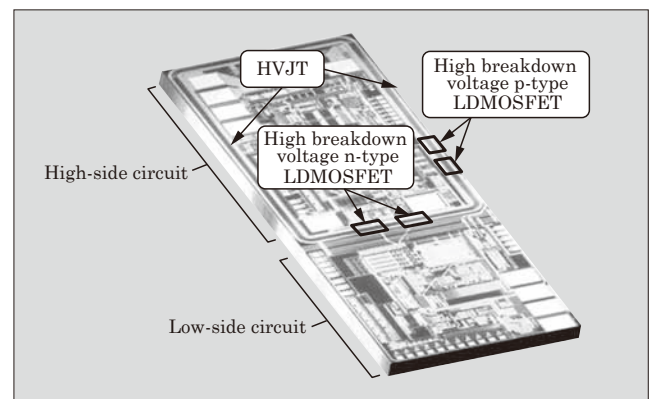


Fig.1 1,200-V breakdown voltage guaranteed HVIC chip

* Electronic Devices Business Group, Fuji Electric Co., Ltd.

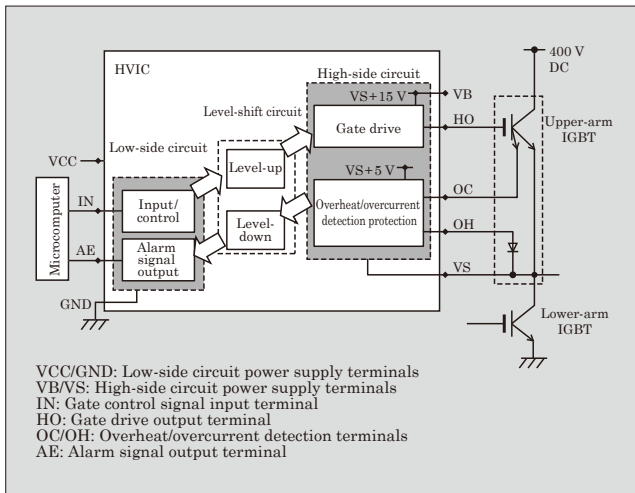


Fig.2 Block diagram of 1,200-V breakdown voltage guaranteed HVIC circuit and peripheral circuit

circuits.

With the HVIC, the control signal based on the ground potential input to the low-side circuit is transmitted through the level-shift circuit to the gate drive circuit in the high-side circuit, which drives the upper-arm IGBT. With an IPM incorporating the HVIC, this level-shift function makes it possible to drive the upper-arm IGBT without using an optocoupler or other insulation device.

Features of the 1,200-V breakdown voltage guaranteed HVIC include:

- (a) Guaranteed breakdown voltage of 1,200 V, power supply voltage of up to 24 V (guaranteed breakdown voltage 800 V with the previous

product)

- (b) Provision of overheat/overcurrent detection protective function for upper-arm IGBT
- (c) Provision of level-down function for alarm signals
- (d) Reduction of circuit area and adoption of high breakdown voltage technology (in-chip wire bonding high potential wiring technology with the previous product)
- (e) Enhanced noise immunity (dV/dt noise immunity $\pm 50 \text{ kV}/\mu\text{s min.}$)

3. Device-Process Technology

To achieve a compact and high-reliability HVIC with advanced-functionality, we have developed 600-V/1,200-V high breakdown voltage CMOS process that introduces a new well structure and high breakdown voltage technology. For device isolation, the self-isolation method has been employed.

3.1 Reduction of circuit area by using divided high-side well structure

Figure 3 shows the cross-sectional structure of the HVIC. The HVIC is provided with a low-side well for forming the low-side circuit and high-side well for forming the high-side circuit. Both are composed of an n-type diffusion layer on the p-type substrate. The high-side well is separated from the low-side well by the high-voltage junction termination (HVJT) and the HVJT functions to maintain the high breakdown voltage between the high-side and low-side circuits.

- (1) Issue with conventional high-side well structure

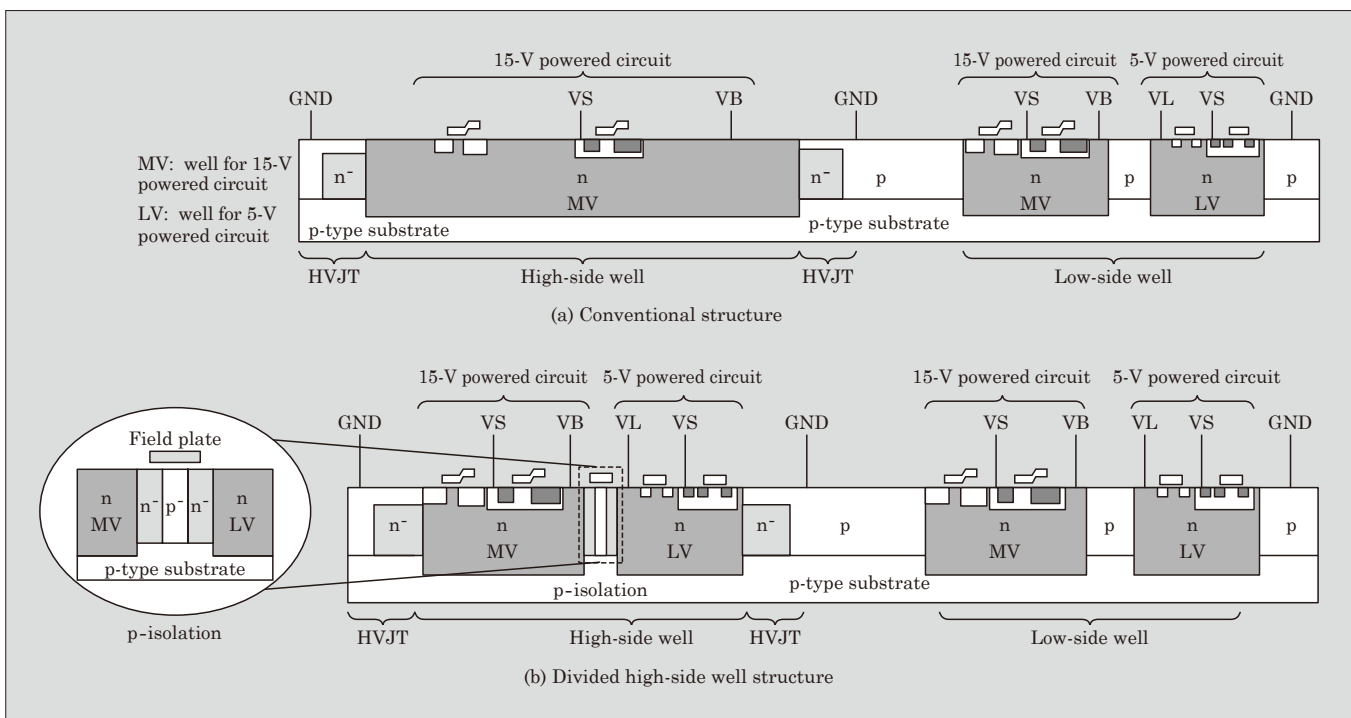


Fig.3 Cross-sectional structure of HVIC

As shown in Fig. 3(a), the low-side well is composed of multiple diffusion layers corresponding to the power supply voltages of the individual circuits. However, the high-side well is composed of a single diffusion layer in the conventional HVIC. This is because it was difficult to divide the high-side well while maintaining the high breakdown voltage with the conventional technology. For that reason, the high-side circuit could only support one power supply voltage, which reduced the degree of freedom of circuit design.

(2) Divided high-side well structure

For the purpose of solving the issue described above, we have developed the divided high-side well structure. Figure 3(b) shows the cross-sectional structure of the HVIC that uses the divided high-side well structure. The high-side well is composed of 2 diffusion layers corresponding to 2 power supply voltages. A structure called p-isolation, which consists of low-concentration n-type and p-type diffusion layers, is used to separate the 2 diffusion layers from each other while the high breakdown voltage of the high-side well is maintained. This allows multiple power supply voltage circuits to be used for configuring a circuit for the high-side circuit in the same way as the low-side circuit. This improvement of the degree of design freedom has made it possible to realize a high-side circuit such as the protective circuit with an area reduced by approximately 20% from the previous product.

3.2 High breakdown voltage technology using area-saving self-shielding method

The level-shift circuit has the role of transmitting signals from the low-side circuit to the high-side circuit. And, when the high-side circuit is activated based on 400 V, for example, the level-shift circuit must convert signals based on the ground potential to those based on 400 V. This level-up function is realized by using high breakdown voltage n-type laterally diffused metal-oxide-semiconductor field-effect transistors (LDMOSFETs). Figure 4 shows the n-type LDMOSFETs of the 600-V breakdown voltage guaranteed HVIC chip.

(1) Conventional high breakdown voltage n-type LD-

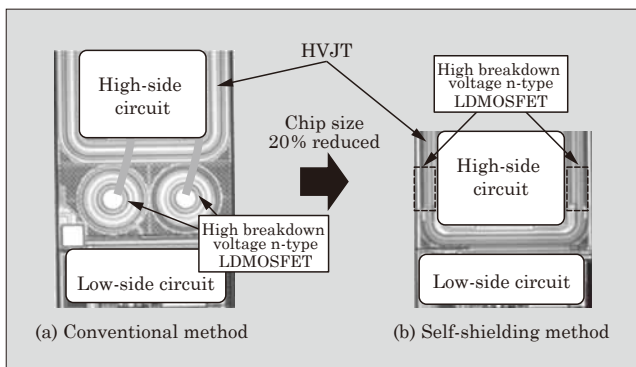


Fig.4 n-type LDMOSFETs of 600-V breakdown voltage guaranteed HVIC chip

MOSFET

Figure 4(a) shows the 600 V guaranteed HVIC chip with conventional high breakdown voltage n-type LDMOSFETs that use wire bonding. With the conventional HVIC, the high breakdown voltage n-type LDMOSFETs occupied a large portion of the area in the chip.

(2) High breakdown voltage n-type LDMOSFET of self-shielding type

In order to reduce the chip size, we have employed the self-shielding method that makes a high breakdown voltage possible with a reduced area. We have developed 600-V and 1,200-V guaranteed HVICs incorporating high breakdown voltage n-type LDMOSFETs. Figure 4(b) shows the 600-V guaranteed HVIC chip with the high breakdown voltage n-type LDMOSFETs using the self-shielding method. The self-shielding method integrates the high breakdown voltage n-type LDMOSFET and HVJT. It allows the device footprint to be reduced from the conventional method that requires independent high breakdown voltage n-type LDMOSFETs. This technology has meant we could successfully reduce the chip size by 20% from the previous product⁽³⁾.

3.3 Level-down high breakdown voltage device technology

(1) Level-down function

The prototyped 1,200-V breakdown voltage guaranteed HVIC is equipped with the level-down function for alarm signals. This allows alarm signals for notification of errors of the upper-arm IGBT chip, such as overheat and overcurrent, to be transmitted to the external microcomputer without requiring any external insulation device or level-shift circuit.

An alarm signal output from the abnormal detection circuit in the high-side circuit is converted into a signal based on the ground potential by the level-down function of the level-shift circuit to be transmitted to the microcomputer through the low-side circuit. While the level-up function of the level-shift circuit is realized by using the high breakdown voltage n-type LDMOSFET, the level-down function uses the high breakdown voltage p-type LDMOSFET.

(2) Device structure

Figure 5 shows the device structure of the 1,200-V breakdown voltage guaranteed p-type LDMOSFET that has been developed. As with the high breakdown voltage n-type LDMOSFET, the structure integrates the HVJT by using the self-shielding method. In order to guarantee the 1,200-V breakdown voltage, a high breakdown voltage structure called the double RESURF structure and resistive field plate (RFP) structure have been employed. The double RESURF structure consists of a 3-layer structure including the p-type substrate, n-type diffusion layer and p-type diffusion layer on the surface. The n-type diffusion layer and the p-type diffusion layer of the surface become

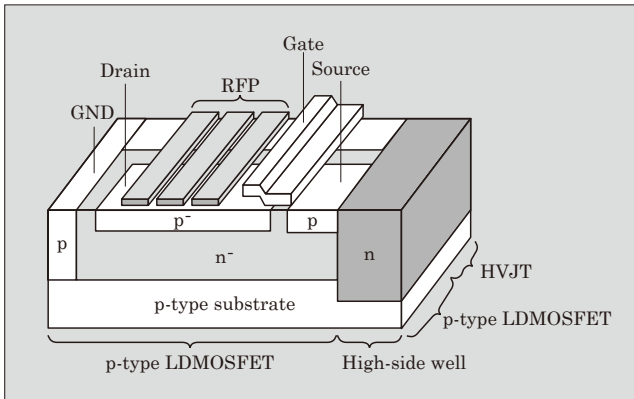


Fig.5 Device structure of 1,200-V breakdown voltage guaranteed p-type LDMOSFET

completely depleted when a high voltage is applied, which mitigates the electric field. The RFP structure has a polysilicon resistor with the electrodes at both ends connected to the high potential and ground potential provided in the high breakdown voltage region. The uniform potential gradient generated in the polysilicon resistor mitigates the electric field in the high breakdown voltage region. These structures are also used for the HVJT and high breakdown voltage n-type

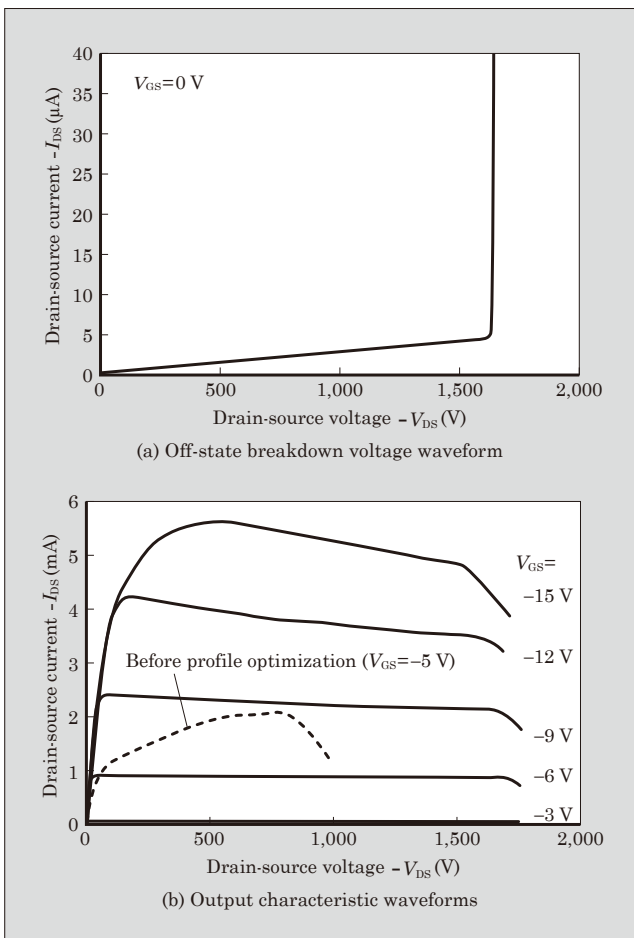


Fig.6 Characteristics of 1,200-V breakdown voltage guaranteed p-type LDMOSFET

LDMOSFET.

(3) Characteristics

Figure 6 shows the characteristics of the 1,200-V breakdown voltage guaranteed p-type LDMOSFET. Figure 6(a) shows an off-state breakdown voltage waveform. Although being a lateral device, it realizes an actual breakdown voltage of approximately 1,640 V. The leakage current observed in the region under 1,700 V is due to the current flowing in the RFP structure. By optimizing the resistance value of the RFP structure, a low leakage current of 5 μA or less at room temperature is achieved while the high breakdown voltage is maintained.

Figure 6(b) shows output characteristic waveforms. At the gate-source voltage of -15 V and drain-source voltage of -400 V , a drain current of 5.4 mA is obtained and the on-state breakdown voltage of approximately 1,500 V is realized. The dotted line in Fig. 6(b) shows the characteristic of the device prototyped in the initial stage of development. The current decrease observed around -800 V is due to the substrate leakage phenomenon recently discovered, which has limited the on-state breakdown voltage to -800 V . Fuji Electric has clarified the detailed mechanism of how this phenomenon is generated and used the results as the basis for optimizing the diffusion layer profile. This has led to a reduction in the substrate leakage phenomena to $-1,500\text{ V}$, which has resulted in the realization of a high on-state breakdown voltage.

4. Circuit Component Technology

4.1 High noise immunity level-shift circuit technology

(1) Conventional level-shift circuit

Figure 7 shows the conventional level-shift circuit for level-up shifting. It is composed of 2 sets of common-source amplifier circuits each using a level-shift resistor and a high breakdown voltage n-type LDMOSFET and the latch circuit in the high-side circuit.

By inputting a control signal from the low-side circuit to the common-source amplifier circuits, a voltage drop according to the control signal is generated in

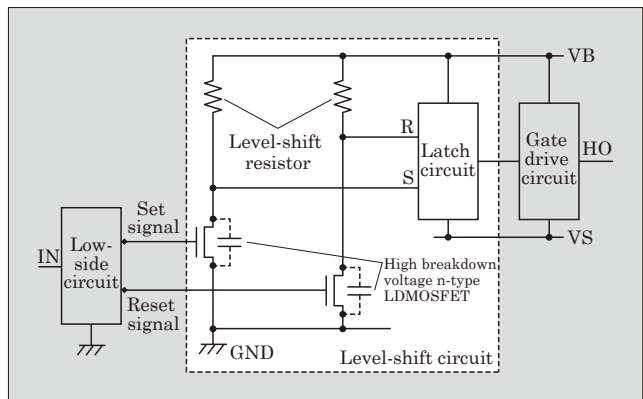


Fig.7 Conventional level-shift circuit for level-up shifting

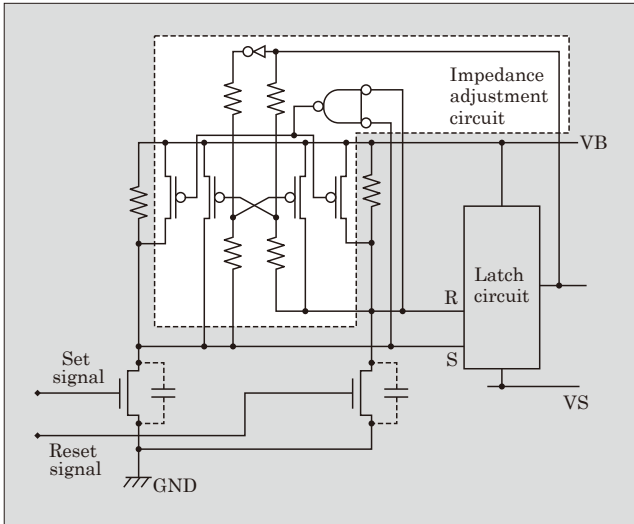


Fig.8 Impedance conversion type level-shift circuit

the level-shift resistors, which switches the output of the latch circuit. This operation transmits the signals from the low-side circuit to the high-side circuit.

(2) Circuit malfunction caused by dV/dt noise of conventional circuit

The conventional level-shift circuit had an issue of being susceptible to malfunctions due to dV/dt noise. The dV/dt noise is generated by rapid variations in the reference potential of the high-side circuit due to switching of the upper-arm IGBT. This dV/dt noise causes a noise current to flow in the level-shift resistors, which generates a voltage drop. And the output of the latch circuit and the output of the subsequent gate drive circuit might be inverted erroneously.

(3) Impedance conversion type level-shift circuit

Figure 8 shows the impedance conversion type level-shift circuit⁽⁴⁾ newly developed for improving the dV/dt noise immunity. The MOSFETs for impedance adjustment are connected in parallel with the level-shift resistors. This structure dynamically optimizes the impedance of the level-shift resistors according to the output status of the latch circuit. In this way, the voltage drop in the level-shift resistors due to the dV/dt noise current is controlled to prevent a malfunction.

4.2 Overheat/overcurrent protection circuit technology

The HVIC developed is equipped with an overheat/overcurrent protection circuit in the high-side well for protecting the upper-arm IGBT from overheating and overcurrent.

Overcurrent detection is achieved by monitoring the current flowing in the current sensing IGBT integrated in the IGBT chip. This is done by using the shunt resistor integrated in the HVIC. Overheat detection is achieved by monitoring the junction voltage

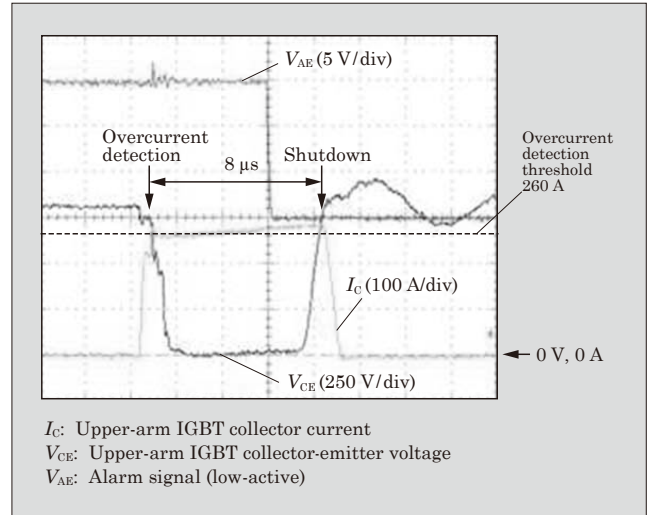


Fig.9 Overcurrent test waveforms of 1,200-V/100-A class IPM incorporating HVIC

of the temperature sensing diode.

Figure 9 shows overcurrent test waveforms of the 1,200-V/100-A class IPM that incorporates the HVIC prototyped. Immediately after an overcurrent exceeding 260 A flows in the upper-arm IGBT, an alarm signal indicating an overcurrent is output and the gate output of the HVIC is shut down. The time from the generation of the overcurrent to the shutdown is around 8 μ s, which indicates that high-speed response sufficient for protecting the IGBT is possible.

5. Postscript

This paper has described the new HVIC technology for IPMs that has been developed. This technology realizes enhanced functionality and improved reliability of IPMs and helps to improve the reliability and reduce the size of power conversion systems. We intend to continue developing power IC technologies that help enhance the value of power conversion systems.

References

- (1) Shimizu, N. et al. V-Series Intelligent Power Modules. FUJI ELECTRIC REVIEW. 2010, vol.56, no.2, p.60-64.
- (2) Yamaji, M. et al. 800 V Class HVIC Technology. FUJI ELECTRIC REVIEW. 2011, vol.57, no.3, p.96-102.
- (3) Yamaji, M. et al. A 600 V High-Voltage IC Technique With a New Self-Shielding Structure for High Noise Tolerance and Die Shrink. IEEE Trans. Electron Devices, 2015, vol.62, no.5, p.1524-1529.
- (4) Akahane, M. et al. A new level up shifter for HVICs with high noise tolerance. Proc. ECCE-ASIA, p.2302-2309.

3rd-Generation Direct Liquid Cooling Power Module for Automotive Applications

ARAI, Hirohisa* HIGUCHI, Keiichi* KOYAMA, Takahiro*

ABSTRACT

Fuji Electric has developed a 3rd-generation direct liquid cooling power module for hybrid and electric vehicles. The power module has a rated capacity of 750 V/800 A, which is designed for motor capacity of 100 kW. The market for automotive application based power modules has been requiring increased efficiency and module miniaturization. To meet these demands, we have improved exothermicity by adopting a water jacket for integrating the cooling fins and cover while also increasing the reliability of the solder, thus enabling the module to achieve continuous operation at 175 °C. Furthermore, we have miniaturized the power module by adopting an RC-IGBT that integrates IGBT and FWD.

1. Introduction

There is a need to reduce CO₂ emissions in order to prevent global warming, and hybrid electric vehicles (HEVs) and electric vehicles (EVs) driven by electric motors are raising expectations with their significant effectiveness for CO₂ reduction. Inverters used for HEVs and EVs are mounted in a limited space of vehicles and are required to offer high power and low loss. Accordingly, in-vehicle power modules, which are a major part of inverters, need to be made smaller and have improved efficiency.

Fuji Electric has developed the 3rd-generation direct liquid cooling power module for automotive applications as an in-vehicle power module for the next generation (see Fig. 1). This power module has achieved higher heat dissipation performance than the previous product by using an optimized flow channel design. In addition, it employs a cover-integrated aluminum water jacket and a flange structure for the refrigerant inlet and outlet⁽¹⁾. All the user has to do is to make sure that the refrigerant is run at the specified flow rate.

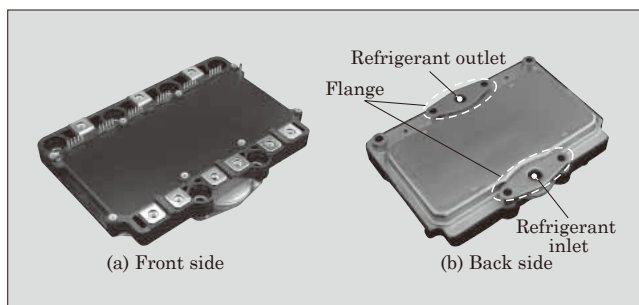


Fig.1 3rd-generation direct liquid cooling power module for automotive applications

Furthermore, the 7th-generation chip technology has been used for the insulated-gate bipolar transistor (IGBT) to reduce losses. Moreover, a reverse-conducting IGBT (RC-IGBT), which requires no free wheeling diode (FWD), has been used to make the module smaller.

2. Features

The following describes the features of the 3rd-generation direct liquid cooling power module for automotive applications. Table 1 lists the major specifications.

(a) Cooling technology to realize high heat dissipation performance

A water jacket integrating the liquid cooling fins and cover has been used to improve heat dissipation performance.

(b) Guaranteed continuous operation at 175°C

This feature has improved the reliability of the solder.

(c) Module size reduction

An RC-IGBT that integrates an IGBT and FWD has been applied.

Of these features, this paper describes the cooling technology and the RC-IGBT application technology.

Table 1 Major specifications of 3rd-generation direct liquid cooling power module for automotive applications

Item	Rating
Collector-emitter voltage	750 V
Rated current	800 A
Maximum operating temperature	175°C
Dimensions	162×116×24 (mm)
Mass	520 g

* Power Electronics Business Group, Fuji Electric Co., Ltd.

3. Cooling Technology to Realize High Heat Dissipation Performance

Inverters used for power control of vehicles are mounted in a limited space. This means they must be compact, have a high degree of freedom of the mounting method and undergo weight reduction and efficiency improvement for a better fuel efficiency. Power modules mounted in inverters also require size and weight reduction and efficiency improvement. We have successfully achieved a size and weight reduction of over 20% with each generation. With in-vehicle power modules, in particular, the heat dissipation performance has been improved by using a direct liquid cooling structure. The weight has also been reduced by using an aluminum cooler.

For improved heat dissipation performance, Fuji Electric has enhanced the heat dissipation performance of the aluminum cooling fins in the direct liquid cooling structure of the power module, achieving a 30% reduction in the thermal resistance.

3.1 Issue with cooling technology

Figure 2 shows a cross-sectional view of the conventional structure in the 2nd-generation aluminum direct liquid cooling intelligent power module (IPM). This structure has the module and heat sink directly joined by solder. The water jacket is independently designed by the user, and consequently the heat sink and water jacket need to be separate parts. A design that considers watertightness and tolerance is required in addition to flow channel design. For that reason, the material and thickness of the base must be carefully selected so that the device can resist buckling and deformation. This has been a factor causing an increase in the thermal resistance. The issue is to ensure both improved heat dissipation performance and high reliability of the aluminum direct liquid cooling structure. To solve this issue, we have developed an aluminum cooler integrating a heat sink and water jacket.

3.2 Third-generation cooling design technology

The heat dissipation performance of a power module can be represented by 2 factors: thermal resistance

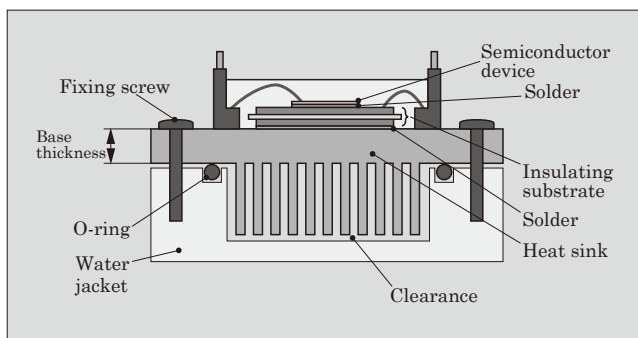


Fig.2 Cross-sectional view of conventional structure

and heat transfer coefficient. Thermal resistance and heat transfer coefficient have a relationship as represented by Equation (1).

$$h = \frac{1}{R_{th} \cdot A} \dots\dots\dots(1)$$

- h : Heat transfer coefficient [W/(m²·K)]
- R_{th} : Thermal resistance (K/W)
- A : Fin surface area (m²)

The heat transfer coefficient h represents the heat exchanging performance of the refrigerant and fins. To reduce the thermal resistance, it is effective to increase the heat exchanging performance of the fins. In addition, a higher flow speed on the fin surface provides a larger heat transfer coefficient representing the heat exchanging performance (Equation (2)).

$$h = \frac{0.664 k \times \frac{\eta C_p^{1/3}}{k} \times \frac{\rho L}{\eta} \times \frac{\rho v L^{1/2}}{\eta}}{L} \dots\dots\dots(2)$$

- h : Heat transfer coefficient [W/(m²·K)]
- k : Thermal conductivity [W/(m·K)]
- η : Refrigerant viscosity (Pa·s)
- C_p : Specific heat [J/(kg·K)]
- L : Characteristic fin length (m)
- ρ : Refrigerant density (kg/m³)
- v : Refrigerant flow speed (m/s)

With the conventional cooling structure that uses a sealant, the water jacket is designed and prepared by the user, and hence a clearance is needed between the fin ends and the water jacket. We made a trial calculation of the effect of this clearance on the heat dissipation performance by using a simplified model.

The fins were specified to be 1 mm thick, provided at intervals of 1 mm and have a height of 10 mm and we assumed the refrigerant would run evenly at 1 L/min into the refrigerant inlet. As a result of the trial calculation, it has been found that a larger clearance causes the thermal resistance to increase, which is undesirable. The refrigerant flows through places where the pressure resistance is low, causing it to flow out to the clearance with a large opening. Further, the flow speed between fins, which contributes to the heat dissipation performance, decreases. In addition, it can be expected that connecting modules in parallel will make the decrease of the refrigerant flow speed more significant. Eliminating the clearance by integrating the heat sink and water jacket is effective for increasing the speed of the refrigerant flow between fins to reduce the thermal resistance⁽²⁾.

Figure 3 shows a cross-sectional view of the new structure adopted for the 3rd-generation direct liquid cooling power module for automotive applications. With the new structure, the fin shape has been elaborated and the clearance has been eliminated by joining the water jacket and fin ends. In this way, the cooling structure can make use of the refrigerant more efficiently. Furthermore, the thickness of the part corre-

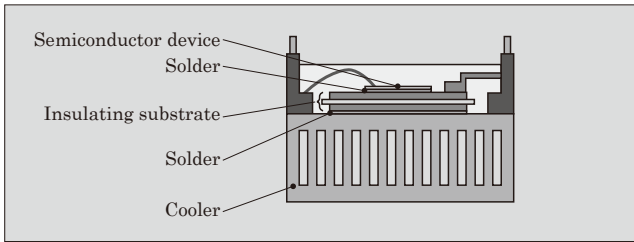


Fig.3 Cross-sectional view of new structure

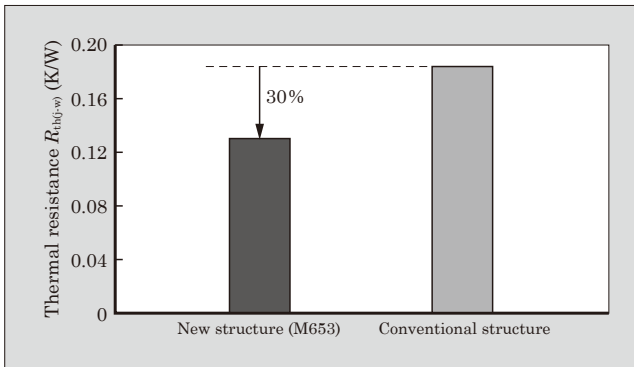


Fig.4 Thermal resistance

sponding to the base has been reduced.

Figure 4 shows the result of comparing thermal resistances. The new structure, which takes the refrigerant and heat transfer into consideration, has achieved a 30% reduction in thermal resistance from the conventional structure.

4. RC-IGBT Application Technology

In the development of 750-V/800-A class power modules for automotive applications, Fuji Electric has developed a 750-V withstand voltage RC-IGBT integrating an IGBT and FWD into one chip. The aim is to meet the requirements for a module size reduction in addition to loss reduction so as to improve the fuel efficiency. RC-IGBTs have been put to practical use as small-capacity chips for consumer electronics. However, as large-capacity chips required for automotive applications, the technological hurdle to overcome before loss can be reduced has been too high⁽³⁾. This section describes the design technology in RC-IGBT application and the effect of application.

4.1 RC-IGBT design technology

Figure 5 shows the schematic structure of the RC-IGBT. The structure uses a field stop (FS) IGBT as the basis and has the IGBT and FWD regions alternately laid out in stripes. Accordingly, integrating 2 chips into one makes it possible to reduce the invalid region (region called a guard ring for ensuring withstand voltage around the chip) to achieve a size reduction⁽⁴⁾. The heat generated during IGBT operation is dissipated also from the FWD section and vice versa. This has

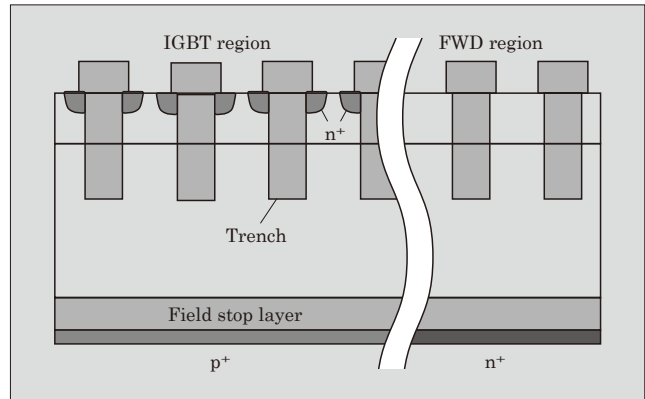


Fig.5 Schematic structure of RC-IGBT

the effect of reducing thermal resistance.

The current capacity of 750-V/800-A class power modules may vary depending on the motor capacity but they generally operate at the power supply voltage V_{cc} of 400 to 450 V and carrier frequency f_{sw} of 5 to 10 kHz. Figure 6 shows the loss generated during inverter operation when the 750-V withstand voltage RC-IGBT is employed to a power module.

If the switching frequency increases to 10 kHz, the switching losses (P_{on} , P_{off} , P_{rr}) also increase but the steady-state losses of the IGBT and FWD (P_{sat} , P_f) account for a large portion: 40%. In order to reduce the steady-state losses, the collector-emitter saturation voltage, which is a parameter determining the steady-state losses, has been minimized. This has been achieved by elaborating the design of the device surface including the trench pitch of the IGBT region⁽⁵⁾. In addition, a thinner chip allows for a greater reduction of the saturation voltage and forward voltage. Accordingly, we have thinned the wafer to the minimum thickness required for 750-V withstand voltage to reduce losses. The collector p-type layer of the IGBT and cathode n-type layer of the FWD have been formed on the back side of the same chip. The switching loss of the IGBT and FWD have a trade-off relationship with the steady-state loss. Therefore, carrier lifetime control has been provided so as to optimize the trade-

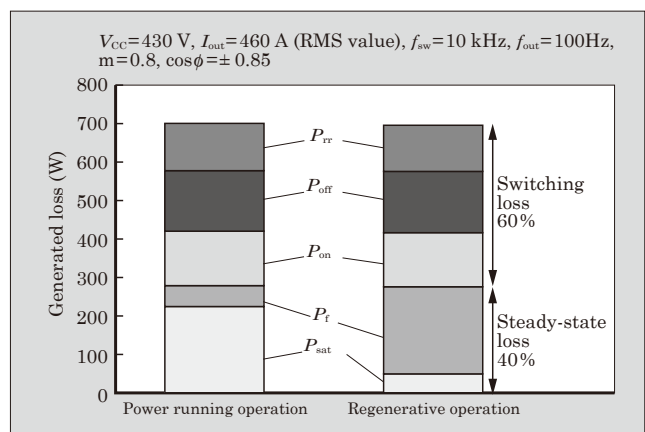


Fig.6 Loss generated during inverter operation

off.

4.2 Improvement of loss of RC-IGBT

This section describes the electrical characteristics of the RC-IGBT based on the same active area as that with the common combination of IGBT and FWD.

(1) IGBT characteristics

Figure 7 shows the saturation voltage output characteristics of the RC-IGBT and a common IGBT. The RC-IGBT realizes a lower saturation voltage than that of a common IGBT by wafer thinning and surface optimization. In addition, it has been reported that, with RC-IGBTs, conductivity modulation is unlikely to occur in the low saturation voltage region and snapback*1 is observed in the current-saturation voltage curve⁽⁶⁾. Accordingly, we have optimized the structures of the IGBT and FWD regions so that it is easier to carry out conductivity modulation and thus suppress snapback.

Figure 8 shows the turn-off characteristics of the RC-IGBT and a common IGBT. The RC-IGBT is shown to offer larger dv/dt at turn-off and a higher carrier emission rate as compared with a common

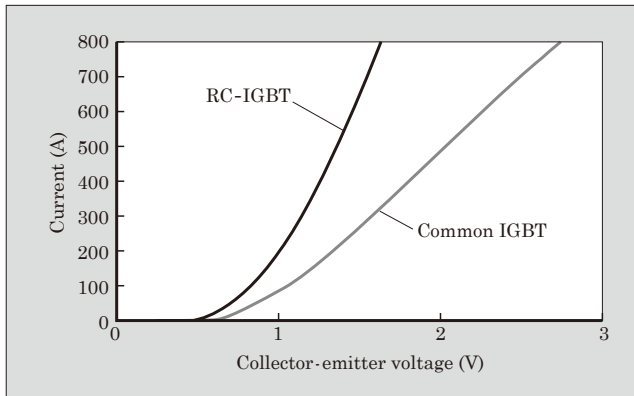


Fig.7 Saturation voltage output characteristics of IGBT

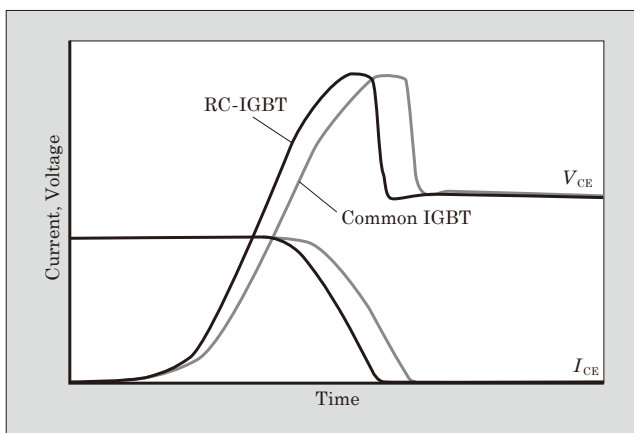


Fig.8 Turn-off characteristics of IGBT

*1: Snapback: Refers to a phenomenon in which the current and saturation voltage increase following a decrease in the process.

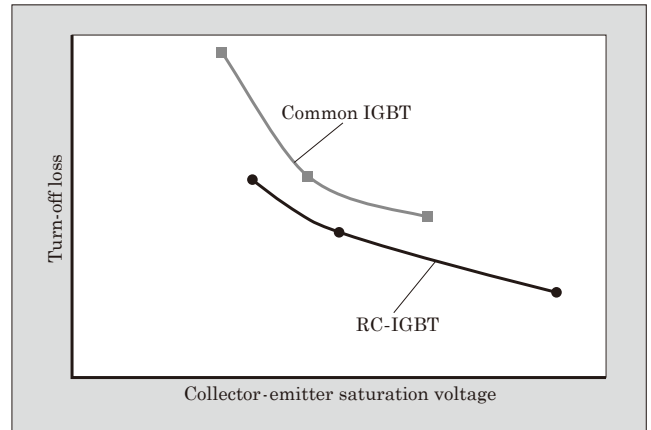


Fig.9 Trade-off characteristics of IGBT

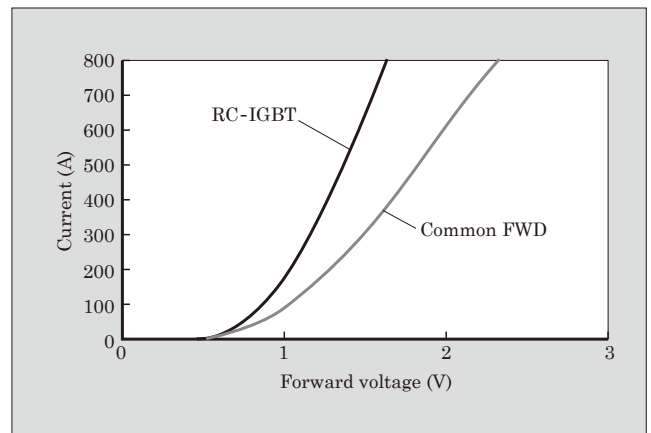


Fig.10 Forward output characteristics

IGBT. This is because the RC-IGBT has the collector short-circuited, in which the p-type layer (IGBT region) and n-type layer (FWD region) are short-circuited on the back side. This causes electrons to be emitted at turn-off not only from the collector p-type layer but also from the cathode n-type layer in the adjacent FWD region. As a result, the RC-IGBT offers a lower turn-off loss than a common IGBT. With the RC-IGBT, the turn-off loss can be reduced as compared with that of a common IGBT even if adjustment is made in the direction to improve the steady-state losses (to reduce the saturation voltage). This has significantly improved the trade-off characteristics (see Fig. 9).

(2) FWD characteristics

Figure 10 shows the forward output characteristics of the RC-IGBT and a common FWD. As with the steady-state losses of the IGBT, with the RC-IGBT, wafer thinning and optimization of the surface structure have led to a reduction in the forward voltage drop from that of a common FWD.

4.3 Heat dissipation performance

The RC-IGBT has the IGBT and FWD integrated to reduce the chip and module areas. In addition, with the RC-IGBT, the heat generated from the FWD re-

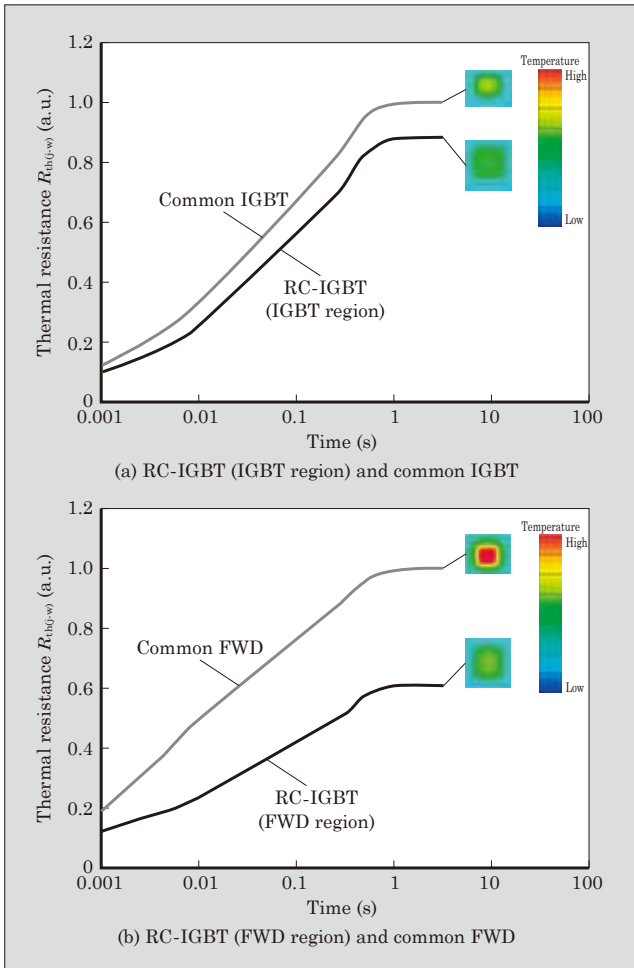


Fig.11 Thermal resistance comparison based on the same active area

gion is released also through the IGBT region. This significantly reduces the thermal resistance from that of a common FWD. We have assumed a module with a direct liquid cooling structure and compared thermal resistance between the RC-IGBT and a common IGBT/FWD based on the same active area (see Fig. 11). With the RC-IGBT, the thermal resistance of the IGBT region is shown to be 12% lower than that of a common IGBT and the thermal resistance of the FWD region 40% lower than that of a common FWD⁽¹⁾.

4.4 Performance achieved

Figure 12 shows the result of calculating the loss generated and temperature during inverter operation for a common IGBT/FWD, an RC-IGBT with the same active area and an RC-IGBT with the area reduced by 30%.

The saturation voltage, forward voltage and turn-off loss have been reduced from those of a common IGBT/FWD. This makes it possible for the RC-IGBT to achieve a reduction in the power loss of over 20% during inverter operation. In addition to loss reduction, the maximum chip temperature can be reduced by about 28 °C thanks to the excellent heat dissipation

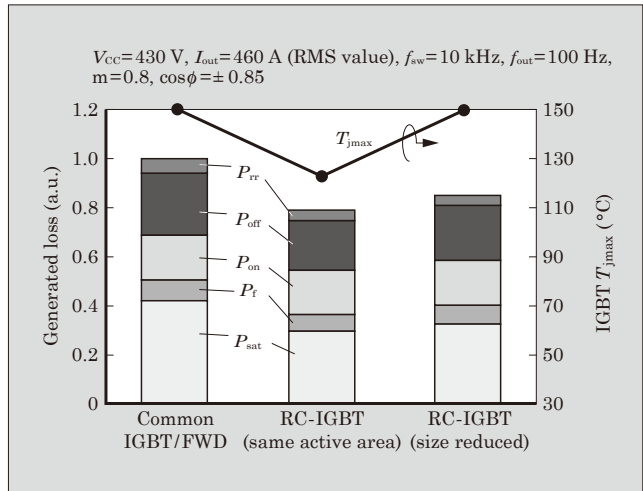


Fig.12 Result of calculating loss generated and temperature during inverter operation

performance. The chip size of a module depends on the maximum temperature during operation. Therefore, this result indicates that, with the RC-IGBT, operation of an inverter with the same rating can be achieved with a smaller chip size than a common IGBT/FWD. The RC-IGBT with the area reduced by 30% offers about the same temperature as that of a common IGBT/FWD and the module area can be reduced by 15%.

5. Postscript

This paper has described the 3rd-generation direct liquid cooling power module for automotive applications. The high heat dissipation performance and continuous operation at 175 °C have been achieved. Moreover, by applying an RC-IGBT, the volume per current capacity has been successfully reduced by 40% from that of the previous product.

In the future, we intend to implement further technological innovations to develop compact, low-loss products.

References

- (1) Higuchi, K. et al. "An intelligent power module with high accuracy control system". Proceedings of PCIM Europe2014, May 20-22, Nuremberg, p.39-46.
- (2) Gohara, H. et al. "Next-gen IGBT module structure for hybrid vehicle with high cooling performance and high temperature operation". Proceedings of PCIM Europe 2014, May 20-22, Nuremberg, p.1187-1194.
- (3) Takahashi, K. et al. "New Reverse- Conducting IGBT (1,200 V) with Revolutionary Compact Package". Proceedings of ISPSDS 2014, p.131-134.
- (4) Laska, T. et al. "The Field Stop IGBT (FS IGBT) -A New Power Device Concept with a Great improvement Potential". Proceedings of ISPSD 2000, p.355-358.
- (5) Momota, S. et al. Plated Chip for Hybrid Vehicles. FUJI ELECTRIC REVIEW. 2008, vol.54, no.2, p.49-51.

- (6) M, Rahimo. et al. "The Bi- mode Insulated Gate Transistor (BIGT) A Potential Technology for Higher power Applications". Proceedings of ISPSD 2009, p.283-286.



Packaging Technology of 3rd-Generation Power Module for Automotive Applications

GOHARA, Hiromichi* TAMAI, Yuta* YAMADA, Takafumi*

ABSTRACT

The development and popularization of hybrid and electric vehicles has been accelerating in recent years. These new vehicles demand miniaturized, light-weight and higher-output power module in order to improve fuel efficiency. Fuji Electric has developed high heat dissipating cooling unit for direct water-cooled structures, an ultrasonic bonding technology for electrodes and copper terminal, and new long-life solder that applies both precipitation strengthening and solid-solution strengthening. By applying these technologies, the 3rd-generation power modules for automotive applications that utilize RC-IGBT dies achieve greater reliability, about 30% smaller footprint and thinner structure compared to the previous generation.

1. Introduction

Recently, advances in energy saving and the tightening of regulations on CO₂ emissions have prompted the automobile industry to accelerate the development and dissemination of hybrid electric vehicles (HEVs) and electric vehicles (EVs). Inverters used for power control in HEVs and EVs are mounted in a limited space and they need to undergo a weight reduction and efficiency improvement for a low fuel consumption. In addition, power modules that accommodate the output of batteries and motors are demanded.

In order to meet these demands, Fuji Electric has been working on technological development for power modules that can achieve a significant improvement in power density. As in-vehicle aluminum direct liquid-cooling power modules, we have developed products improving the power density by over 20% in each generation with the 1st generation in 2012 and 2nd generation in 2015⁽¹⁾. To achieve even higher power density and higher power output, we have employed a reverse-conducting insulated-gate bipolar transistor (RC-IGBT) chip, which integrates an insulated-gate bipolar transistor (IGBT) and free wheeling diode (FWD), in the 3rd-generation aluminum direct liquid-cooling module and successfully realized higher heat dissipation by using cooling fins. This has allowed for a substantial footprint reduction of 30% and made it possible to have thinner devices by optimizing the cooling structure.

This paper describes the packaging technology of the 3rd-generation power module for automotive, specifically the design technologies for a high heat dissipation cooler, ultrasonic bonding and improved solder life expectancy.

2. Design Technology for High Heat Dissipation Cooler

Thermo-fluid analysis technology is used for the design of the direct liquid-cooling structure and we have carried out simulations with the flow of coolant and heat transfer taken into account. We have turned our attention to the dependency of the cooler performance on the coolant flow speed and designed a structure with the focus on how the limited amount of coolant should flow.

2.1 Design accuracy improvement

In thermal design using simulation, the accuracy of analysis is directly linked to the accuracy of the design. Accordingly, we have improved the analysis accuracy by feeding the measurement results of temperature distribution by means of an infrared camera back to the simulation and optimizing the mesh conditions. As a result of product design using an optimization model that uses this improvement effect, we have achieved an error of less than 10% in the thermal resistance between the design values and measurement results and made it possible to design a product by using a simulation.

2.2 Design issues and performance improvement

The coolers of the direct liquid-cooling structure are categorized into 2 types of structures: an open structure with the heat sink and water jacket separated from each other, or a closed structure with the water jacket integrated with heat sink⁽¹⁾⁽²⁾. Figure 1 shows a simulation model for evaluating the chip temperature characteristics.

The open structure uses an O-ring and gasket to tightly seal the heat sink and water jacket. For that reason, a clearance must be provided between the fin

* Corporate R&D Headquarters, Fuji Electric Co., Ltd.

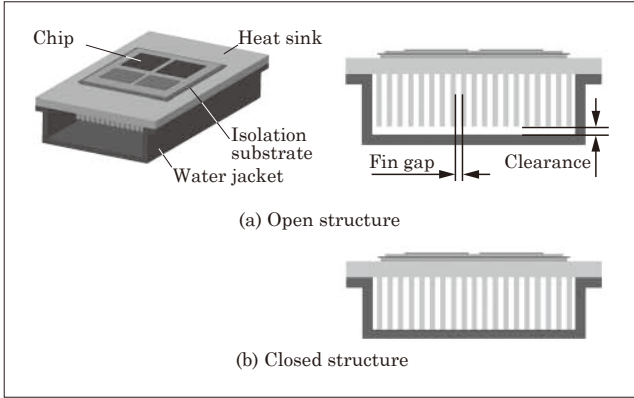


Fig.1 Simulation models

ends and water jacket in view of the respective design tolerances and thermal deformations. This clearance increases the cross section of the flow channel through which the coolant flows. When the clearance is larger than the fin gaps, the flow resistance between the fins increases relatively and the flow speed between the fins decrease, resulting in a deteriorated cooling performance. Meanwhile, the closed structure has no clearance as in the open structure due to the water jacket joined with a heat sink.

Figure 2 shows the speed distribution of cross section obtained by thermal fluid simulation. While the

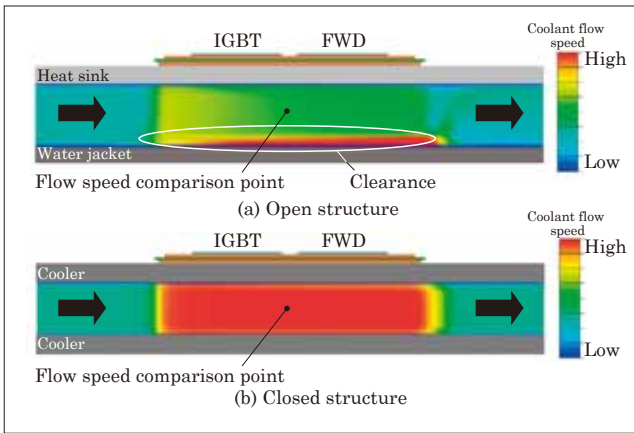


Fig.2 Cross-section flow speed distribution

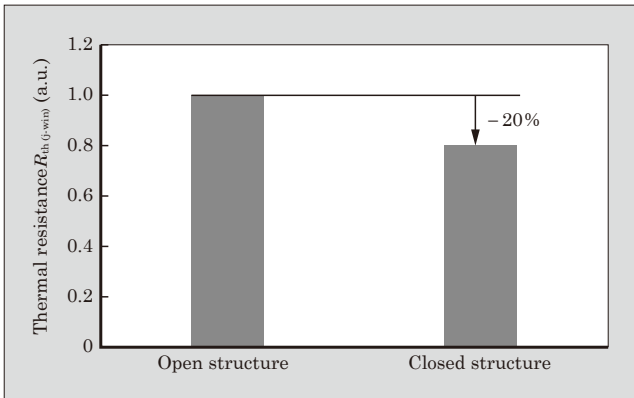


Fig.3 Thermal resistance

open structure has the coolant flowing out to the clearance, in the closed structure, the flow speed distribution is nearly equalized and the flow speed increases by about twice because of no clearance. Figure 3 shows a comparison of the thermal resistance between the open and closed structures. The closed structure exhibits the thermal resistance reduced by 20% because of no clearance and the effect of thinning of the heat sink as compared with the open structure⁽³⁾.

3. Design Technology for Ultrasonic Welding

The increase in the current density of automotive power modules requires wiring in the power module to increase the wiring capacity and reduce the space.

Figure 4 shows a comparison between the conventional aluminum wire structure, copper wire structure and copper terminal structure. The copper terminals molded in the terminal case and the copper pattern on the insulated substrate are connected together by wiring. Copper terminal wiring in which ultrasonic bonding is applied to this wiring that carries the principal current has achieved a current capacity approximately 3.5 times as large as that of the conventional aluminum wire structure, leading to a reduction in the footprint.

3.1 Ultrasonic bonding of terminals in power modules

Figure 5 shows overview of ultrasonic bonding. Ultrasonic bonding is solid-phase diffusion bonding that the surface oxide films on the bonding surfaces

Wiring technology	Aluminum wire bonding	Copper wire bonding	Copper terminal ultrasonic welding
Cross section structure			
External appearance			
Current-carrying capacity	Medium (1.0)	High (1.7)	Very high (3.5)

Fig.4 Wiring structure

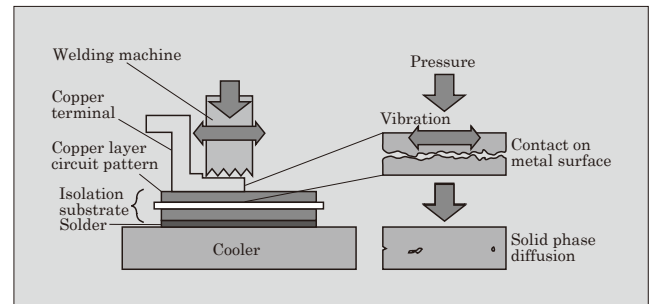


Fig.5 Overview of ultrasonic welding

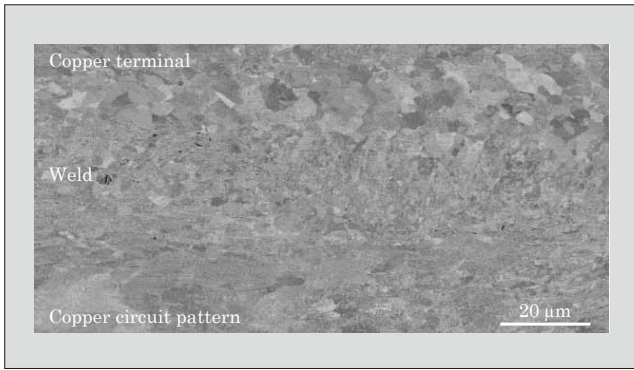


Fig.6 SEM image of cross-section of ultrasonic welding

are broken by ultrasonic vibration and pressure, and metal surfaces are contacted and diffused each other. It allows base materials to be bonded at a temperature lower than the melting point. By using this ultrasonic bonding, copper terminals are directly bonded to the copper circuit pattern on the insulated substrate circuit without any bonding material.

We observed the cross section of a copper terminal, bond and copper circuit pattern to investigate the metallographic structure of ultrasonic bonds with scanning electron microscope (SEM) (see Fig. 6). Ultrasonic bonds have a finer structure (crystal grain size) than that of the copper terminals because of work hardening. The strength depends on the crystal grain size and a smaller grain size tends to exhibit higher strength. Different crystal grain sizes may cause less accurate lifetime predictions. Accordingly, due to the fineness of the crystal grain size of ultrasonic bonds, we used test pieces in the shape of a terminal similar to the actual device to establish a lifetime prediction technology for metal solid-phase diffusion bonds of copper terminals.

3.2 Fatigue testing and study on life expectancy prediction

We built samples for lifetime prediction of ultrasonic welded joint of copper terminals (see Fig. 7) and conducted the cyclic fatigue tests. First, we determined the deformation of the applied product by using full-model thermal-stress analysis to find out the direction of load generated on copper terminals. Under the condition of forced displacement in agreement with this direction of the load, we conducted a stress simulation and fatigue testing by using an element model.

From the result of the stress simulation, we have determined that stress is generated locally on the copper terminal bond interface. In addition, from the result of fatigue testing on the copper terminal, it has been observed that cracks propagate along the bond interface due to the stress generated, causing a fracture at the bond interface. Based on the fact that the origins of the fracture coincide in both the results of simulation and fatigue test, we have used the results to study the method of lifetime prediction.

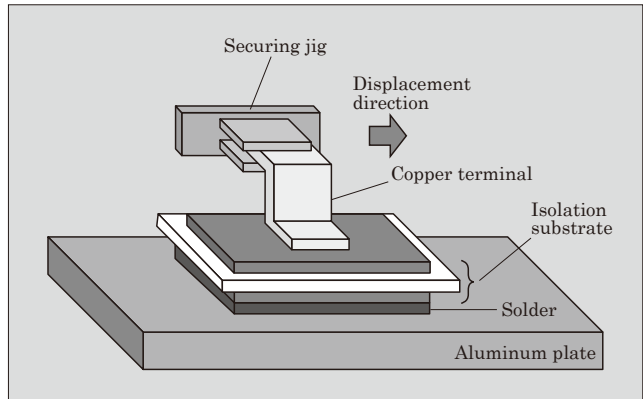


Fig.7 Model to evaluate life expectancy of copper terminals

In fatigue lifetime curves of copper terminals and copper test pieces obtained in this research, the vertical axis indicates the total strain calculated from the stress analysis, and the horizontal axis indicates the number of test repetitions at the time of terminal fracture (see Fig. 8). The copper test pieces are made from an ordinary copper material (C1100, 1/2He) machined into a dumbbell shape. The fatigue lifetime curves of these copper terminals are generally used for lifetime prediction. However, in this case, they cannot be used for the lifetime prediction of ultrasonic-welded copper terminals because the slope of fatigue lifetime curves of the ultrasonic-welded copper terminals and the copper test pieces do not coincide. The reason for the slope difference between the ultrasonic-welded copper terminals and the copper test pieces is assumed that the crystal grain sizes of the ultrasonic-welded interface are different from those of the copper test pieces⁽⁴⁾. Accordingly, we conducted fatigue testing with the actual product to verify the validity of the fatigue lifetime curve of the element model.

Consequently, the result of a lifetime evaluation of the actual product nearly matched with the fatigue lifetime curve of the ultrasonic-welded copper terminal, A fracture mode in which fracture occurs at the bond interface can be replicated by using samples for

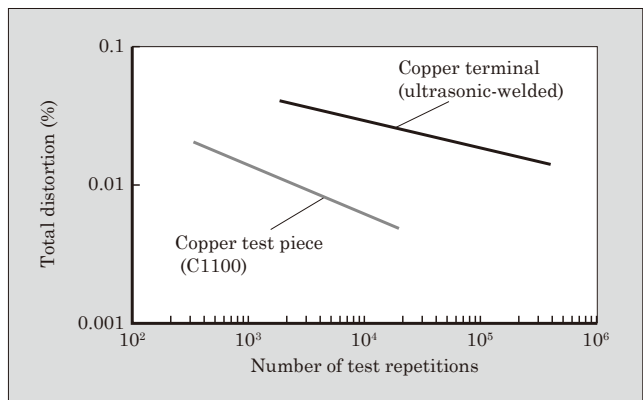


Fig.8 Fatigue life expectancy curves of copper test pieces and copper terminals

copper terminal lifetime evaluation. From these results, it was determined that this methodology can be used to estimate the lifetime evaluation of ultrasonic welded copper terminal.

4. Design Technology for Solder Lifetime

A module can achieve higher power density by increasing the guaranteed operation temperature. Meanwhile, expanding the operation temperature range of a module causes a reduction in the lifetime of the solder under the insulated substrate which is the most likely to fail in the power module. With conventional solders, changes of the physical properties due to thermal aging*1 reduce the strength, leading to a shorter life expectancy. In addition, in solders affected by this thermal aging, the lifetime designs based on the Coffin-Manson Law are difficult to achieve the required accuracy. In order to deal with these issues, we have developed a new solder that suppresses the strength reduction under high-temperature conditions.

A test piece as shown in Fig. 9 was used to conduct a comparative evaluation between the conventional and new solders. As the evaluation results, Fig. 10, Fig. 11 and Fig. 12 show the crack development speeds, SEM images of the solder structure before and after the thermal cycle test and the tensile strength after heating at 175 °C for 1,000 hours.

(1) Conventional solder

With the conventional solder (Sn-Ag solder), the crack propagation speed increases at an accelerated pace as the temperature change ΔT increases in thermal cycling (see Fig. 10). An SEM image of the solder structure shows that, before the test, intermetallic compounds precipitate at the grain boundaries of the Sn matrix and form a network (see Fig. 11). After the test, this network of intermetallic compounds has disappeared, Ag_3Sn phase has precipitated and the Sn matrix has become coarser. Because thermal cycling

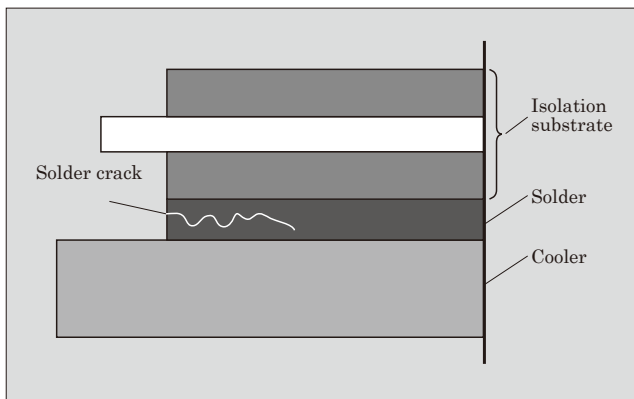


Fig.9 Test piece construction

*1: Aging: Refers to a phenomenon in which metal properties (e.g. hardness) change over time.

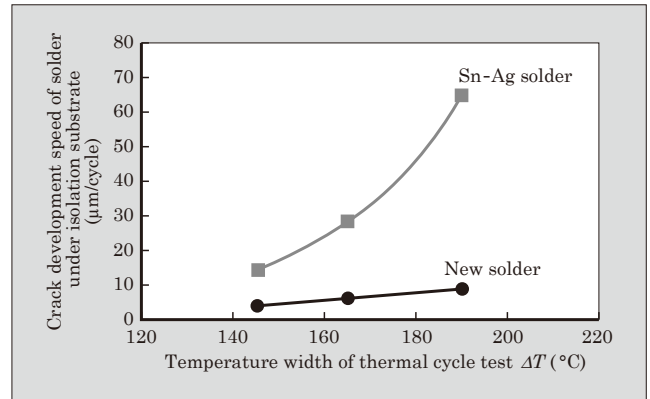


Fig.10 Solder crack development speeds

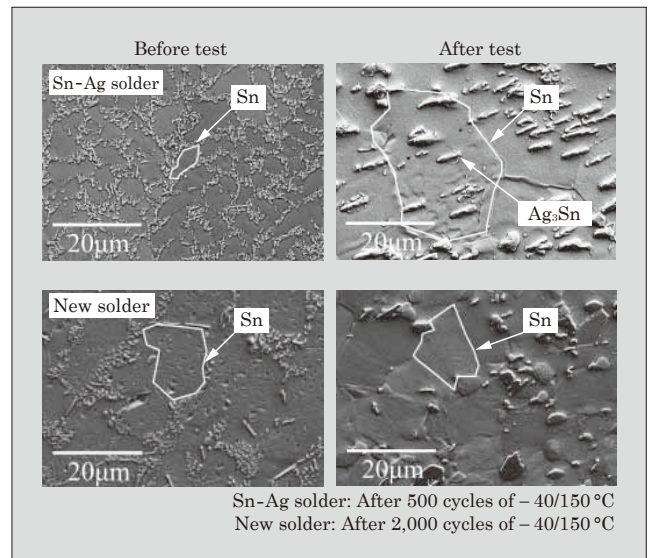


Fig.11 SEM images of solder structures

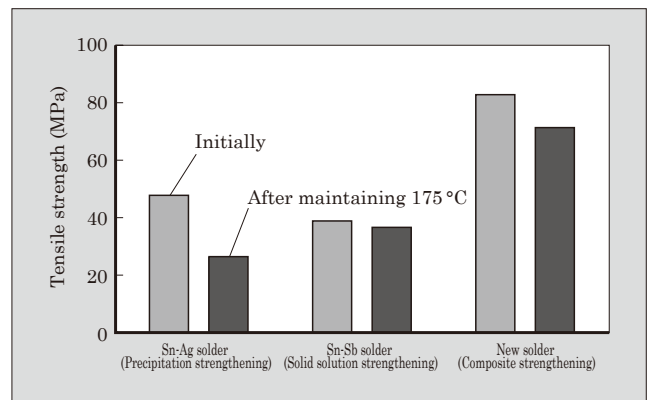


Fig.12 Tensile strengths of solders

causes thermal deterioration of the solder structure and it leads to reduce the strength, the crack propagation speed increases as ΔT increases⁽⁴⁾.

(2) New solder

While the Sn matrix of Sn-Ag solder becomes coarser as ΔT increases, with Sn-Sb solder, coarsening of the Sn matrix is suppressed by solid solution of Sb. The new solder is strengthened by conventional precip-

itation strengthening in addition to this solid solution strengthening. Therefore, the strength reduction of the new solder under high temperature is less than those of Sn-Ag solder and their high strength is maintained (see Fig. 12).

The crack propagation speed of the new solder exhibits small change as ΔT increases and the increase is not at an accelerated pace but almost linear. For this reason, predict the lifetime prediction technology based on the Coffin-Manson Law can be applied and an improvement of the prediction accuracy and reliability can be achieved at the same time. With the new solder, the crack propagation speed is less than one fifth of that of Sn-Ag solder even if ΔT increases to 190 °C, which allows for a further operating temperature increase (see Fig. 10).

5. Postscript

This paper has described the packaging technology for the 3rd-generation power module for automotive applications. By improving the consistency of the re-

sults between the actual device and simulation, highly accurate design technology has been developed. We intend to work on improving elemental technologies and reducing product development periods to take advantage by using this design technology.

References

- (1) Gohara, H. et al. Packaging Technology of IPMs for Hybrid Vehicles. FUJI ELECTRIC REVIEW. 2014, vol.59, no.4, p.235-240.
- (2) Gohara, H. et al. "Next-gen IGBT module structure for hybrid vehicle with high cooling performance and high temperature operation" Proceedings of PCIM Europe 2014, May 20-22, Nuremberg, p.1187-1194.
- (3) Nishimura, Y. et al. "Power Module Technology for automotive power-electronics" Proceedings of APE 2015, April 14-15, Paris.
- (4) Momose, F. et al. "The New High Power Density Package Technology for the 7th Generation IGBT Module". Proceedings of PCIM Europe 2015, May 19-21, Nuremberg p.772-778.



RC-IGBT for Automotive Applications

YOSHIDA, Soichi* NOGUCHI, Seiji* MUKAI, Koji*

ABSTRACT

The number of hybrid electric vehicles and electric vehicles in use on the road has been increasing as a measure to reduce CO₂ emissions in order to protect the environment from phenomena such as global warming. In order to improve fuel efficiency for these types of vehicles, they need to reduce loss in mounted semiconductor devices, while also decreasing the size of the inverter. To meet these needs, Fuji Electric has been working to develop an RC-IGBT that integrates an IGBT and FWD into one chip. Moreover, we have optimized trench gate spacing, a field stop layer and lifetime control for the RC-IGBT for automotive applications. As a result, the inverter achieves an about 20% reduction in generated loss during the operation compared to using conventional RC-IGBTs for automotive applications.

1. Introduction

There has been an increase in global attention to environmental protection such as preventing global warming. Accompanying this, hybrid electric vehicles (HEVs), which use both an engine and motor to reduce CO₂ emissions, and electric vehicles (EVs), which are driven by a motor only, have been spreading.

There are also demands for automotive semiconductor devices that dissipate less power and smaller inverters to improve the fuel economy of HEVs and EVs. In response to this, Fuji Electric has developed a reverse conducting insulated-gate bipolar transistor (RC-IGBT) that integrates an IGBT and a free wheeling diode (FWD) on a single chip. RC-IGBTs have already been in practical use in small-capacity chips for home appliances. Their practical use in large-capacity chips for automotive applications, however, was difficult because of the high technological hurdle—for making them dissipate less power⁽¹⁾. Fuji Electric overcame this technological hurdle and developed a low-loss chip using an RC-IGBT for mild hybrid vehicles⁽²⁾⁽³⁾.

We improved this RC-IGBT for mild hybrid vehicles (conventional RC-IGBT) and have developed an RC-IGBT for automotive applications that dissipates less power (improved RC-IGBT). This improved RC-IGBT can support various motor drive methods including full hybrid and mild hybrid.

2. Challenges and Measures

Figure 1 shows a schematic structure of an RC-IGBT. The RC-IGBT for an HEV has a structure that uses a field stop (FS) IGBT⁽⁴⁾ mass-produced by Fuji

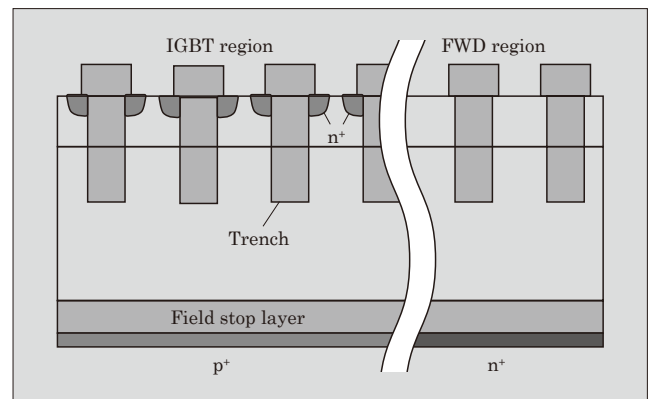


Fig. 1 Schematic structure of an RC-IGBT

Electric as a base. On it, IGBT units and FWD units are arranged alternately in stripes. The sizes of the IGBT units and FWD units are determined so that their characteristics are not negatively affected by mutual interference. Figure 2 shows a constitutive example of the losses generated in the inverter for an HEV. The generated losses are determined by the switching loss generated when a current is turned on/off (P_{on} , P_{off} , P_{rr}) and the steady-state loss of IGBT

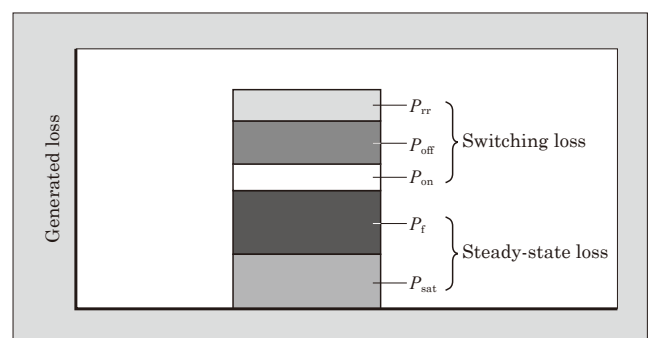


Fig. 2 Example of losses generated in an inverter

* Electronic Devices Business Group, Fuji Electric Co., Ltd.

and FWD (P_{sat} , P_f). Improving the fuel economy of HEVs requires a reduction in the steady-state loss. Consequently, we designed an improved RC-IGBT with the main objective of reducing the steady-state loss. When the loss is reduced, we can suppress the heat generated from the device and make the device smaller. As a result, IGBT modules and inverters can be miniaturized. The following describes the improvements made to the RC-IGBT.

(1) Reducing the conduction loss through the use of IE effect

It is known that the conduction loss of an IGBT can be reduced through a phenomenon called as injection enhanced (IE) effect. With this, a small number of carriers (holes for the case of n-channel IGBT) are accumulated in the drift layer and this reduces the saturation voltage $V_{\text{CE(sat)}}$. One effective way to enhance the IE effect is to make the spacing of the trench gates formed on the device surface smaller. For the improved RC-IGBT, we made improvements to enhance the IE effect. That is we optimized the trench gate spacing compared with conventional RC-IGBTs.

(2) Reducing the conduction loss by using a thinner wafer

It is desirable to make the chip as thin as possible. Because the thinner the chip is, the more the saturation voltage and forward voltage can be suppressed to reduce the steady-state loss. The thinner the chip is, however, the more often oscillation occurs when IGBT and FWD switch off. Consequently, we could not make the wafer sufficiently thin for the conventional RC-IGBT. But for the improved RC-IGBT, we were able to suppress the oscillation of both IGBT and FWD by optimizing the FS layer. This has led us to make the wafer sufficiently thin and achieve reduction in the conduction loss. The optimization of the FS layer also allowed for a reduction in the collector-emitter leak current I_{CES} at elevated temperatures.

(3) Reducing the conduction loss and switching loss through lifetime control

We added an improvement to optimize lifetime control, and reduce the conduction loss of IGBTs and switching loss of FWDs. This also reduced I_{CES} at elevated temperatures, resulting in better high-temperature characteristics.

3. Loss Characteristics

3.1 Electrical characteristics

RC-IGBT is a device made by integrating an IGBT and an FWD on a single chip. This section describes the IGBT characteristics and FWD characteristics of the RC-IGBTs respectively.

(1) IGBT characteristics

Figure 3 shows the IGBT saturation voltage output characteristics. The saturation voltage of the improved RC-IGBT is lower than that of the conventional RC-IGBT due to the measures described in Chapter 2.

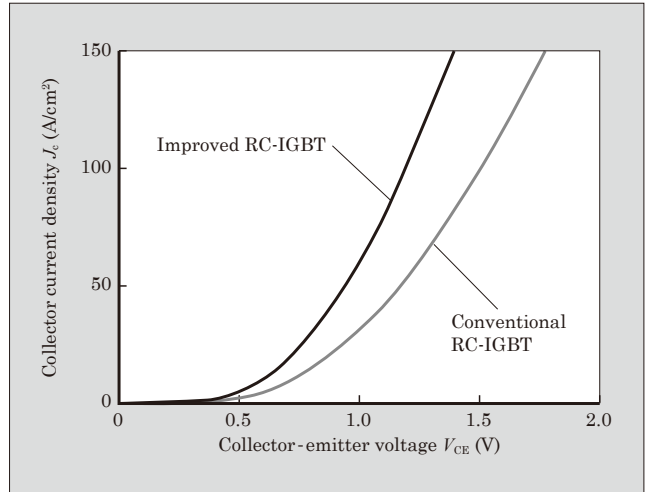


Fig. 3 IGBT Saturation voltage output characteristics

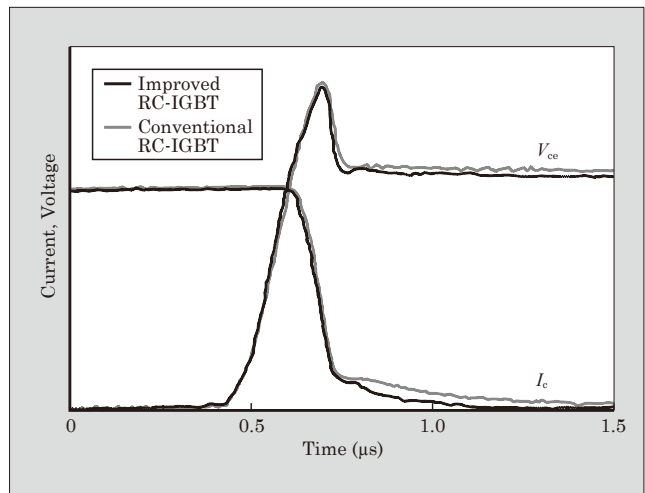


Fig. 4 IGBT turn-off characteristics

Figure 4 shows the IGBT turn-off characteristics. When the waveforms are compared, we notice that the tail current of the improved RC-IGBT at the time of turn-off is smaller and the turn-off time is also shorter than those of the conventional RC-IGBT. This indicates less turn-off loss. This is a result of the reduced saturation voltage and the optimized impurity concentration of the collector at the improved RC-IGBT. The oscillation at turn-off has also been suppressed by optimizing the collector section and FS layer.

As a result, we succeeded in significantly improving the trade-off characteristics of the improved RC-IGBT (see Fig. 5). This was achieved by taking advantage of its ability to maintain a low saturation voltage even when the turn-off loss is reduced. The values of the turn-off loss in the graph have been normalized with the loss of the conventional RC-IGBT being assumed as 1.

Figure 6 shows the I_{CES} characteristics under a high-temperature condition of the case (package) temperature $T_C = 150^\circ\text{C}$. As a result of optimizing the FS layer and lifetime control, the value of the improved

RC-IGBT has decreased to 30% or less of the conventional RC-IGBT.

(2) FWD characteristics

Figure 7 shows the FWD forward characteristics.

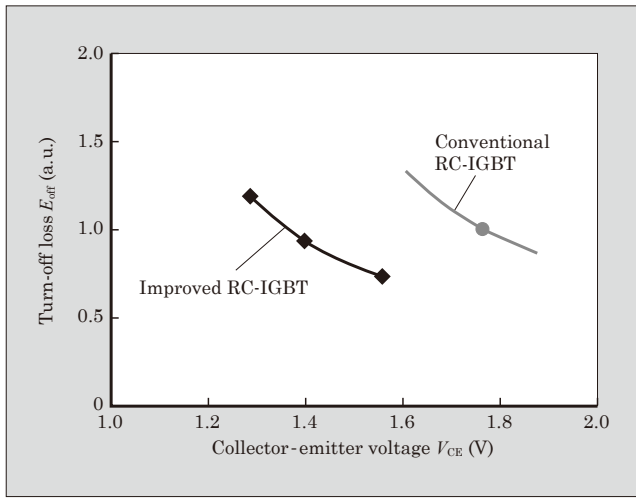


Fig. 5 IGBT trade-off characteristics

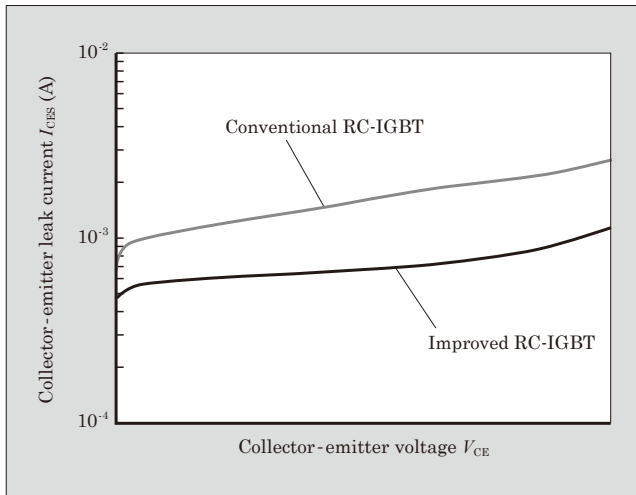


Fig. 6 I_{CES} characteristics ($T_c = 150\text{ }^\circ\text{C}$)

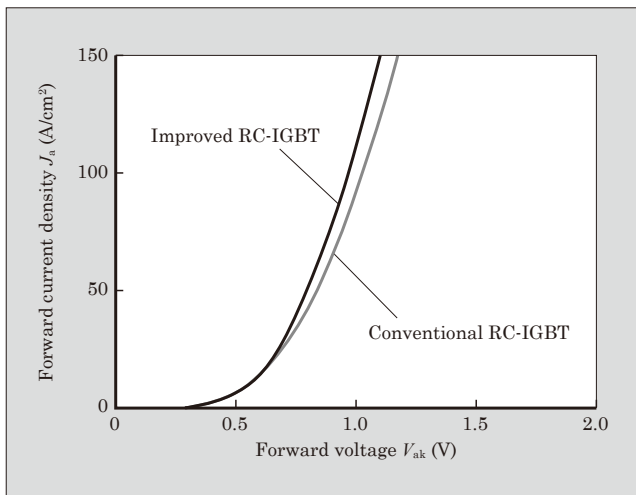


Fig. 7 FWD forward characteristics

The improved RC-IGBT has reduced the drop in the forward voltage compared with the conventional RC-IGBT due to the effect of using a thinner wafer.

Figure 8 shows the switching waveforms during reverse recovery operation. For the improved RC-IGBT, we have optimized the FS layer and lifetime control. This means that even the use of a thinner wafer can provide a soft-recovery characteristics to reduce the re-

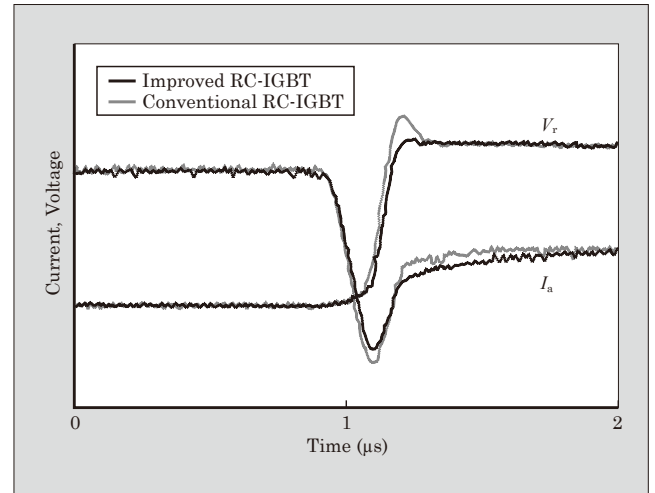
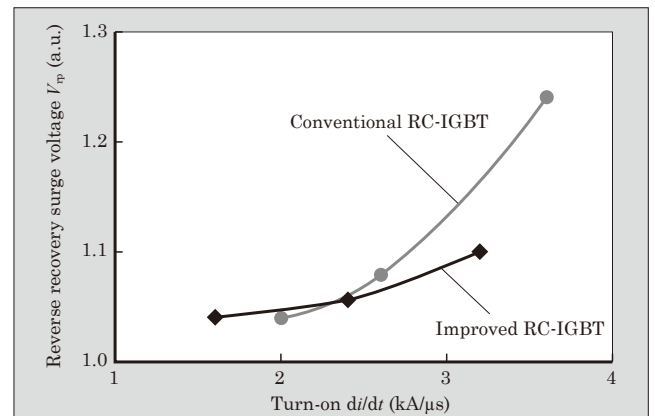
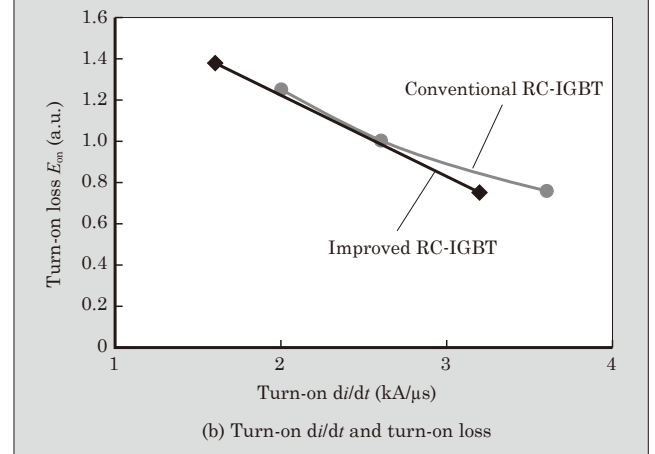


Fig. 8 Switching waveforms during reverse recovery operation



(a) Turn-on di/dt and reverse recovery surge voltage



(b) Turn-on di/dt and turn-on loss

Fig. 9 Characteristics at turn-on

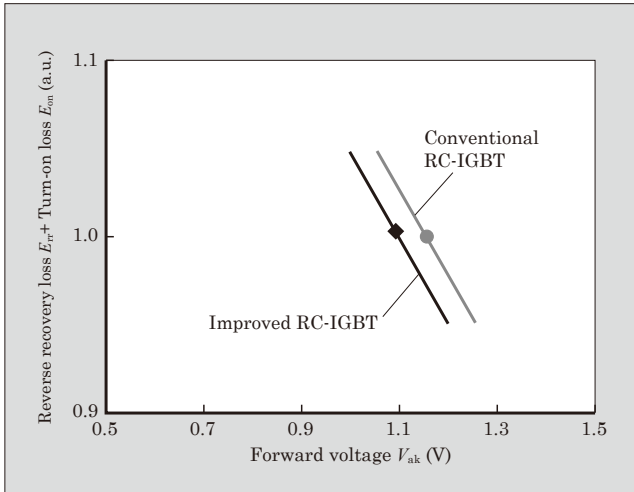


Fig. 10 FWD trade-off characteristics

verse recovery surge voltage.

Figure 9 shows the characteristics at turn-on. The reverse recovery surge voltage shown in Fig. 9(a) is a value normalized with the power supply voltage being assumed as 1. As the relationships between turn-on di/dt and reverse recovery surge voltage and between turn-on di/dt and turn-on loss show, the improved RC-IGBT can suppress the reverse recovery surge voltage at high-speed turn-on. A faster switching speed at turn-on can effectively improve the turn-on loss. Hence, we have reduced the turn-on loss at high-speed switching by driving with a lower gate resistance.

Figure 10 shows the trade-off characteristics between the forward voltage and reverse recovery loss + turn-on loss in an FWD. Reverse recovery characteristic and turn-on characteristic are phenomena that occur in the same transient period, and the amounts of them are determined by the difference in the voltage sharing ratio. For this reason, the Y-axis shows the added loss of two amounts. The values have been normalized with the loss in the conventional RC-IGBT being assumed as 1. The trade-off characteristic has been improved by reducing the loss that resulted from the drop in the forward voltage. We achieved this by using a thinner wafer and by reducing the turn-on loss through faster switching.

3.2 Loss generated during inverter operation

The losses generated during the inverter operation of the RC-IGBTs are shown in Fig. 11. A driving mode of a typical HEV is assumed as the condition for the loss calculation. With the improved RC-IGBT, the gen-

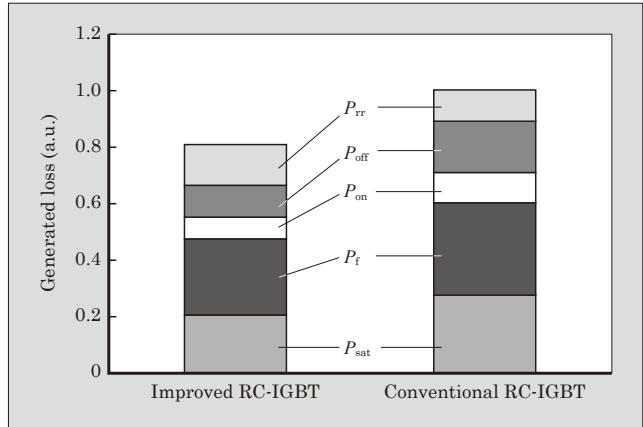


Fig. 11 Loss generated during inverter operation

erated loss has been reduced by about 20% compared with the conventional RC-IGBT. This was due to the significant improvement of the IGBT characteristics. Reducing the generated loss leads to a decrease in the temperature caused by heat generated in the device. This enables the use of smaller devices, raising expectations for a lower inverter volume.

4. Postscript

This paper described RC-IGBTs for automotive applications. From the need to solve environmental problems, major developments of hybrid electric vehicles and electric vehicles are expected to continue also in the future. The miniaturization of in-vehicle equipment seems to be one of the important challenges, and RC-IGBTs can be highly effective in achieving this objective. We will continue contributing to the improvement of devices and the development of devices using new materials.

References

- (1) Takahashi, K. et al. "New Reverse-Conducting IGBT (1200V) with Revolutionary Compact Package". Proceedings of ISPSD 2014, p.131-134.
- (2) Noguchi, S. et al. RC-IGBT for Mild Hybrid Electric Vehicles. FUJI ELECTRIC REVIEW. 2014, vol.60, no.4, p.224-227.
- (3) Higuchi, K. et al. "New standard 800 A/750 V IGBT Module technology for Automotive Applications". Proceedings of PCIM Europe 2015, p.1137.
- (4) Laska, T. et al. "The Field Stop IGBT (FS IGBT)- A New Power Device Concept with a Great Improvement Potential". Proceedings of ISPSD 2000, p.355-358.

Relative Pressure Sensor for Automobile Fuel Tanks

KATO, Hirofumi* ASHINO, Kimihiro* SATO, Eisuke*

ABSTRACT

In recent years, there has been increasing regulation to reduce the environmental burden of automobiles. One example of such regulation is the requirement to detect fuel leaks in the United States. Fuji Electric has developed a relative pressure sensor for automobile fuel tanks capable of being directly mounted to a pipe inside the engine room. The sensor is used for controlling vaporized fuel exhaust suppression devices that recover vaporized fuel to incinerate it in the cylinder. Based on our 6th-generation compact pressure sensor technology, we have successfully improved resistance to vaporized fuel, enhanced protective functions and reinforced EMC to both ensure durability and achieve high-precision detection.

1. Introduction

Automobiles have come to be demanded strictly to reduce the environmental burden in addition to the provision of safety and comfort. One example is the obligatory requirement to detect fuel leaks by on-board diagnostics (OBD) regulations in the U.S. market. Emission of vaporized fuel into the atmosphere may cause danger of ignition due to static electricity or change into air pollutants through chemical reactions. These regulations are intended for suppressing leaks of vaporized fuel in order to reduce danger and environmental burden. For the purpose of meeting these regulations, Fuji Electric developed the relative pressure sensor that is capable of detecting the differential pressure between 2 points with one chip for detecting fuel tank leaks⁽¹⁾, which was commercialized in 2007.

For controlling fuel evaporative gas emission control units that return vaporized fuel to the cylinder to incinerate it, we have now developed a relative pressure sensor for detecting the automobile fuel tank pressure (tank pressure sensor) that can be directly mounted in the evaporation line*¹.

2. Features of Tank Pressure Sensor

Figure 1 shows the external appearance of the tank pressure sensor. Conventionally, the basic concept of Fuji Electric's pressure sensors has been to maximize the features of the one chip technology for providing compact, high-reliability products. Tank pressure sensors incorporate additional new features as described below.

(1) Improvement of resistance to vaporized fuel

Vaporized fuel may cause deterioration of the die

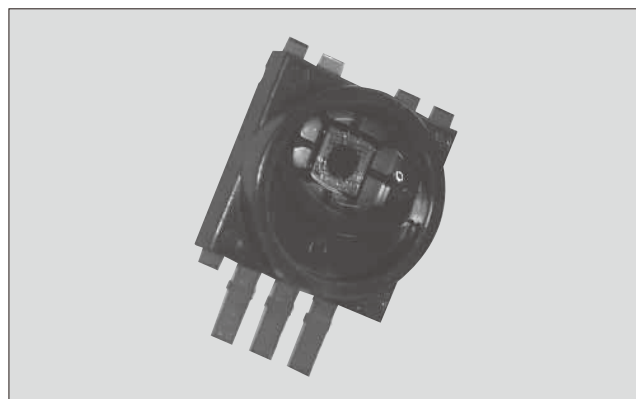


Fig.1 Appearance of tank pressure sensor

bond material that constitute pressure sensors and destruction failure arising from it. The tank pressure sensor has achieved resistance to pressure media containing vaporized fuel while ensuring the conventional high reliability by selecting a material not degenerated by contact with vaporized fuel.

(2) Improvement of protective function

The tank pressure sensor, which is mounted inside an engine, is a relative pressure sensor that detects the differential pressure between the atmospheric pressure and the fuel pipe pressure, which subjects it to the constant risk of foreign objects from inside and outside the automobile. To deal with this problem, we have covered the both pressure receiving sides with a gelatinous protective material to achieve protection of the sensor chip from foreign objects and high-precision pressure detection at the same time. In addition, an air filter is provided on the atmospheric pressure receiving side of the sensor cell. Thus, the protective

*1: Evaporation line: Fuel carrying line for returning vaporized fuel to a cylinder to incinerate it

* Electronic Devices Business Group, Fuji Electric Co., Ltd.

function against foreign objects from outside is further improved.

(3) Enhancement of EMC

Recently, various electronic devices are mounted on automobiles and enhancement of electromagnetic compatibility (EMC) against the electromagnetic noise from those devices is needed. We have followed the conventional technology of integrating the sensing unit, signal processing unit and surge protection device into one chip. Additionally, we have mounted a chip capacitor on it to achieve the improvement of EMC while maintaining the same size.

3. Structure of Tank Pressure Sensor

3.1 Pressure detection unit

Figure 2 shows the pressure detection unit. Part of the Si substrate is processed into a thin film by etching to form a diaphragm. On top of the diaphragm, piezoresistors made of diffusion line are provided and 4 piezoresistors constitute a Wheatstone bridge. The 3D etching technology at which Fuji Electric excels has made it possible to form a diaphragm in a round and isotropic shape with high precision, which ensures high sensitivity and resistance to excessive pressure.

Diaphragm pressure sensors detect the deformation generated by the pressure difference (differential pressure) between the 2 sides of the diaphragm as the resistance change of the piezoresistor formed on the surface. Conventional pressure sensors of Fuji Electric are absolute pressure sensors that measure the pressure with reference to a vacuum and the vacuum chamber is provided by bonding the glass spacer using the electrostatic bonding process. Meanwhile, the tank pressure sensor is provided with a pressure medium inlet port in the glass spacer to allow measurement of the differential pressure with the atmospheric pressure.

3.2 Signal processing circuit

Figure 3 shows the basic configuration of the signal processing circuit. The signal processing circuit uses the technology for the 6th-generation low pressure sensor (100 to 400 kPa)⁽²⁾ developed in FY2010 for mass production. The circuit has been optimized for

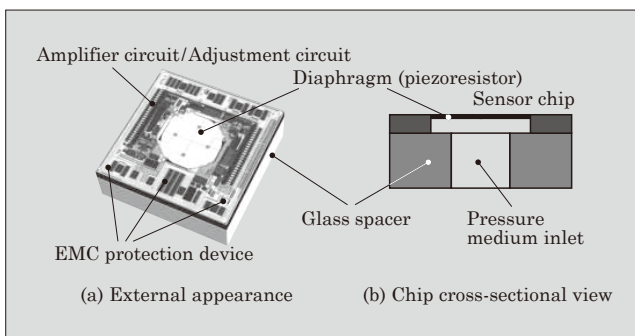


Fig.2 Pressure detection unit

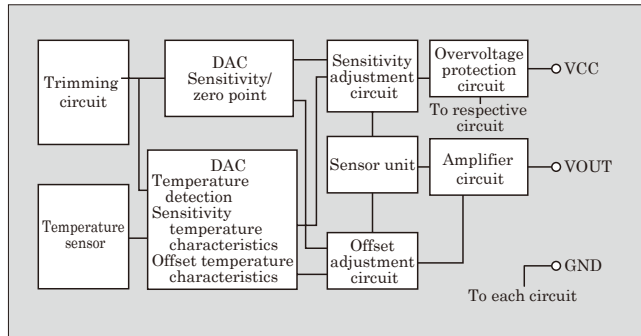


Fig.3 Basic configuration of signal processing circuit

applying it to the tank pressure (-80 to $+5$ kPa). It is equipped with a high-precision amplifier that amplifies the voltage signal output from the Wheatstone bridge and adjustment circuit that corrects the sensor characteristics. It is also equipped with protective devices for protecting the internal circuit from surge waveforms generated by the engine control system of the automobile, static electricity in the assembly process and electromagnetic waves from outside.

3.3 Structure of sensor cell

Figure 4 shows the cross-sectional structures of the sensor cells in the pressure sensor (absolute pressure sensor) and tank pressure sensor (relative pressure sensor). Both sensor cells integrate a chip capacitor for improving EMC. The tank pressure sensor is provided with a pressure inlet port to measure relative pressure. In addition, for ensuring easy replacement with conventional products, dimensions at many points are designed to be the same.

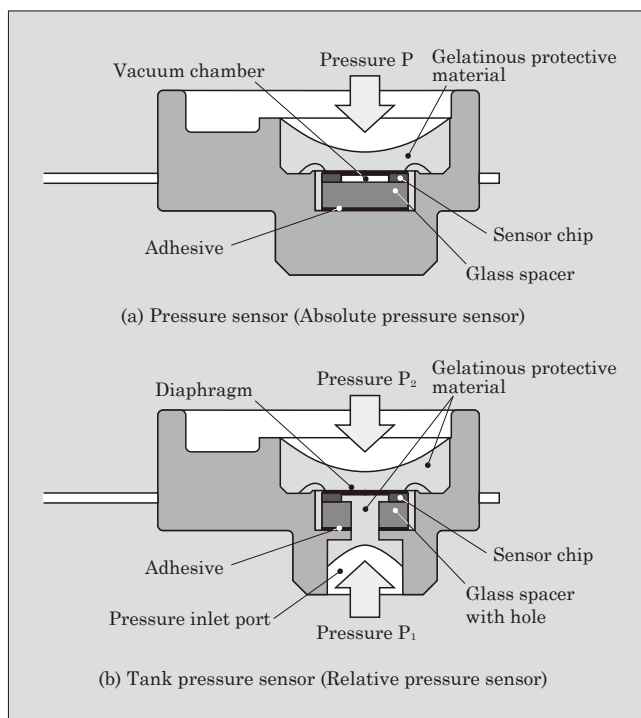


Fig.4 Cross-sectional structure of sensor cell

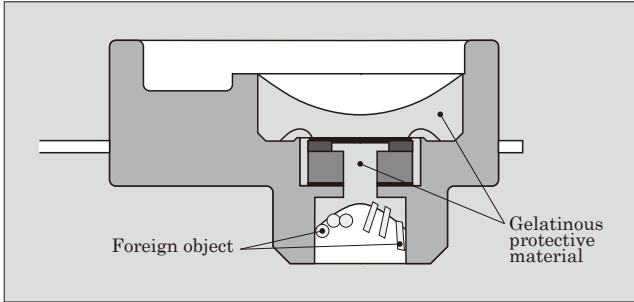


Fig.5 Protection from foreign objects by gelatinous protective material

Fuji Electric's sensor cells have the sensor chip attached by using an adhesive. The tank pressure sensor measures the pressure inside the fuel tank. Therefore, a new adhesive with resistance to fuel has been selected.

Furthermore, as shown in Fig. 5, the entire sensor chip is covered entirely with a gelatinous protective material, which allows for detection of the applied pressure while protecting the internal structure including the sensor chip and wire bonding against foreign objects from outside. This has achieved both higher precision of pressure detection and longer life of the product.

3.4 Outer housing structure

Figure 6 shows the cross-sectional structure of the package, which fixes the sensor cell with a resin adhesive to the resin housing case of a direct mount type. This structure can be directly mounted in the evaporation line and we call this an "outer housing structure." The resin adhesive used to fix the sensor cell also has the role of ensuring airtightness and prevents the air containing vaporized fuel entering through the pressure inlet port from flowing into the atmospheric pressure side. The pressure sensor uses an O-ring with the temperature characteristics taken into account for

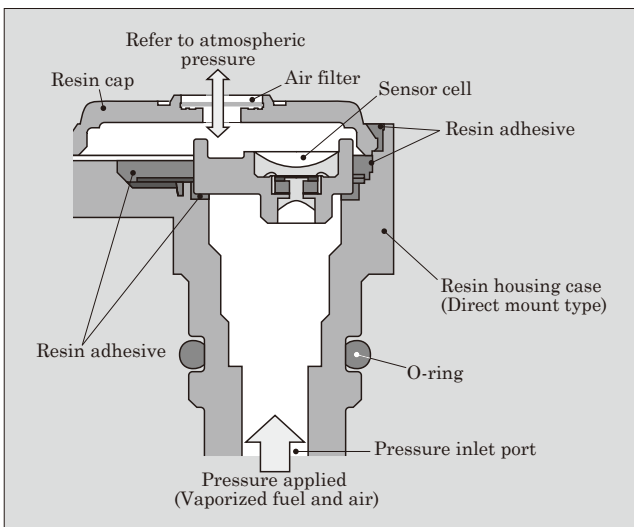


Fig.6 Outer housing structure

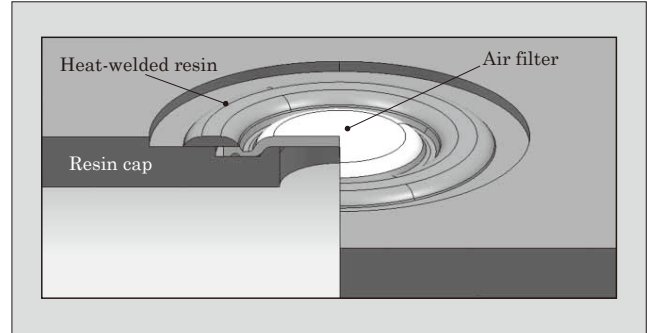


Fig.7 Cross-sectional view of air filter mounting part

ensuring the airtightness at the pressure port. On the other hand, the tank pressure sensor employs an O-ring with resistance to fuel, which has been confirmed to show durability against 32 types of fuel in various countries around the world as well as the temperature characteristics.

This outer housing can be mounted directly in an engine and accommodates various pressure ranges by changing of the internal sensor cell. In addition, the same shape of the outer housing allows the layout around the mounting and the wire harness part to be used without change as they are.

One side of the tank pressure sensor is open to the atmospheric pressure. The pressure sensor is mounted on the pipe in the engine room, so that the sensor is exposed to dust, rainwater, and muddy water, In an environment that allows easy entry of foreign objects and moisture, failure due to wire disconnection and short circuits resulting from such environmental conditions and sensor characteristic errors due to dew condensation and freezing are assumed to occur.

In order to address this problem, we use the gelatinous protective material for the sensor cell to protect the internal structure and provide a resin cap equipped with an air filter for the outer housing. Figure 7 shows a cross-sectional view of the air filter mounting part.

This filter is mounted on the resin cap by heat welding to ensure durability higher than the maximum load to the air filter assumed for use in the engine room. As durability of the filter itself, it satisfies the dust resistance (IP6KX) and water resistance (IPX9K) regulation according to the road vehicle IP test standards specified by the ISO 20653 and JIS D 5020.

This air filter has a property to allow passage of air only and not dust of large particle sizes or liquid. This filter is also water repellent and waterproof. By providing air filter on the resin cap at the atmospheric pressure side, stable pressure detection is realized in an engine room, which is exposed to the entry of dust and muddy water, without being affected by contamination.

3.5 Application to EGR and DPF

By using the sensor chip and sensor cell structure

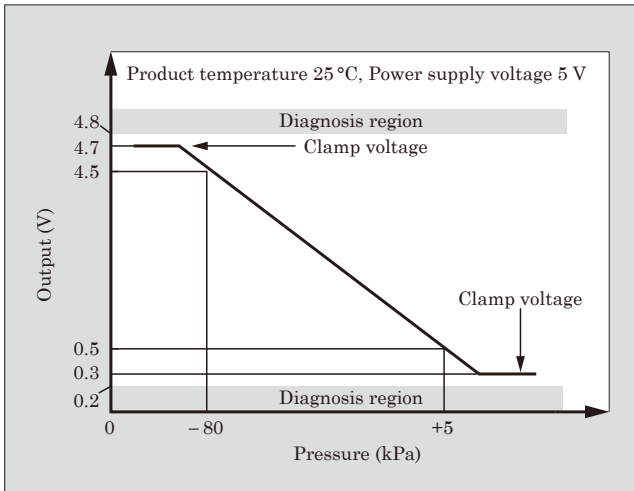


Fig.8 Pressure-output characteristics of tank pressure sensor

Table 1 Basic specifications of tank pressure sensor

Item	Unit	Specification
Operating temperature range	°C	-40 to +135
Operating pressure range*1	kPa	-80 to +5
Sensor output range	V	0.5 to 4.5
Interface	kΩ	Pull up = 300 or Pull down = 100
Clamp region	V	< 0.3 / > 4.7
Diagnosis region*2	V	< 0.2 / > 4.8
Sink current	mA	1
Source current	mA	0.1
Pressure error	%F.S.	< 1.5
Temperature error	times	2.0 (max.)
Applicable EMC standard		ISO 11452-2 (100 V/m, CW, 10 kHz to 2 GHz) ISO 11452-4 (100 m, CW, 1 to 400 MHz) ISO 7637 (Level IV)
Applicable fuel		Gasoline Diesel gass oil (DIN EN 590) E10, E25, E85, M15, M100 Biodiesel (DIN EN 14214)
Dust resistance of filter		IP6KX
Water resistance of filter		IPX9K
Terminal assign		(Output) - (GND) - (Power supply)

*1: Value for pressure applied through pressure inlet port

*2: Detection of power supply line disconnection and output line disconnection

and outer housing structure described previously, the tank pressure sensor has achieved high durability and high-precision detection performance less affected by air containing vaporized fuel or foreign objects. In addition, combining anti-corrosion treatment of the sensor chip allows them to be used for other applications with even harsher installation environment such as exhaust gas recirculation (EGR) or diesel particulate filter (DPF), which suppress generation and emission of environmentally hazardous substances including suspended particulate matters (SPMs), nitrogen oxides and sulfur oxides in exhaust gas.

4. Specifications

Figure 8 shows the pressure-output characteristics and Table 1 shows the basic specifications of the tank pressure sensor. The product is configured to have an outer housing structure.

5. Postscript

This paper has described the relative pressure sensor for automobile fuel tanks. In the future, the needs of pressure sensors for automotive applications are expected to further increase along with the environmental and safety regulations in various countries of the world. Meanwhile, the requirements for accuracy, quality, environmental friendliness and cost of products are estimated to be more stringent than ever. In order to meet these requirements, Fuji Electric have an intention of committing to constant development of the world's top-level technologies and products appreciated by customers.

References

- (1) Uematsu, K. et al. Development of Pressure Sensor Cell for Fuel Leak Detection. FUJI ELECTRIC REVIEW. 2007, vol.53, no.3, p.77-80.
- (2) Nishikawa, M. et al. 6th Generation Small Pressure Sensor. FUJI ELECTRIC REVIEW. 2011, vol.57, no.3, p.103-107.

PWM Power Supply Control IC “FA8B00 Series” Capable of Handling Peak Loads

MATSUMOTO, Shinji* YAMANE, Hiroki* YABUZAKI, Jun*

ABSTRACT

In recent years, the notebook computer and inkjet printer market requires increasing the maximum output power for new CPUs and motor drive loads. To meet these requirements, Fuji Electric has developed the “FA8B00 Series” of pulse width modulation (PWM) power supply control IC capable of handling Peak loads. This IC can increase the switching frequency up to 130 kHz in accordance with rise in FB terminal voltage, allowing it to increase the maximum output power of a power supply without increasing the volume of a transformer. Furthermore, the IC comes equipped with an expansion function for switching frequency jitter that enables it to achieve low EMI noise characteristics even against varying loads.

1. Introduction

In recent years, it has become increasingly important to work toward the creation of a low-carbon society in order to mitigate the severity of global warming. There is currently a need for the various electronic equipment that support our modern society to operate at high efficiency, low standby power and low noise levels from the view point of increased energy savings and electromagnetic compatibility (EMC). Fuji Electric has been working to meet these social needs by developing and releasing into the market a number of high efficiency current-mode power supply control ICs that come equipped with built-in low standby power functions. At the same time, the notebook computer and inkjet printer industries have been requiring a peak power output capable of corresponding to new CPUs and motor drive loads.

Fuji Electric has developed the peak-power compatible “FA8B00 Series” pulse width modulation (PWM) power supply control IC as a current-mode PWM control IC capable of meeting these social and industrial needs.

2. Product Overview

Figure 1 shows the external appearance of the FA8B00 Series. This IC is characterized by a 3-stage switching frequency that is compatible with the peak loads of power supplies, and it has made it possible to increase the maximum output power without changing the size of power supply components. Moreover, it ensures power supply safety because it comes equipped with various protective functions optimized for power supply systems. Furthermore, the IC has an expansion

function for switching frequency jitter*1 that enables it to achieve low electro-magnetic interference

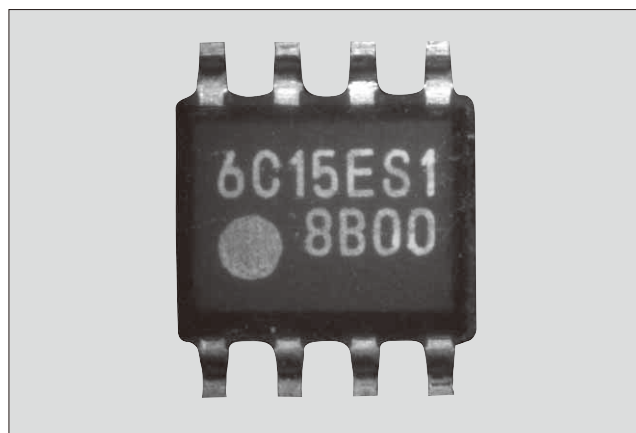


Fig. 1 “FA8B00 Series”

Table 1 Function overview of “FA8B00 Series”

Item	FA8B00 Series		FA8A00 Series (conventional model)	
Switching frequency characteristics	3-stage frequency characteristics (25 kHz - 65 kHz - 130 kHz)		2-stage frequency characteristics (25 kHz - 65 kHz)	
OCP line correction	±3.7%		±6.5%	
IC output voltage	With output voltage clamp		Without output voltage clamp	
Switching frequency jitter	With expansion function		Fixed	
Standby power	25.7 mW		29.0 mW	
Power supply average efficiency	90.0% ($V_i = 115V AC$)	90.7% ($V_i = 230V AC$)	89.7% ($V_i = 115V AC$)	90.5% ($V_i = 230V AC$)

*1: Switching frequency jitter: It refers to an IC function for reducing EMI noise, especially conduction noise, by changing the switching frequency via a fixed interval and width.

* Fuji Electric Taiwan Co., Ltd.

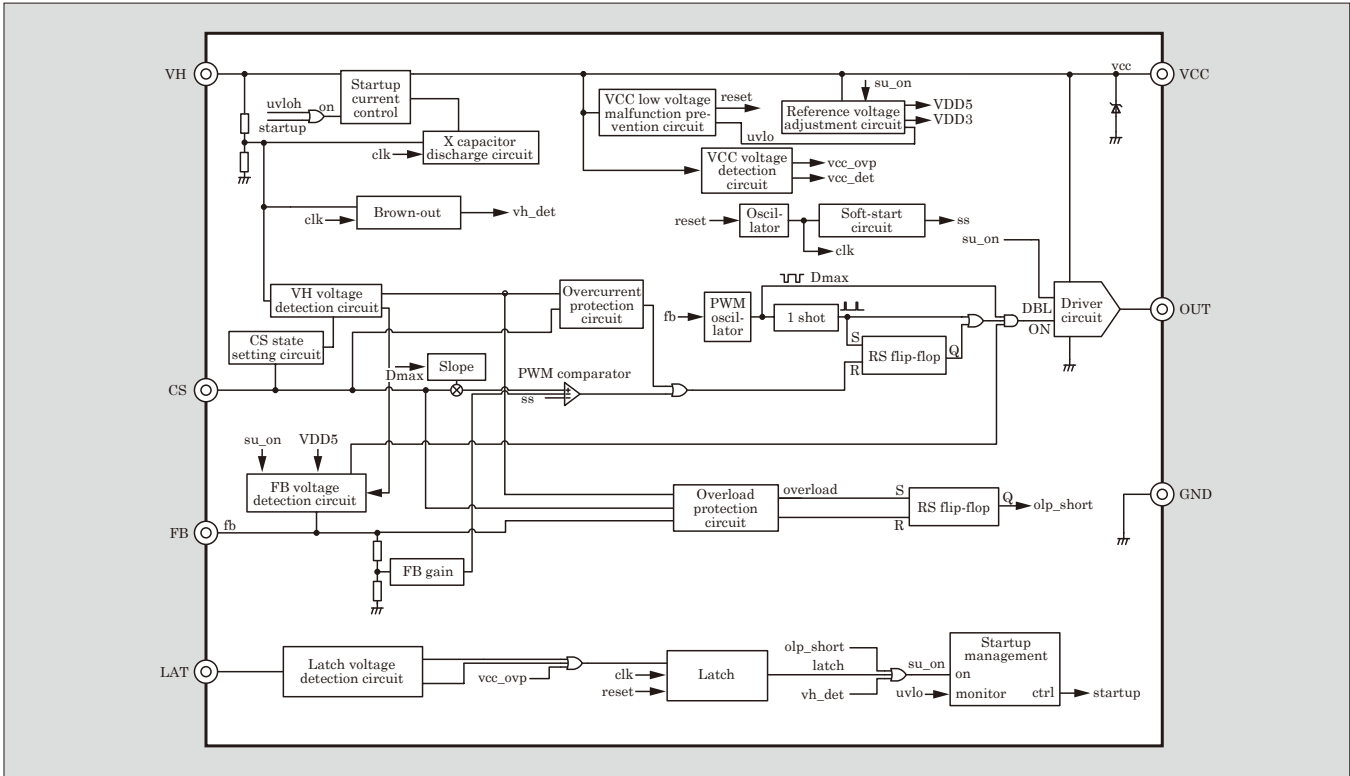


Fig. 2 Block diagram of “FA8B00 Series”

(EMI) noise characteristics even against fluctuating loads.

Table 1 provides a function overview of the FA8B00 Series, and Fig. 2 shows the block diagram.

3. Main Features

3.1 Switching frequency characteristics compatible with peak loads

The FA8B00 Series comes equipped with a new 3-stage switching frequency characteristic (25 kHz to 65 kHz to 130 kHz) that is compatible with the peak loads of power supplies, and in accordance with increasing FB terminal voltage, switching frequency has also been increased to a maximum of 130 kHz (see Fig.

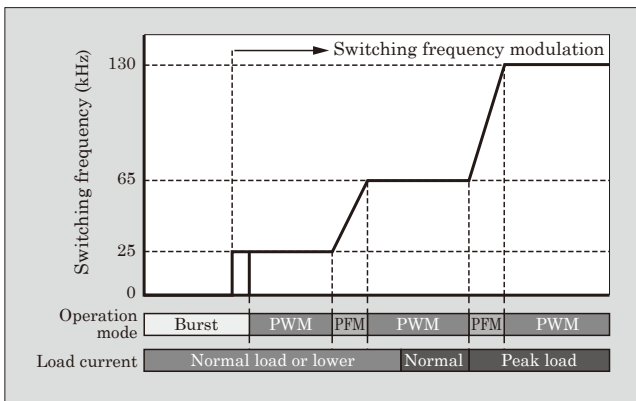


Fig. 3 3-stage switching frequency characteristics

3). Since conventional models of the “FA8A00 Series” could only support a switching frequency up to 65 kHz, a larger-volume transformer was needed to obtain a larger maximum output, and this resulted in extra costs. In contrast, the FA8B00 Series is capable of providing higher switching frequencies, and it can increase maximum output without needing to change the volume of the transformer.

3.2 High-precision OCP line correction

The output current during overload has the property that it increases in proportion to AC input voltage. As a result, power supply has a large difference in the detecting current of over load between low input voltage (approximately 100 V AC) and high input voltage (approximately 230 V AC). The conventional model came built-in with an over current protection (OCP) line correction function for adjusting the threshold voltage of the CS terminal changed by the AC input voltage, allowing it to reduce the output current fluctuation width to $\pm 6.5\%$ during overload within an AC input voltage range of 90 to 265 V.

The FA8B00 Series is designed to achieve high-precision control so that this function has more flat characteristics versus AC input voltage. Figure 4 shows a comparison with the conventional model regarding output current during overload. The FA8B00 Series has reduced the output current fluctuation width to $\pm 3.7\%$. In addition, it is enabled to select between 3 correction levels (Weak, Middle, Strong) for OCP line correction, thus improving design flexibility.

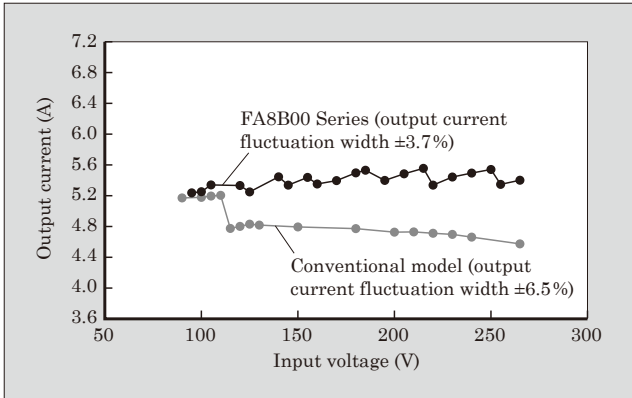


Fig. 4 Comparison of output current during overload

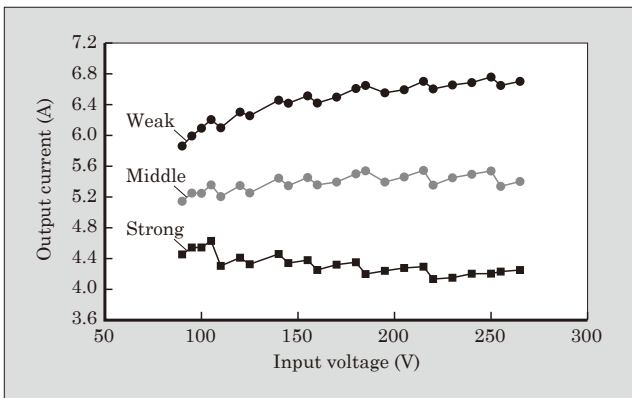


Fig. 5 Selection of OCP line correction

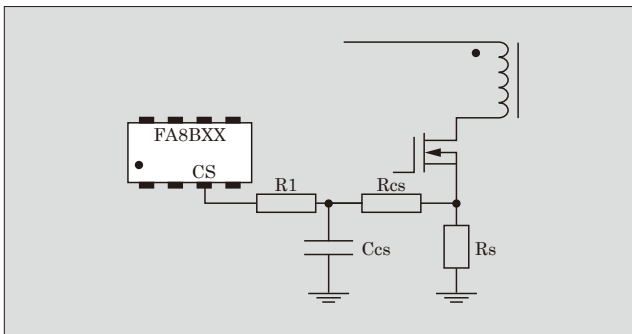


Fig. 6 Circuit configuration example for CS terminal

Table 2 Adjustment of correction amount

Input voltage dependence correction amount	Resistance value
Strong(correction amount: large)	$0.3\text{ k}\Omega \leq R_{cs}$ or $R_1 + R_{cs} \leq 0.5\text{ k}\Omega$
Middle(correction amount: medium)	$1.4\text{ k}\Omega \leq R_{cs}$ or $R_1 + R_{cs} \leq 2.1\text{ k}\Omega$
Weak(correction amount: small)	$3.9\text{ k}\Omega \leq R_{cs}$ or $R_1 + R_{cs} \leq 5.2\text{ k}\Omega$

Correction levels can be selected via the value of the external resistor connected to the CS terminal (see Fig. 5, Fig. 6, Table 2).

3.3 Various protective functions

The FA8B00 Series comes with built-in protective functions especially suited for power supply systems,

and with fewer external components, it is capable of achieving safe and stable power supply.

(1) Load short-circuit protective function

The IC comes with a built-in load short-circuit protective function for preventing metal-oxide-semiconductor field-effect transistor (MOSFET) damage from occurring at the time of power supply output short circuit. This function can be used according to application need because it has 2 types of methods for detecting load short circuit. In a type using a method of detection based on VCC terminal voltage, it instantly terminates switching when the VCC terminal voltage falls to a certain threshold in the overload state. In another type using a method of detection based on FB terminal voltage, it terminates switching when voltage continuously exceeds the FB load short-circuit protection detection voltage for longer than a certain fixed period of time.

(2) Brown-in/brown-out function

It is also equipped with a built-in brown-in/brown-out function for preventing power circuit malfunction when there is some drop in AC input voltage. This function terminates the output pulse from the OUT terminal when AC input voltage drops to the VH brown-out threshold voltage for longer than a certain fixed period of time. Moreover, it starts switching once the AC input voltage reaches the VH brown-in threshold voltage.

(3) Overvoltage protective function

It comes with a built-in overvoltage protective function for monitoring VCC terminal voltage. This function terminates switching when the VCC terminal voltage continuously exceeds the overvoltage protection threshold voltage for longer than a certain fixed period of time.

(4) Low voltage malfunction prevention function

It also comes with a built-in low voltage malfunction prevention function for preventing IC malfunction when there is some drop in VCC terminal voltage, i.e. the power supply voltage of the IC. It terminates operation when the VCC terminal voltage drops to the OFF threshold voltage, and starts operation when the VCC terminal voltage reaches the ON threshold voltage.

4. Application Effect on the Power Circuit

4.1 EMI countermeasures

The conventional model came equipped with a built-in jitter function as an EMI countermeasure for implementing a frequency variation of $\pm 7\%$ for a switching frequency of 65 kHz. This function made it possible to reduce conduction noise because switching noise energy was dispersed more efficiently comparing with a fixed frequency system. However, the real jitter width would fall below 7% when the switching frequency was changing from 130 kHz to 65 kHz or from 65 kHz to 25 kHz (frequency reduction region), and this, in turn, would create the problem of a weak-

ened noise reduction effect. This was the result of the jitter amplitude width decreasing due to the FB terminal voltage based frequency variation offsetting the jitter based frequency variation. Therefore, the FA8B00 Series newly comes equipped with a built-in switching frequency jitter expansion function for expanding the jitter width in the frequency reduction region from 7% to 14%. An overview of the switching frequency jitter expansion function is shown in Fig. 7, the evaluation results of the switching frequency jitter expansion function is shown in Fig. 8 and the evaluation results of the conduction noise generating power supply in Fig. 9. We verified that the jitter effect can be maintained in the frequency reduction region and that a standard compliant noise margin can be secured at approximately 10 dB and above.

4.2 Effect of reducing power supply components

In order to reduce the conduction noise generated from the power supply, common mode choke coils and

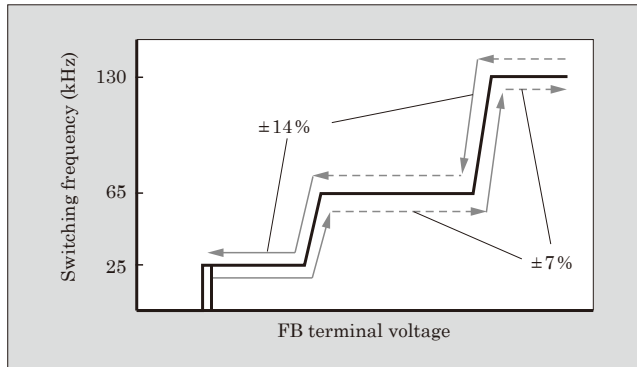


Fig. 7 Overview of switching frequency jitter expansion function

capacitors are inserted as noise filters into power supply input portion. The FA8B00 Series newly comes equipped with a built-in switching frequency jitter expansion function as described in Section 4.1, and thus it is capable of reducing the capacity and number of input filters since it can reduce conduction noise more

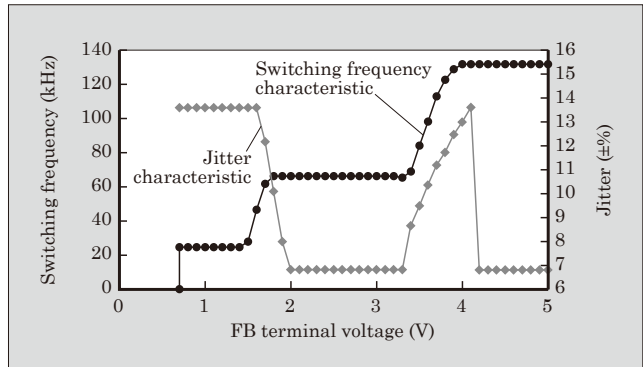


Fig. 8 Evaluation results for switching frequency jitter expansion function

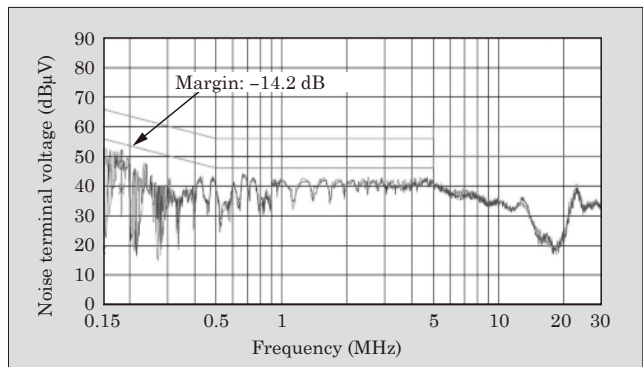


Fig. 9 Evaluation results for power supply conduction noise

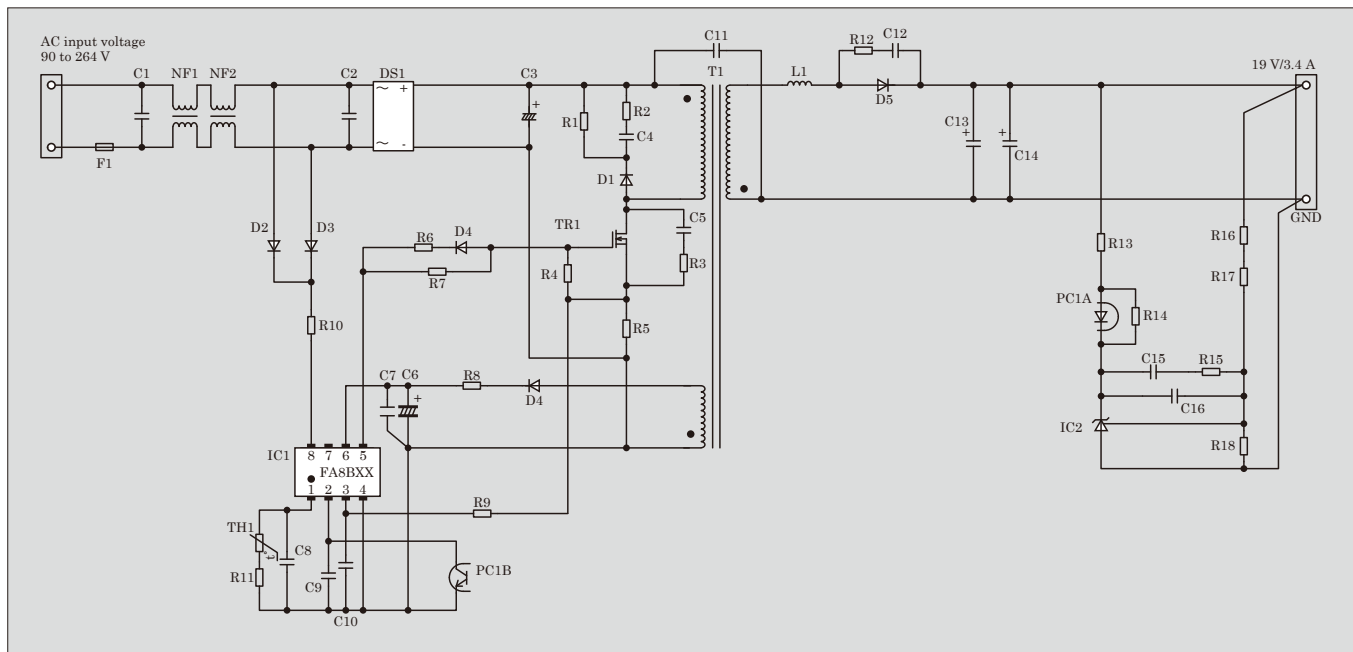


Fig. 10 Circuit of evaluation-use power supply board

than the conventional model

4.3 Improvement in power supply safety

The FA8B00 Series comes with a built-in OUT terminal voltage clamp function for the IC, and is capable of clamping the output voltage of the IC at approximately 18 V to prevent the OUT terminal voltage from rising any further even when a VCC terminal voltage of 20 V or more has been applied. This function makes it possible to use a power MOSFET with a gate protection and gate voltage specification of 20 V or less, thus facilitating improvement in power supply safety and making it possible to reduce the cost of components. Figure 10 shows the circuit of an evaluation-use power supply board. In addition, the results of measuring standby power and power supply efficiency using the power supply board are compared with the conven-

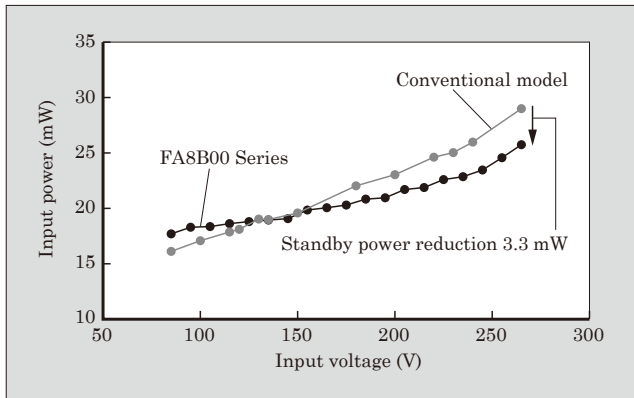


Fig. 11 Standby power

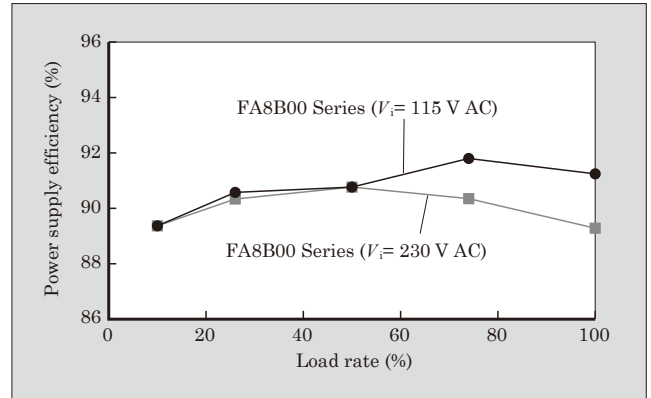


Fig. 12 Power supply efficiency

tional model in Fig. 11 and Fig. 12. The FA8B00 Series achieves a reduction in standby power of 3.3 mW compared with the conventional model, while also maintaining a power supply efficiency capability equal to or greater than the conventional model.

5. Postscript

This paper described the “FA8B00 Series” PWM power supply control IC, that is compatible with the peak power of switching power supply circuits.

In the future, we plan on advancing our efforts to establish new technologies for achieving even higher efficiency, lower standby power and lower noise so that we can continue to develop products that meet the needs of the market.

2nd-Generation Low-Loss SJ-MOSFET “Super J MOS S2 Series”

WATANABE, Sota* SAKATA, Toshiaki* YAMASHITA, Chiho‡

ABSTRACT

In order to use energy efficiently, there has been increasing demand for enhanced efficiency in power conversion equipment, and power metal-oxide-semiconductor field-effect transistors (MOSFETs) that are equipped with it have been required to be compact, low loss and low noise. Fuji Electric has developed the easy-to-use 2nd-generation low-loss SJ-MOSFET “Super J MOS S2 Series” that reduces on-resistance $R_{on} \cdot A$, which is standardized by unit area, and improves the trade-off characteristic between turn-off switching loss E_{off} and the V_{DS} surge at turn-off switching. The adoption of this product is expected to improve the efficiency of power conversion equipment.

1. Introduction

In recent years, renewable energy sources such as photovoltaic power generation and wind power generation have been spreading against the background of global warming prevention and other concerns. On the other hand, energy consumption is increasing in the social infrastructure, automotive, industrial machinery, IT equipment and home appliance fields. In order to use energy more efficiently, power conversion technology has become of increasing importance. Various types of equipment have a power converter that uses semiconductor switching elements such as power metal-oxide-semiconductor field-effect transistors (MOSFETs). Such power converters are required to ensure high efficiency, high power density and low noise, and the semiconductor switching elements need to have characteristics of small size, low loss and low noise.

In order to meet such requirements, Fuji Electric developed the 1st-generation low-loss SJ-MOSFET “Super J MOS S1 Series” (S1 Series) in 2011. It achieved both low on-resistance and low switching loss by adopting a superjunction (SJ) structure and we have been establishing its product line^{(1) to (3)}.

This paper describes the 2nd-generation low-loss SJ-MOSFET “Super J MOS S2 Series” (S2 Series) that offers higher usability and improved conversion efficiency of power converters. This has been achieved by further improving the trade-off relationship between the withstand voltage of the element (BV_{DSS}) and the on-resistance normalized with a unit area ($R_{on} \cdot A$) and through suppressing the V_{DS} surge at the time of turn-off switching.

* Electronic Devices Business Group, Fuji Electric Co., Ltd.

‡ Sales Group, Fuji Electric Co., Ltd.

2. Design

2.1 Design policy

Improving the power conversion efficiency of a switching power supply requires a reduction in the conduction loss, switching loss and drive loss of the power MOSFET. There is a contradictory relationship among them: attempting to increase the switching speed and thus reduce the switching loss increases the V_{DS} surge at the time of turn-off switching, which generates noises and causes a malfunction. It is desirable to suppress the V_{DS} surge to 80% or less of the maximum rated voltage also in terms of reliability.

Consequently, we set the objective of developing the S2 Series to reduce the switching loss at turn-off (E_{off}) and suppress the V_{DS} surge and noises at the same time while reducing $R_{on} \cdot A$ so that it is lower than that of the conventional S1 Series.

2.2 Reducing the conduction loss

To reduce the conduction loss, we need to lower $R_{on} \cdot A$. As Fig. 1 shows, the superjunction structure

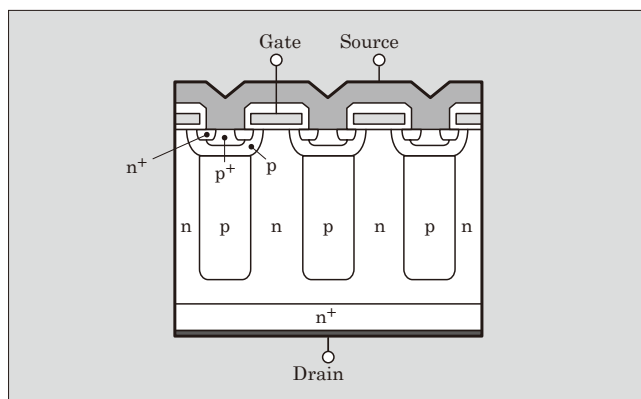


Fig. 1 Superjunction structure of SJ-MOSFET

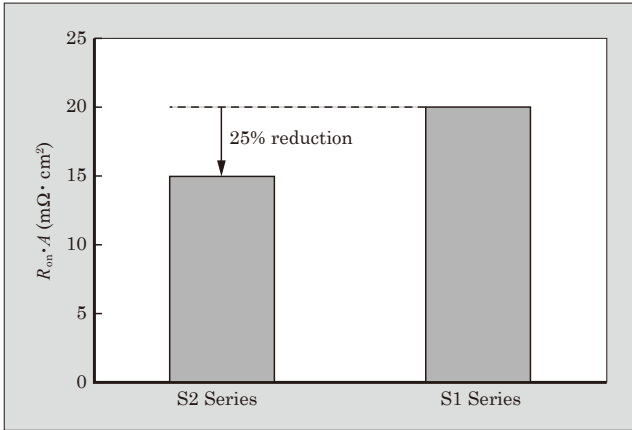


Fig. 2 $R_{on} \cdot A$ characteristics of 600-V rated products

has p-type regions and n-type regions arranged alternately in the drift layer. In this way, the depletion layers of p-n junctions connect horizontally when voltage is applied and a withstand voltage is provided on the entire surface^{(4) to (8)}.

To reduce $R_{on} \cdot A$, we need to increase the impurity concentration of the n-type region to lower the resistance. For the S2 Series, we improved the impurity diffusion process and maintained a high impurity concentration in the n-type region to allow resistance to be reduced⁽⁹⁾.

Figure 2 shows the $R_{on} \cdot A$ characteristics of the 600-V rated products of the S1 and S2 Series. We have reduced the resistance of the S2 Series by 25% to 15 $m\Omega \cdot cm^2$ from 20 $m\Omega \cdot cm^2$ of the S1 Series. As a result, in the TO-247 package, the S2 Series can mount up to 600-V/25.4-m Ω chips, whereas the S1 Series was limited to up to 600 V/40 m Ω .

2.3 Reducing the switching loss and suppressing the V_{DS} surge

We evaluated the power supply shown in Fig. 3 by mounting 600-V/70-m Ω products of the S1 and S2 Series in a MOSFET of a continuous conduction mode power-factor control circuit (CCM-PFC circuit). The conversion efficiency of the power supply against the external gate resistance R_g at 100-V input and

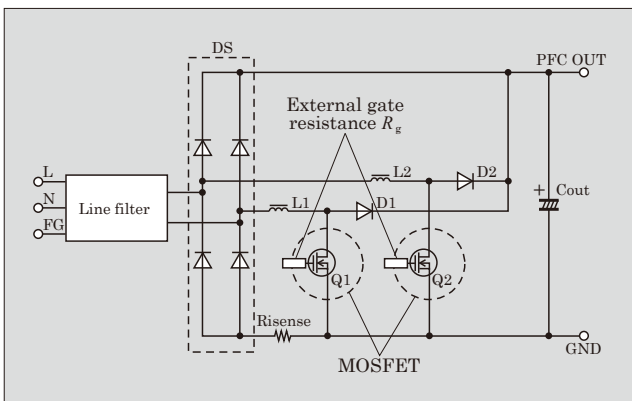


Fig. 3 CCM-PFC circuit of power supply

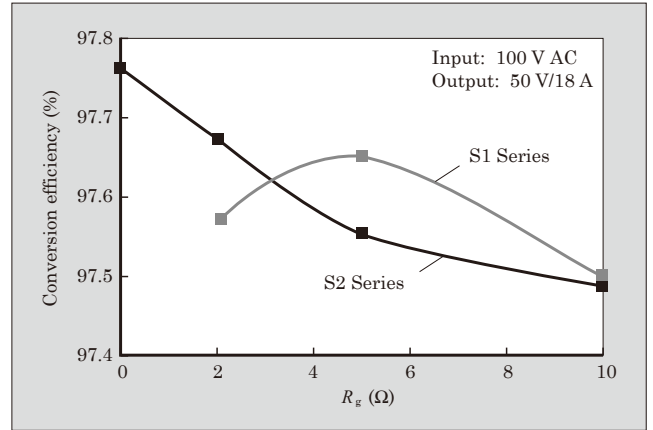


Fig. 4 Power supply conversion efficiency against external gate resistance R_g

50-V/18-A output is shown in Fig. 4. As the figure shows, the power supply efficiency normally increases when R_g is reduced. However, the efficiency decreases with the S1 Series. This is caused by erroneous ON due to the large wiring inductance of the source. In general, it is necessary to suppress such erroneous ON to prevent loss.

It is, however, impossible to eliminate the wiring inductance of the source completely because a power supply circuit is sometimes designed by reusing previous design patterns and its design is restricted by various factors such as the part layout. We thus took measures for the device so that we did not have to change the pattern design or parts circuit constant. The S2 Series attempts to suppress erroneous ON by increasing the threshold voltage $V_{GS(th)}$. For this purpose, increasing $V_{GS(th)}$ alone makes the turn-off speed faster. This might cause erroneous ON caused by gate vibration and the V_{DS} surge at turn-off switching. Therefore, we took measures including the optimization of $V_{GS(th)}$ and R_g .

Figure 5 shows the turn-off waveforms when R_g of the S1 and S2 Series is 2 Ω . Compared with the S1 Series, the S2 Series produces a smaller gate vibration and V_{DS} surge to suppress erroneous gate ON. This makes it possible to improve the power supply efficiency without changing the customer's R_g .

Figure 6 shows the trade-off characteristics between E_{off} and V_{DS} surge. When the V_{DS} surge is the same, the E_{off} value of the S2 Series is smaller than that of the S1 Series. This shows there is an improvement in the trade-off characteristic between E_{off} and V_{DS} surge. The S2 Series suppresses the V_{DS} surge and erroneous gate ON in this way. Figure 4 shows the conversion efficiency of a power supply against R_g when the S2 Series is mounted in the CCM-PFC circuit of the power supply. The S1 Series shows low conversion efficiency when R_g is small, but the S2 Series shows an improvement in the conversion efficiency when R_g is decreased.

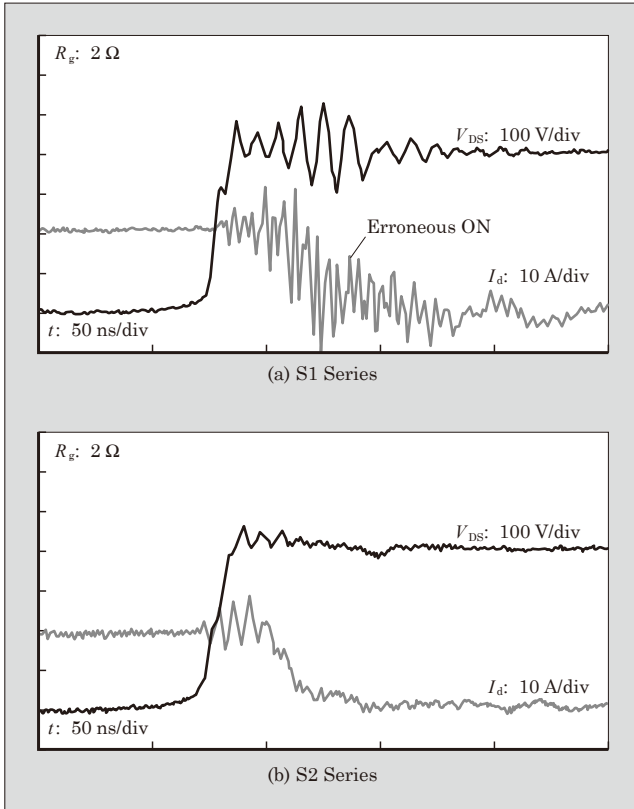


Fig. 5 Turn-off waveforms

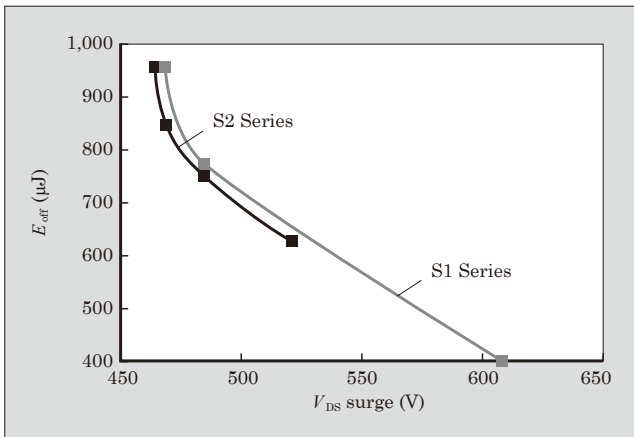


Fig. 6 E_{off} - V_{DS} trade-off characteristics

2.4 Reducing the loss under light load

When a light load is applied to a power supply, the current flowing in the MOSFET is small. Consequently, the proportion of the conduction loss in the total loss decreases. This results in an increase in the proportion of the drive loss and the loss generated when the output capacitance C_{oss} is charged/discharged (E_{oss}). We hence optimized the surface structure and reduced the total gate charge Q_g that is an index of the drive loss by approximately 30% compared with the S1 Series, achieving a reduction of $R_{on} \cdot Q_g$ by approximately 20%. Figure 7 shows the result of comparing Q_g between the S1 and S2 Series.

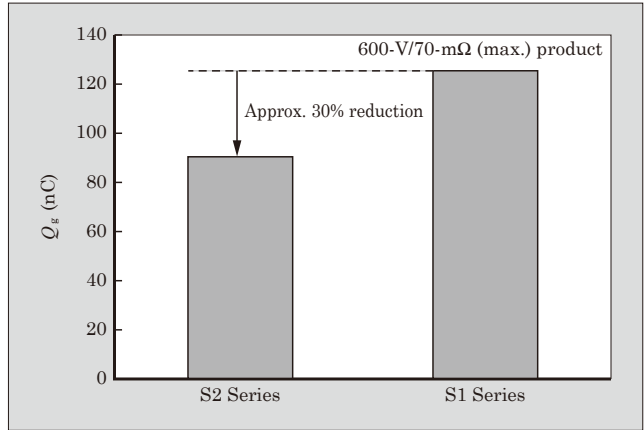


Fig. 7 Q_g characteristics

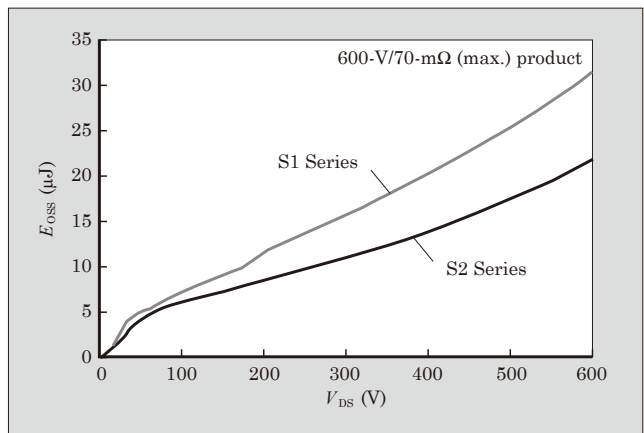


Fig. 8 E_{oss} characteristics

Figure 8 shows the result of comparing E_{oss} against V_{DS} between the S1 and S2 Series. When V_{DS} is 400 V, E_{oss} is approximately 30% less than that of the S1 Series.

3. Application Effect

We conducted a comparative evaluation by mounting the 600-V/70-mΩ products of the S1 and S2 Series in the CCM-PFC circuit of the power supply shown in Fig. 3 (see Fig. 9). The I/O conditions for the evalua-

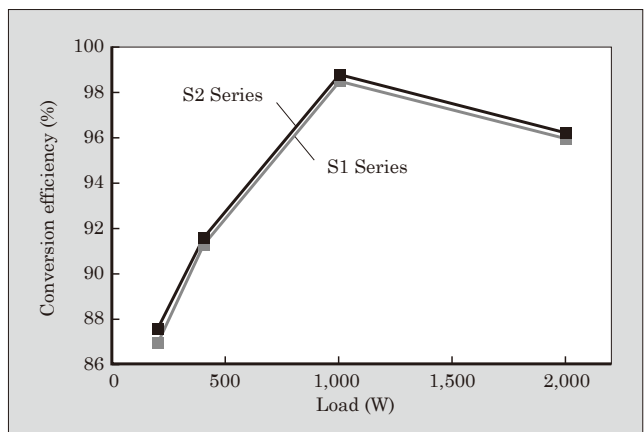


Fig. 9 Conversion efficiency-load characteristics

Table 1 Product lineup and major characteristics of “Super J MOS S2 Series”

V_{DS} (V)	$R_{DS(on)}$ max. (mΩ)	I_D (A)	Product lineup			
			TO-247 package 	TO-3P package 	TO-220 package 	TO-220F package 
600	25.4	95.5	FMW60N025S2	-	-	-
	40	66.2	FMW60N040S2	-	-	-
	55	49.9	FMW60N055S2	-	-	-
	70	39.4	FMW60N070S2	-	-	FMV60N070S2
	79	37.1	FMW60N079S2	-	FMP60N079S2	FMV60N079S2
	88	32.8	FMW60N088S2	-	FMP60N088S2	FMV60N088S2
	99	29.2	FMW60N099S2	-	FMP60N099S2	FMV60N099S2
	125	22.7	FMW60N125S2	-	FMP60N125S2	FMV60N125S2
	160	17.9	FMW60N160S2	-	FMP60N160S2	FMV60N160S2
	190	15.5	FMW60N190S2	FMH60N190S2	FMP60N190S2	FMV60N190S2
	280	10.4	-	FMH60N280S2	FMP60N280S2	FMV60N280S2
	380	8.1	-	-	FMP60N380S2	FMV60N380S2

tion includes input voltage of 200 V, output voltage of 53.5 V and R_g of 2 Ω. The S2 Series ensures higher efficiency than the S1 Series in the entire load region by suppressing erroneous ON by gate vibration, improving the trade-off characteristics between E_{off} and V_{DS} surge and reducing Q_g and E_{oss} . As a result, we can expect a power supply design offering higher efficiency and reliability by applying the S2 Series to a switching power supply.

4. Product Lineup

Table 1 lists the product lineup and major characteristics of the S2 Series. The lineup includes products rated at $R_{DS(on)}$ 25.4 to 160 mΩ for relatively large-capacity power supplies and those rated at 190 to 380 mΩ for small-capacity power supplies.

5. Postscript

The 2nd-generation low-loss SJ-MOSFET “Super J MOS S2 Series” is a product achieving both low power dissipation and V_{DS} surge suppression. The evaluation of a prototype mounted in a CCM-PFC circuit showed that the product could achieve higher efficiency than the conventional products. The developed device could make a great contribution to the efficiency improvement and miniaturization of switching power supplies.

In order to provide the better performance required by the market, we will continue to expand the lineup

of high-breakage products and the products for high-speed switching of built-in diodes. At the same time, we will improve performances such as $R_{on} \cdot A$ reduction.

References

- (1) Tamura, T. et al. “Super J-MOS” Low Power Loss Superjunction MOSFETs. FUJI ELECTRIC REVIEW. 2012, vol.58, no.2, p.79-82.
- (2) T. Tamura et al. Reduction of Turn- off Loss in 600 V-class Superjunction MOSFET by Surface Design. PCIM Asia 2011, p.102-107.
- (3) S. Watanabe et al. A Low Switching Loss Superjunction MOSFET (Super J-MOS) by Optimizing Surface Design. PCIM Asia 2012, p.160-165.
- (4) T. Fujihira. Theory of Semiconductor Superjunction Devices. Jpn. J. Appl. Phys. 1997, vol.36, p.6254-6262.
- (5) G. Deboy et al. A New Generation of High Voltage MOSFETs Breaks the Limit Line of Silicon. Proc. IEDM, 1998, p.683-685.
- (6) Y. Onishi et al. 24 m·cm² 680 V Silicon Superjunction MOSFET. Proc. ISPSD’02, 2002, p.241-244.
- (7) W. Saito et al. A 15.5 m·cm²-680 V Superjunction MOSFET Reduced On- Resistance by Lateral Pitch Narrowing, Proc. ISPSD’06, 2006, p.293-296.
- (8) Oonishi, Y. et al. Superjunction MOSFET. FUJI ELECTRIC REVIEW. 2010, vol.56, no.2, p.65-68.
- (9) T. Sakata et al. A Low- Switching Noise and High-Efficiency Superjunction MOSFET, Super J MOS® S2. PCIM Asia 2015, p.419-426.

High-Speed Discrete IGBT “High-Speed W-Series”

HARA, Yukihiro* NAITO, Tatsuya* KATO, Yoshiharu*

ABSTRACT

Since power conversion efficiency is an important factor for uninterruptible power systems (UPSs) and power conditioning sub-systems (PCSs) for photovoltaic power generation, switching devices used in the equipment are required to reduce the power loss. For compact inverter welding machines, utilized devices are required to have low-loss characteristics and high-speed switching to make conveyance easier. The high-speed discrete insulated-gate bipolar transistor (IGBT) that we have developed and released reduces parasitic capacitance in active parts and optimizes the field stop layer, thereby achieving a 10% reduction in loss for 650-V products and a 19% reduction in loss for 1,200-V products when compared to the conventional product.

1. Introduction

In recent years, the demand for energy in the world has been steadily increasing. The servers and data centers that support our Internet based society require highly reliable power supplies. On the other hand, the spread of renewable energies such as photovoltaic power generation and wind power generation has advanced the diversification of energy supply, and as a result, the demand for power conversion has been increasing. The increasing demand for power savings in servers and data centers, as well as the need for higher power conversion efficiency in energy supply has created very high expectations for the field of power electronics technology.

As worldwide data usage increases, uninterruptible power systems (UPSs) are being adopted for servers and data centers to ensure the integrity of data. In the past, it was common to adopt a single large capacity UPS for applications requiring 100 kVA or more. However, servers and data centers require a redundant configuration to ensure high reliability, and as such, the recent trend has been to combine medium capacity units with a rated capacity of approximately 10 to 50 kVA in parallel to achieve redundant operation. In addition, photovoltaic power generation facilities are adopting power conditioning sub-systems (PCSs) to convert generated DC power to AC power. The power conversion efficiency of these UPS and PCS is a very important factor in performance, and thus, there has been strong demand for switching devices to dissipate less power. In either case, since insulated-gate bipolar transistor (IGBT) switching is implemented very frequently at 20 to 40 kHz, there is increasing demand to reduce the switching loss caused by high-speed switch-

ing.

At the same time, compact inverter welding machines used on construction sites are being required to be smaller and lighter to make for easier conveyance. The miniaturization of transformers and coils, achieved through reducing the loss in utilized devices during high-speed switching and by driving them at high frequencies, can contribute to reducing the size and weight of welding machine units.

In order to increase the performance of UPS, PCS and inverter welding machines, we have recently developed and released to the market the high-speed discrete IGBT “High-Speed W-Series” as a device capable of improving on-voltage and switching characteristic trade-off. This paper provides an overview and describes the application effects of the High-Speed W-Series, which has a product lineup featuring a maximum rated voltage of 650 V and 1,200 V.

2. “High-Speed W-Series” Overview

The external appearance of the High-Speed

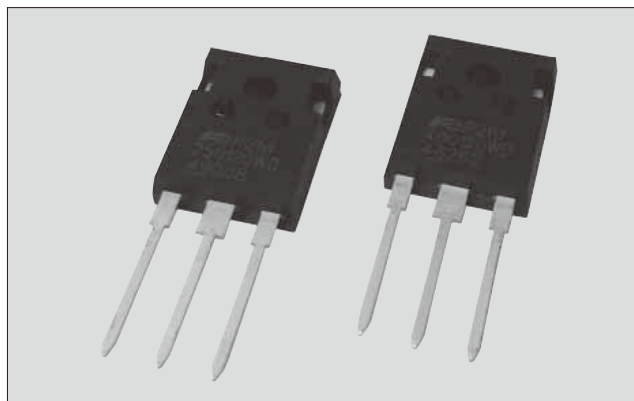


Fig.1 High-speed discrete IGBT “High-Speed W-Series”

* Electronic Devices Business Group, Fuji Electric Co., Ltd.

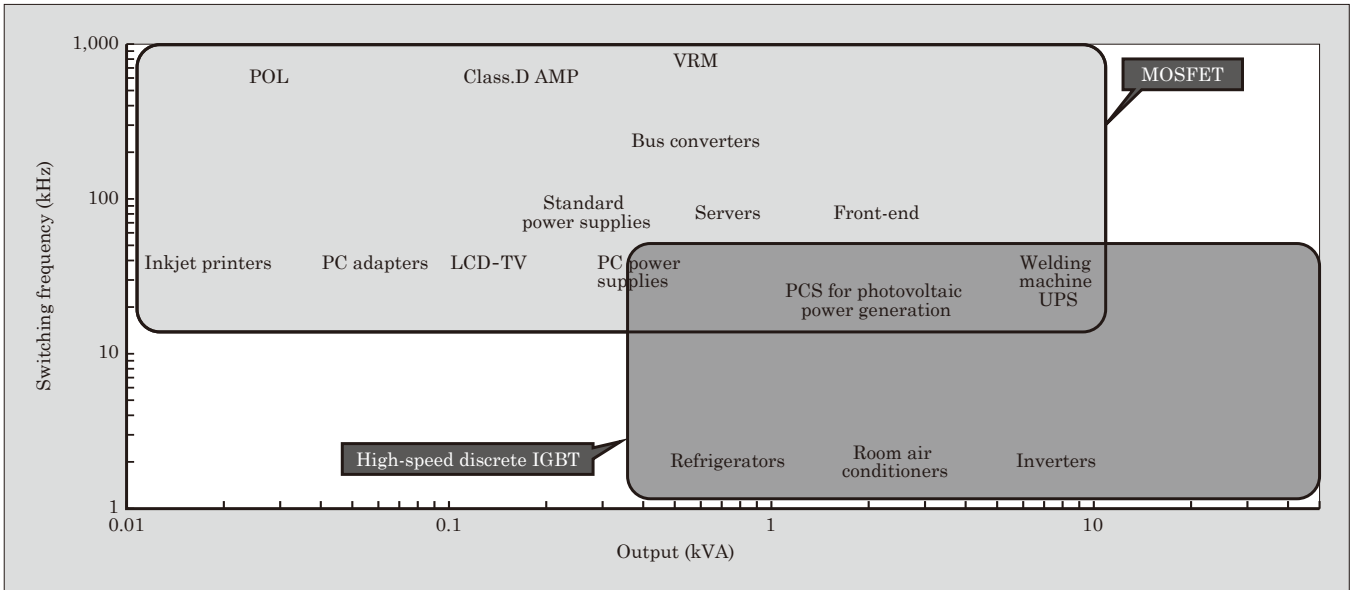


Fig.2 Main applications of “High-Speed W-Series”

W-Series is shown in Fig. 1, and its main applications are shown in Fig. 2. The primary maximum ratings and electrical characteristics of the High-Speed W-Series are shown in Table 1.

The 650-V series equips its common discrete product package TO-247 with a 40- to 60-A IGBT chip and 20- to 60-A free wheeling diode (FWD) chip, and the 1,200-V series equips it with a 25-, 40-A IGBT chip and 12-, 20-, 40-A FWD chip. This product lineup is designed to allow users to select a specification depending on equipment power supply capacity and utilized

circuits.

3. Issues Facing Discrete IGBT

An application example of a discrete IGBT in a UPS is shown in Fig. 3, and an application example in a PCS is shown in Fig. 4.

It is important for a UPS to minimize power loss, and for a PCS to minimize loss when converting DC power generated by photovoltaic panels to AC power.

In order to improve the power efficiency of invert-

Table 1 Primary maximum ratings and electrical characteristics of “High-Speed W-Series”

Type	Product type	Package	Maximum ratings				Electrical characteristics			
			IGBT			FWD	IGBT		FWD	
			V_{CES}	I_C ($T_j = 100^\circ\text{C}$)	I_{CP}	I_F ($T_j = 100^\circ\text{C}$)	$V_{CES(sat)}$ ($T_j = 25^\circ\text{C}$ typ.)	$V_{CES(sat)}$ ($T_j = 125^\circ\text{C}$ typ.)	V_F ($T_j = 25^\circ\text{C}$ typ.)	V_F ($T_j = 125^\circ\text{C}$ typ.)
			(V)	(A)	(A)	(A)	(V)	(V)	(V)	(V)
FGW40N65 WD	Ultra Fast FWD	TO-247	650	40	160	20	1.80	2.05	2.5	1.9
FGW50N65 WD	Ultra Fast FWD	TO-247	650	50	200	25	1.80	2.05	2.5	1.9
FGW60N65 WD	Ultra Fast FWD	TO-247	650	60	240	30	1.80	2.05	2.5	1.9
FGW40N65 WE	Ultra Fast FWD	TO-247	650	40	160	40	1.80	2.05	2.5	1.9
FGW50N65 WE	Ultra Fast FWD	TO-247	650	50	200	50	1.80	2.05	2.5	1.9
FGW60N65 WE	Ultra Fast FWD	TO-247	650	60	240	60	1.80	2.05	2.5	1.9
FGW40N65 W	w/o FWD	TO-247	650	40	160	–	1.80	2.05	–	–
FGW50N65 W	w/o FWD	TO-247	650	50	200	–	1.80	2.05	–	–
FGW60N65 W	w/o FWD	TO-247	650	60	240	–	1.80	2.05	–	–
FGW25N120 WD	Ultra Fast FWD	TO-247	1,200	25	100	12	2.0	2.4	2.2	2.05
FGW40N120 WD	Ultra Fast FWD	TO-247	1,200	40	160	20	2.0	2.4	2.2	2.05
FGW40N120 WE	Ultra Fast FWD	TO-247	1,200	40	160	40	2.0	2.4	2.4	2.2
FGW25N120 W	w/o FWD	TO-247	1,200	25	100	–	2.0	2.4	–	–
FGW40N120 W	w/o FWD	TO-247	1,200	40	160	–	2.0	2.4	–	–

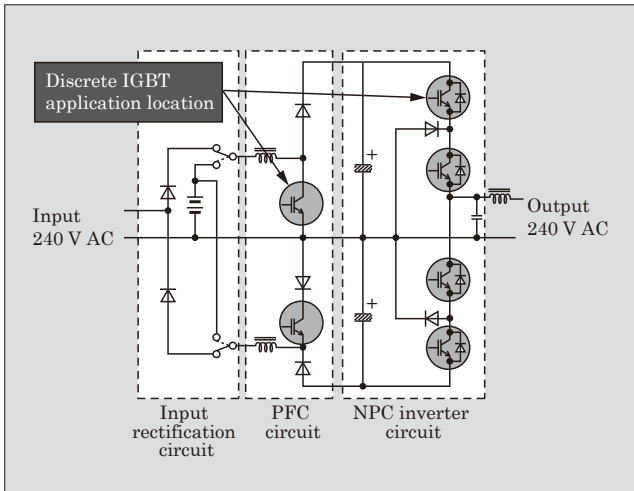


Fig.3 Application example of discrete IGBT in UPS (3-level I-Type)

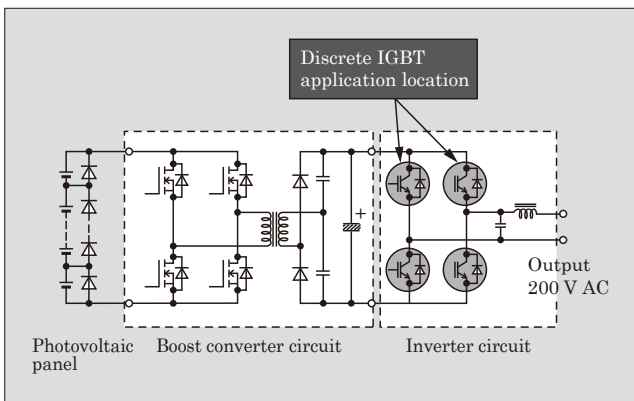


Fig.4 Application example of discrete IGBT in PCS

ers in a UPS and PCS capacity range from several kVA to several tens of kVA, the use of 3-level power conversion technology has become more widespread, and operation is often implemented at a discrete IGBT switching frequency of approximately 20 to 40 kHz.

In order to reduce the size and weight of welding machines, it is necessary to reduce the size of the transformer, which occupies a large portion of the volume and mass. Therefore, there has been an increasing trend in recent years to raise the switching frequency. A portion of the welding machines released to the market are performing discrete IGBT switching at frequencies of 50 kHz or higher.

Figure 5 shows the analysis results of discrete IGBT loss in the inverter of a 5-kVA class UPS and an 8.5-kVA class welding machine. The percentage of IGBT switching loss $E_{on} + E_{off}$ accounted for approximately 50% of the total amount of loss for the UPS and approximately 60% of the total amount of loss for the welding machine. Moreover, the IGBT on-voltage loss V_{on} was about 40% for both of them. Based on these results, in order to achieve low loss discrete IGBT switching at high-speed switching operations, it is important to improve the $V_{CE(sat)}-E_{off}$ trade-off, while si-

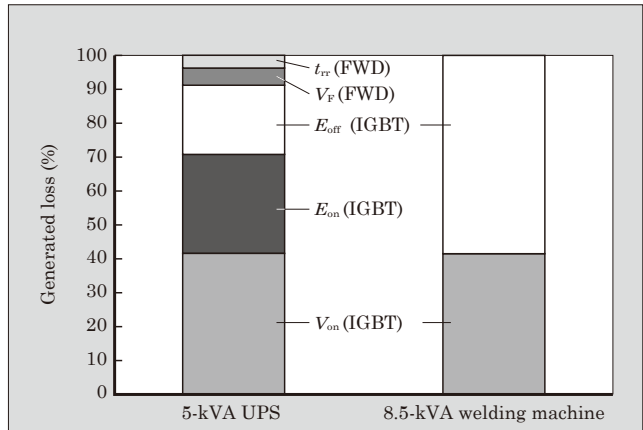


Fig.5 Loss analysis results for discrete IGBT ($f_c=40$ kHz)

multaneously establishing low switching loss and low V_{on} . In particular, emphasis is currently being placed on having a low E_{off} characteristic to ensure also compatibility with increases in drive frequency. In addition, it has also become an important issue to reduce recovery loss in FWD in order to respond to the higher frequencies.

4. Features of “High-Speed W-Series”

The discrete IGBT is a device that mounts an IGBT chip and FWD chip in a single package. The following describes some of the characteristics of the IGBT and FWD chips.

4.1 Features of 650-V series IGBT chip

The rated voltage of the conventional “High-Speed V-Series” product was 600 V. The rated voltage has currently been raised to 650 V to meet the market demand of securing voltage margin.

Figure 6 shows the cross sectional structure of the 650-V IGBT chip. The conventional product was designed to improve the $V_{CE(sat)}-E_{off}$ trade-off based on a V-Series IGBT for the module⁽¹⁾. Against this backdrop, the High-Speed W-Series has newly incorporated design measures to improve the $V_{CE(sat)}-E_{off}$

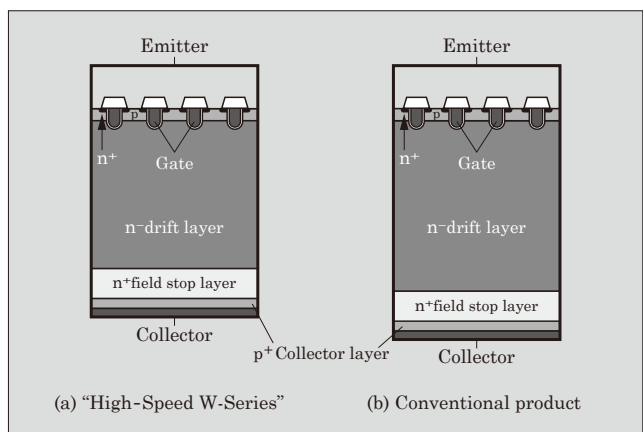


Fig.6 IGBT chip cross sectional structure

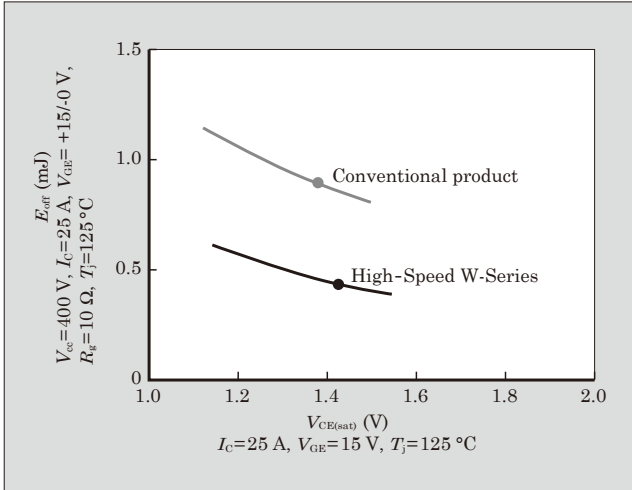


Fig.7 $V_{CE(sat)}$ - E_{off} characteristics of 600-V series/50-A IGBT chip

by including an active structure for significantly reducing parasitic capacitance, optimizing the field stop (FS) layer, incorporating a collector layer that suppresses hole injection and thinning the substrate.

Figure 7 shows the $V_{CE(sat)}$ - E_{off} characteristics of the 600-V series/50-A IGBT chip. Compared with the conventional product, the High-Speed W-Series minimizes degradation of $V_{CE(sat)}$, while also reducing E_{off} by approximately 48%.

4.2 Features of 650-V series FWD chip

The conventional FWD was designed specifically for high-speed switching. The High-Speed W-Series has enhanced the FWD to support a capacity of 650 V, while maintaining low recovery loss characteristics by optimizing the thickness of the drift layer based on the conventional FWD.

4.3 Features of 1,200-V series IGBT chip

The 1,200-V series IGBT chip incorporates the same measures that were implemented for the 650-V series IGBT chip described above, which include a reduction in parasitic capacitance in active parts, suppression of hole injection in the collector layer and thinning of the substrate. Figure 8 shows the turn-off waveform

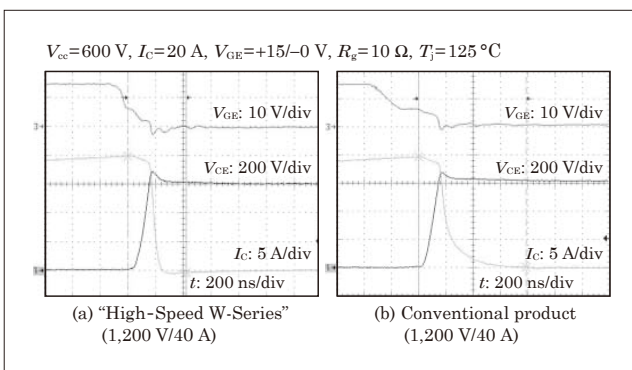


Fig.8 Turn-off waveform of 1,200-V/40-A IGBT

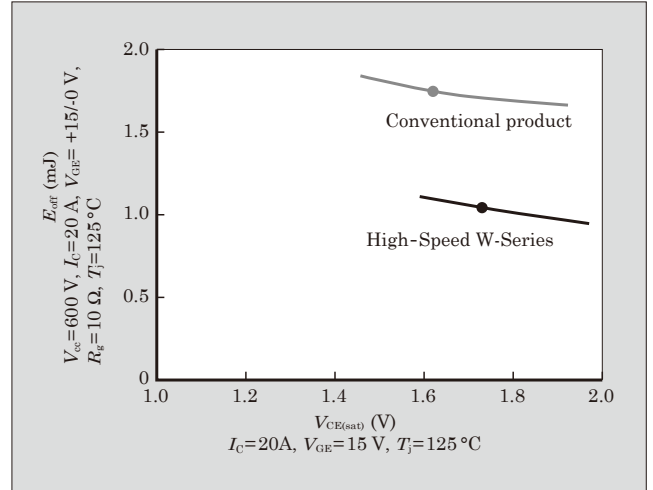


Fig.9 $V_{CE(sat)}$ - E_{off} characteristics of 1,200-V/40-A IGBT

waveform of the 1,200-V/40-A IGBT. The High-Speed W-Series has significantly improved tail current at the time of turn-off, while also greatly reducing E_{off} . Figure 9 shows the $V_{CE(sat)}$ - E_{off} characteristics. The High-Speed W-Series reduces E_{off} by approximately 40%.

4.4 Features of 1,200-V series FWD chip

The High-Speed W-Series utilizes an FWD that has the same low recovery loss characteristics as the conventional product.

5. Application Effects of “High-Speed W-Series”

The results of a generated loss simulation for a UPS with a 5-kW output are shown in Fig. 10 and Fig. 11. We simulated a full-bridge circuit pulse width modulation (PWM) of 40 kHz for the switching frequency.

Based on the 600-V series IGBT in Fig. 10 it is expected that the High-Speed W-Series will reduce total loss by approximately 10% compared with the conventional product. Furthermore, based on the 1,200-V series IGBT in Fig. 11, it is expected that loss will be reduced by about 19%. The large reduction of E_{off} , which

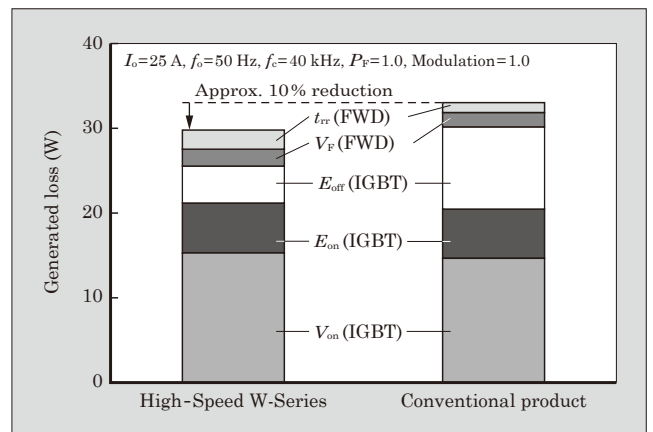


Fig.10 Loss simulation for 600-V series/50-A IGBT

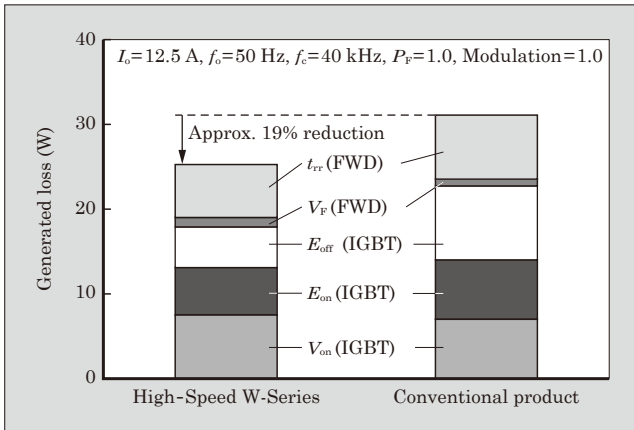


Fig.11 Loss simulation for 1,200-V series/25-A IGBT

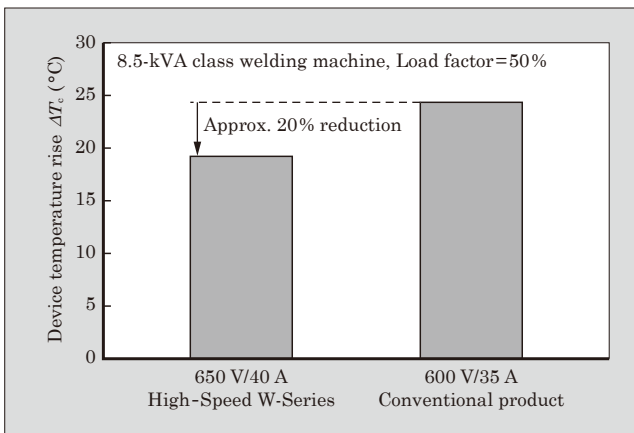


Fig.12 Device temperature evaluation results for welding machine mounted with 600-V series IGBT

occupies approximately 30% of the generated loss in either case, contributes greatly to reducing total loss.

The evaluation results for device temperature when mounting a 600-V series IGBT to an 8.5-kVA

class welding machine are shown in Fig. 12. There is strong demand for the IGBT in general welding machines to have a small temperature rise width because welding machine operations are terminated when the temperature protection function begins to operate. As shown in Fig. 5, approximately 60% of the total loss in welding machines is occupied by the loss caused by E_{off} . Therefore, the High-Speed W-Series has achieved a significant application effect, because it reduces E_{off} much more than the conventional product. It suppresses device temperature rise approximately 5°C (approximately 20%) more than the conventional product. As a result, the High-Speed W-Series makes it possible to lengthen continuous operation of welding machines more than the conventional product.

6. Postscript

This paper provides an overview and describes the application effects of the 650-V and 1,200-V high-speed discrete IGBT “High-Speed W-Series.” This product was designed mostly for UPS, PCS and welding machines, and it can be also used in a wide range of applications such as industrial equipment and the power factor correction (PFC) circuits of switching power supplies.

In the future, we will pursue even greater reductions in power loss, while offering products that meet market needs so that we can continue to contribute to even greater energy savings, higher power conversion efficiency, and the development of smaller and lighter equipment.

References

- (1) Watashima, T. et al. “High Speed V-Series” of Fast Discrete IGBTs. FUJI ELECTRIC REVIEW. 2011, vol.57, no.3, p.91-95.

Amorphous MOLTRA “FM-AT14”

WATANABE, Kenji*

Against the backdrop of global warming prevention, power-saving measures for substation equipment have become an important topic and the need for highly energy-efficient electric equipment is increasing. At present, there are approximately 2.6 million high-voltage distribution transformers installed in Japan and if their total energy loss is calculated based on the loss characteristics per production year, total number of units shipped, and average capacity, the result is a huge amount of approximately 16.5 billion kWh/y (corresponding to CO₂ emissions of 6.2 billion kgCO₂/y). Thus, replacing these older transformers with high efficiency transformers would result in a significant energy savings effect. For molded transformers, as specified equipment under the “Act on the Rational Use of Energy” (Energy Saving Act), second Top Runner Standards*¹ were introduced in FY2014.

Fuji Electric released a “top runner MOLTRA 2014” lineup of single-phase (10 to 500 kVA) and 3-phase (20 to 2,000 kVA) models in June 2013. Compared to conventional products, the generated loss of the transformers was lower by 40%, and the second Top Runner Standards were satisfied. In addition, in June 2015, Fuji Electric released the amorphous MOLTRA “FM-AT14” that realizes an achievement rate of 130%*² with respect to the target efficiency of the secondary top runner criteria (see Fig. 1). This paper describes features of the amorphous alloys used as



Fig.1 “FM-AT14”

* Industrial Infrastructure Business Group, Fuji Electric Co., Ltd.

the iron core material in transformers and features of the FM-AT14.

1. Features of Amorphous Alloy

The FM-AT14 uses an amorphous alloy for the iron core material of the transformer instead of conventional grain-oriented electrical steel sheets. Features and characteristics of amorphous alloy and grain-oriented steel sheets are shown in Fig. 2 and Fig. 3,

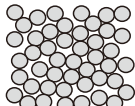
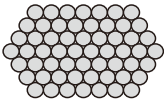
Item	Amorphous alloy	Grain-oriented electrical steel sheets
Atom arrangement	 Irregular (non-crystalline) →Small hysteresis loss	 Regular (crystalline) →Large hysteresis loss
Plate thickness	0.025 mm →Small eddy current loss	0.23 to 0.35 mm →Large eddy current loss that is proportional to thickness

Fig.2 Features of amorphous alloys and grain-oriented electrical steel sheets

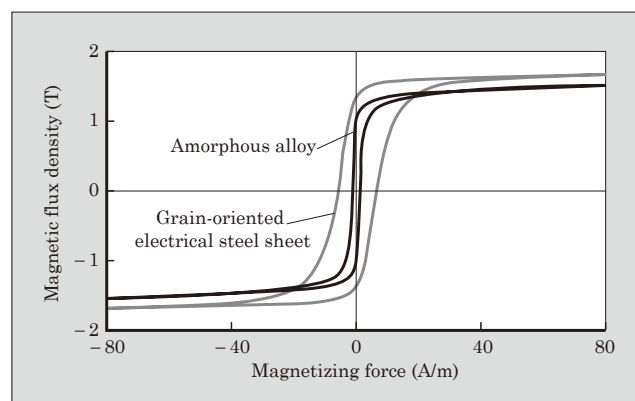


Fig.3 Characteristics of amorphous alloys and grain-oriented electrical steel sheets

*1: Second Top Runner Standards: Indicates secondary judgment criteria for top runner transformers. Prescribed by JIS C 4306 6 kV Encapsulated-winding distribution transformers

*2: Achievement rate: Indicates the percentage of suppression with respect to the reference energy consumption rate (W) of the top runner transformer secondary judgment criteria.

respectively. Amorphous means non-crystalline and in an amorphous alloy the atoms solidify in an irregular state rather than being arranged in a periodic crystalline structure. The loss in a transformer consists of a no-load loss (iron loss) that is generated regardless of the load and a load loss (copper loss) that is generated in proportion to the square of the load current. Amorphous alloy material has characteristics that suppress hysteresis loss and eddy current loss, which account for a large percentage of the no-load loss, and in transformers that use an amorphous alloy, the no-load loss can be suppressed to extremely low levels.

An amorphous alloy has such characteristics, but when used as the iron core material of a transformer, various issues such as an increase in volume, as well as rigidity and processing ease must be addressed.

2. Overview of “FM-AT14”

2.1 Features

- (a) Reduces standby power to 1/3 of that of the Top Runner MOLTRA 2014.
- (b) Realizes energy savings with a 130% achievement rate with respect to the target efficiency of the second Top Runner Standards.
- (c) Employs vacuum cast coils in models of all capacities to realize high insulation reliability of the molded windings.
- (d) Realizes high flame retardancy and has obtained certification of compliance with IEC 60076-11.
- (e) Realizes excellent earthquake resistance in conformance with JEM-TR 252.

2.2 Specifications

Table 1 lists specifications of the FM-AT14.

2.3 Manufacturing issues and measures

Amorphous alloys have a lower saturation magnetic flux density than do grain-oriented electrical steel sheets and the density of flux that can pass through them is also lower. For this reason, the volume of the iron core is larger for the FM-AT14 than for the Top

Table 1 “FM-AT14” specifications

Item	Specification	
Number of phases	1 phase	3 phase
Frequency	50, 60 (Hz)	
Rated capacity	50, 75, 100, 150, 200, 300 (kVA)	75, 100, 150, 200, 300, 500 (kVA)
Primary voltage	R6600-F6300-6000 (V) (Single-phase 50 kVA only) F6750-R6600-F6450-F6300-6150 (V)	
Secondary voltage	210-105 (V)	210, 420, 440 (V)
Thermal class	F	

Runner MOLTRA 2014 which uses grain-orientated electrical steel sheets. In addition, because the plate thickness is one-tenth that of the grain-oriented electrical steel sheets and the strength is low, a clever structural design is needed in order for the iron core of the transformer to become self-standing. Furthermore, so the size and distribution of the load applied to the amorphous alloy does not cause noise or otherwise adversely affect the characteristics, the structural design must also consider rigidity and the ease of processing

Because the MOLTRA is installed within a distribution board as a distribution transformer, space savings must be considered. The FM-AT14 is designed to expand in the vertical direction so as to accommodate an increase in volume without allowing its footprint to become large. The expansion in the vertical direction, however, has an adverse effect on rigidity and leads to a rise in the temperature of the transformer.

In the development stage this time, the above issues were resolved by adopting the following measures, and the products were then commercialized.

- (a) Optimization of the method for affixing the amorphous alloy in consideration of the effect on characteristics
- (b) Increased rigidity of the entire transformer in consideration of earthquake durability
- (c) Optimal assembly method for the transformer
- (d) Application of an optimal winding design and cooling structure

3. Selection of Transformer Type and Capacity

A comparison of the total loss and efficiency when changing the load factor of the FM-AT14 and the Top Runner MOLTRA 2014 is shown in Fig. 4. The FM-

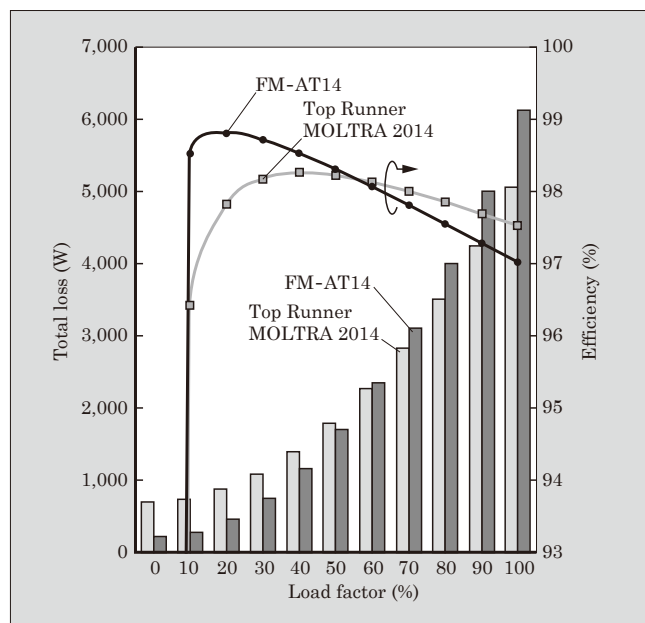


Fig.4 Total loss and efficiency of “FM-AT14” and “Top Runner MOLTRA 2014”

AT14 exhibits particularly excellent efficiency when the load factor is low. However, as the load factor increases, the volume of the FM-AT14 becomes larger and its windings become longer, and consequently, the load loss has a large effect on the total loss and the top runner MOLTRA 2014 exhibits superior efficiency.

The amount of power used and the time bands of that usage vary for factories, office buildings, shopping malls, and so on. Thus, when selecting the type and capacity of a transformer, it is crucial that an appropriate transformer be selected in consideration of the power fees per time band as set by the power companies so that energy waste and cost can be minimized during operation.

Fuji Electric has arranged a lineup of the FM-

AT14 and the Top Runner MOLTRA 2014 transformers and has prepared a system capable of supplying users with the MOLTRA model best suited for their needs.

Launch time

June 2015

Product Inquiries

Design Department I, Chiba Factory, Industrial Infrastructure Business Group, Fuji Electric Co., Ltd.

Phone: +81-436-42-8130



Circuit Protector “CP30F Series”

EMURA, Takeshi*

Circuit protectors are circuit breakers that are equipped with both an overcurrent protection function, to protect circuitry that is inside a device, and a switching function. Circuit protectors have come into widespread use with recent developments in FA equipment, OA equipment, computers and peripheral devices.

As circuit protectors for use in control circuit applications, Fuji Electric previously released the “CP-D Series” in 1983 and the “SP-F Series” in 1993, both of which were favorably received in the marketplace. Since that time, however, user needs have diversified and become more sophisticated. In response to these needs, Fuji Electric has recently developed the “CP30F Series” (Fig. 1) of circuit protectors that feature improved safety and greater ease of wiring. This paper describes features of the CP30F Series.

1. Aim of Development

The main user requirements of components to be used in control panels, including circuit protectors for use with control circuits, are as follows.

- (a) Component miniaturization that supports smaller-sized control panels
- (b) Enhanced safety for advanced-function, sophisticated machinery
- (c) A product structure that allows an overall cost reduction through improved ease of wiring, and the like
- (d) Specifications that enable the same design to be

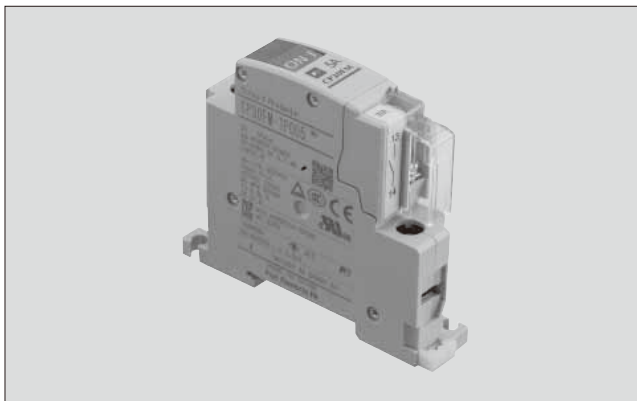


Fig.1 “CP30F Series”

* Development Group, Fuji Electric FA Components & Systems Co., Ltd.

employed for both domestic and export uses

2. Product Features

Figure 2 shows the internal structure of the product. The main features are as follows:

- (a) The product is miniaturized by integrating the function of the main circuit terminal cover into the main body of the unit, resulting in a 20% reduction in volume and a 20% reduction in footprint size.
- (b) A finger protection (IP20 equivalent) structure is adopted as a standard so that fingers will not touch live parts and to ensure safety.
- (c) A screw lift-up structure that enables wires to be connected to round crimping terminals without having to remove screws has been adopted. Moreover, since there is no need to review the terminal arrangement and to wire main terminals and auxiliary terminals sequentially, the main and auxiliary terminals can be tightened individually, thus improving the ease of wiring.
- (d) Major domestic and overseas standards are supported so that circuit protectors with the same specifications may be used both domestically and abroad. The product series complies with IEC, CCC, UL/SCA, KC, and PSE (JIS) stan-

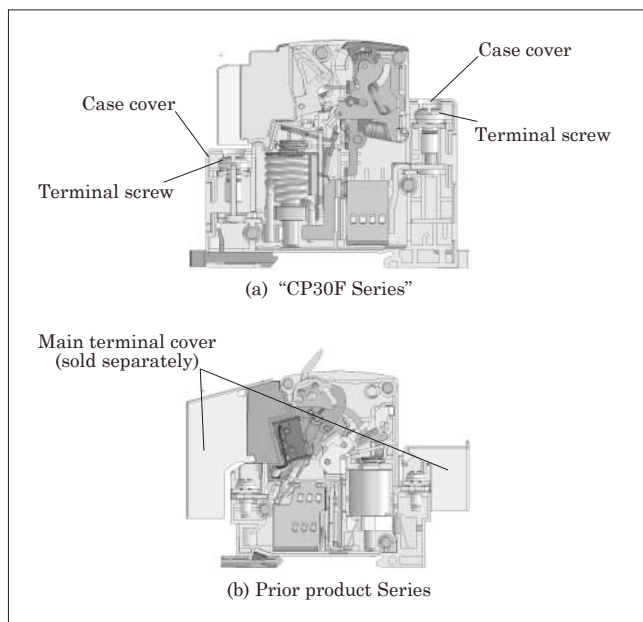


Fig.2 Internal structure of product

Table 1 Main specifications of “CP30F Series”

	CP30F Series	CP-F Series (prior product series)
No. of poles	1, 2, 3	
External dimensions (W×H×D)	17.5×73×66 (mm)	17.5×92.6×65 (mm)
Main terminal structure	Screw lift-up structure	Screw
Main terminal cover	Integrated with case cover	Sold separately
Rated current	0.1 to 30 A	
Rated usage voltage	250 V AC 65 V DC	240 V AC 60 V DC
Operating characteristics	Long time delay Medium time delay Instantaneous tripping	
Circuit breaker capacity	2.5 kA	
Auxiliary terminals	Screw terminal	
Auxiliary terminal cover	Included accessory	Sold separately

dards.

3. Specifications

Table 1 lists the main specifications of the CP30F Series. The required specifications for circuit protectors vary according to the target equipment or device. While maintaining the same varieties of number of poles, rated current and operating characteristics as the prior product series, the CP30F Series also features a revamped terminal area structure to realize a significant improvement in safety and ease of wiring.

4. Improved Terminal Area Structure and Ease of Wiring

With the prior product series, it was necessary to remove the terminal cover when tightening the terminals, and there was the risk of accidentally losing a screw during the wiring process. With the CP30F Series, as shown in Fig. 3, a screw lift-up structure is adopted whereby a spring is positioned on the washer of the terminal screw, and when loosening the termi-

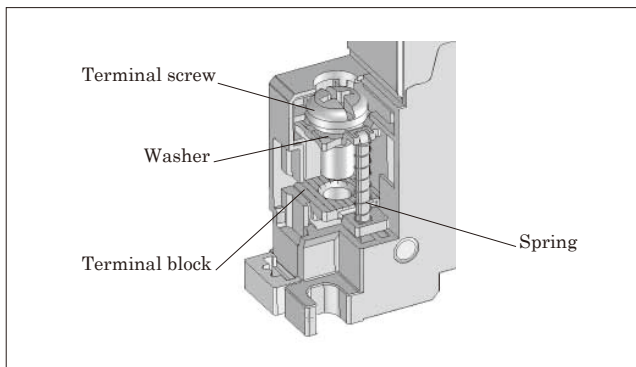


Fig.3 Screw lift-up structure

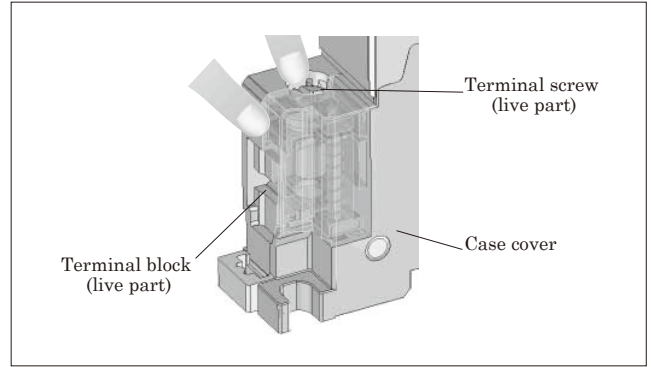


Fig.4 IP20 structure

nal screw, the terminal screw lifts up together with the washer. Thus, wires with round crimp terminals can be connected without removing the terminal screws. Moreover, as shown in Fig. 4, a finger protection (IP20 equivalent) structure is adopted whereby a case cover encloses the exterior of the terminal screws so that fingers will not touch live parts.

By combining both the screw lift-up structure and the IP20-equivalent structure, as shown in Table 2, the CP30F Series requires less labor than the prior product series and allows for easier wiring.

Furthermore, as shown in Fig. 5, the positional relationship between the main terminals and auxiliary terminals has been revised. In the prior product series, wiring connections had to be made sequentially, main terminals first and then auxiliary terminals, since the auxiliary terminals were located on both the left and

Table 2 Required tasks when wiring a main terminal

	CP30F Series	CP-F Series (prior product series)
Loosen screw	—	○
Remove screw	—	○
Align screw with crimp terminal	—	○
Align crimp terminal with terminal block	○	○
Tighten screw	○	○
Attach main terminal cover	—	○

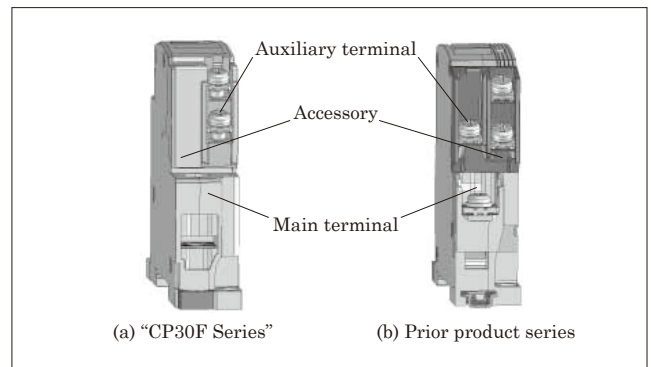


Fig.5 Positional relationship of main terminals and auxiliary terminals

right sides. In addition, when tightening the main terminals during maintenance work, the wires from accessories would get in the way. With the CP30F Series, however, the auxiliary terminals are positioned on the right side so that wiring work can be performed without regard for the order of main terminals and auxiliary terminals, and it is also possible to tighten the main terminals only.

Launch time

July 2015

Product Inquiries

Product Management Department, Business Planning Group, Fuji Electric FA Components & Systems Co., Ltd.

Phone: +81-3-5847-8060



7th-Generation “X Series” IGBT Module

KAWABATA, Junya* MOMOSE, Fumihiko** ONOZAWA, Yuichi*

Recently, the depletion of energy resources due to increased energy consumption and acceleration of global warming because of increased CO₂ emissions have been posing serious global problems. Under these circumstances, application of power conversion equipment that use power semiconductor devices is becoming widespread in the industrial, consumer, automotive, renewable energy and various other fields and insulated-gate bipolar transistor (IGBT) modules are mainly utilized for that purpose. To further disseminate power conversion equipment in the future, it is essential to reduce equipment size (cost savings), improve efficiency (loss reduction) and enhance reliability.

Fuji Electric has developed the 7th-generation “X Series” IGBT modules, which apply new chip and packaging technologies. The aim is to further reduce the size, improve the efficiency and enhance the reliability of power conversion equipment (see Fig. 1). The X Series IGBT modules have made it possible to not only reduce the size and loss of IGBT and free wheeling diode (FWD) chips but also enhance the reliability by improving various characteristics that may be degraded in high-temperature operation. The improvement of heat dissipation, heat resistance and reliability of the package has improved the IGBT’s maximum temperature T_{jop} in continuous operation to 175 °C, which is increased by 25 °C compared to the 6th-generation “V Series” IGBT modules.

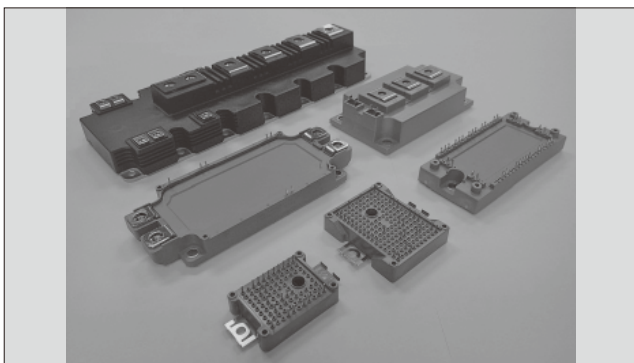


Fig. 1 7th-generation “X Series” IGBT modules

1. Features

Reducing the size and loss of the IGBT modules and achieving a $T_{jop}=175\text{ }^{\circ}\text{C}$ have made it possible to increase the output current by approximately 35% from the V Series IGBT modules as shown in Fig. 2. This has allowed a reduction in the size of power conversion equipment by further increasing the power density.

1.1 Size and loss reduction of IGBT module

The X Series IGBT modules have achieved a further size and loss reduction by using lower-loss IGBTs and FWDs and improving the heat dissipation and reliability of the package.

As an example, this section describes a product with the 1,200-V/75-A rating that uses the EP2 package. While the maximum current rating of the V Series IGBT modules is 50 A, with the X Series IGBT modules, an increase of the rating to 75 A has been achieved with the same package. This has been made possible by reducing the chip size, achieved by reducing the power loss of IGBTs and FWDs and improving heat dissipation of the package. A comparison based on the same current rating shows a footprint reduction of approximately 36% realized by replacing the EP3 package conventionally used with the EP2 package. Figure 3 shows a comparison of power loss and IGBT junction temperature in normal operation. As compared with the V Series IGBT modules, the power loss and junction temperature have been reduced by approximately 10% and 10 °C respectively, allowing for

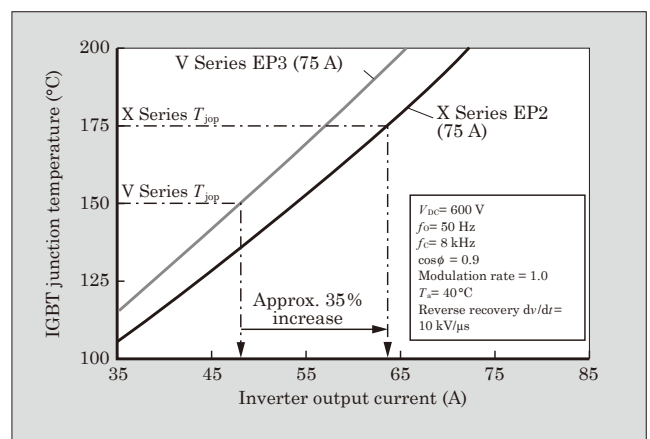


Fig. 2 Inverter output current and IGBT junction temperature

* Electronic Devices Business Group, Fuji Electric Co., Ltd.

** Corporate R&D Headquarters, Fuji Electric Co., Ltd.

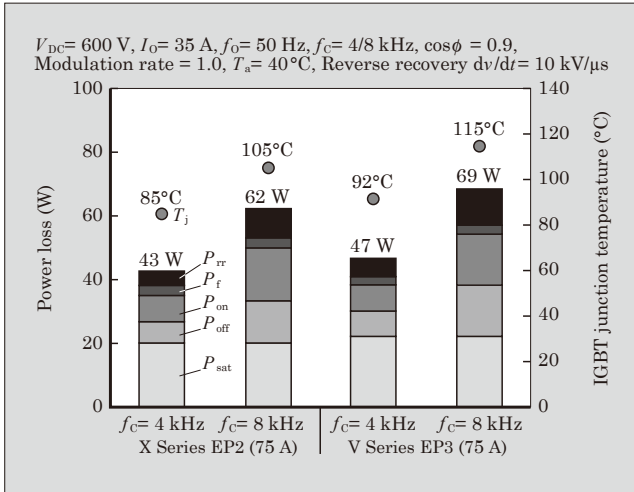


Fig. 3 Power loss and IGBT junction temperature in normal operation

a size and loss reduction.

1.2 Realization of $T_{jop} = 175^\circ\text{C}$

The X Series IGBT modules have achieved an increase of T_{jop} from the conventional 150°C to 175°C . This has been done by improving the characteristics and durability in high-temperature operation and thermal resistance and reliability of the package so that power conversion equipment can have a higher output current.

1.3 Product lineup

Table 1 shows the lineup of the X Series IGBT modules.

2. Underlying Technology

2.1 Loss reduction of IGBT and FWD

To reduce the size of IGBT modules, it is essential

to make the chip size smaller by significantly reducing the loss of IGBTs and FWDs. The trade-off characteristic indicating the relationship between the on-state voltage and switching loss of IGBT and FWD is shown in Fig. 4. The 7th-generation IGBT has significantly reduced the on-state voltage by thinning the drift layer and optimizing the surface gate structure. It has also reduced the turn-off loss as well by reducing the Miller capacitance.

With the 7th-generation FWD, lower reverse recovery loss and smooth reverse recovery waveforms have been realized by optimizing the minority carrier lifetime control in addition to reducing the forward voltage by thinning of the drift layer. This significant loss reduction and other measures have helped reduce the chip size of the 7th-generation IGBT and FWD.

2.2 High heat dissipation AlN insulating substrate

Increasing the power density by reducing the chip and product size correlates with an IGBT junction temperature rise and heat concentration. In order to solve this problem, we have developed a new aluminum nitride (AlN) insulating substrate that features high-heat-dissipation properties. AlN is well-known as a high-heat-dissipation ceramic and has made it possible to further improve the long-term reliability and lower the thermal resistance of the X Series IGBT modules. This AlN insulating substrate has improved the bending strength by revising the ceramic baking conditions so that the AlN insulating substrate is significantly thinner than the conventional one. This has led to mitigation of the thermal stress and significant improvement of the thermal cycling capability. Thermal resistance has also been reduced by approximately 45% and the problem of IGBT junction temperature rise due to size reduction has been solved.

Table 1 Lineup of 7th-generation "X Series" IGBT modules

Package	Circuit structure	Dimensions W × D (mm)	Rated current		
			650-V rated product	1,200-V rated product	1,700-V rated product
Small PIM1	PIM	33.8 × 48	10, 15, 20, 30 A	10, 15 A	-
Small PIM2		56.7 × 48	50 A	25, 35 A	-
EconoPIM*2		45 × 107.5	50, 75, 100 A	35, 50, 75 A	-
EconoPIM3		62 × 122	100, 150 A	75, 100, 150 A	-
EconoPACK*	6 in 1	62 × 122	-	100, 150, 200 A	-
Std. 2in1	2 in 1	34 × 94	100, 150, 200 A	100, 150, 200 A	75, 100, 150 A
		45 × 92	300, 400 A	200, 300 A	-
		62 × 108	400, 600 A	300, 400, 450, 600 A	150, 200, 300, 400 A
		80 × 110	600 A	450, 600 A	300, 400 A
Dual XT		62 × 150	-	300, 450, 600, 800 A	300, 450, 600, 800 A
EconoPACK+	6 in 1	150 × 162	-	300, 450, 600 A	300, 450 A
PrimePACK*2	2 in 1	89 × 172	-	600, 900, 1,200 A	650, 1,200 A
PrimePACK3		89 × 250	-	1,400, 1,800 A	1,000, 1,400, 1,800 A

* EconoPIM, EconoPACK, PrimePACK: Trademark or registered trademark of Infineon Technologies AG

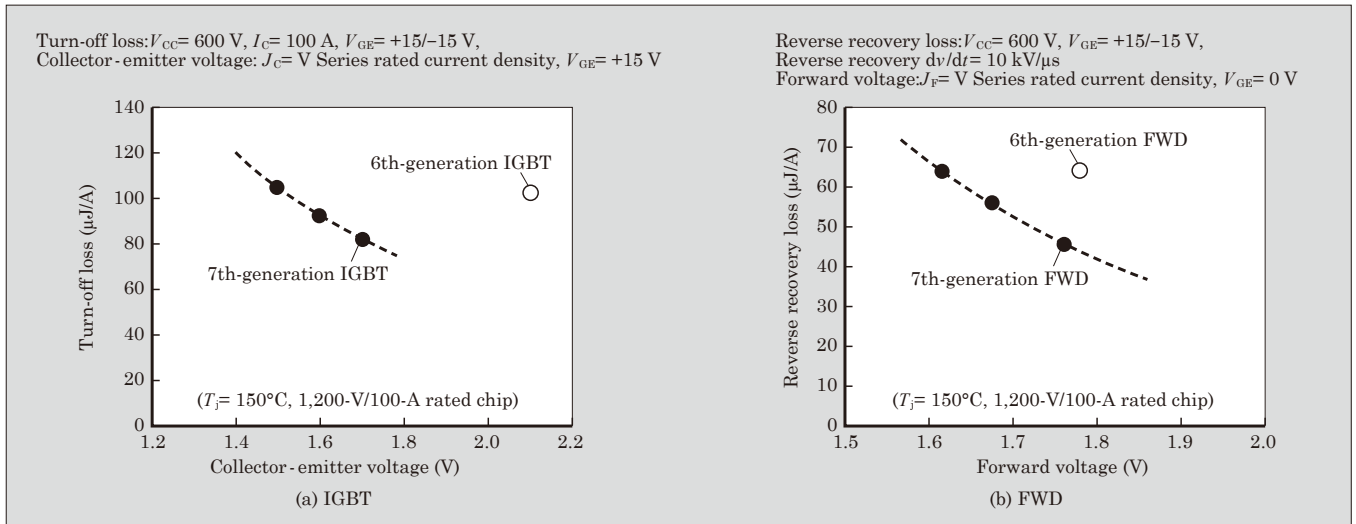


Fig. 4 Trade-off characteristics

2.3 High reliability, high heat resistance package

The problems to be solved before $T_{jop}=175^{\circ}\text{C}$ can be realized include a decrease of the package life expectancy against repetition of thermal stress (ΔT_j power cycle capability) and degradation of the long-term insulation performance of silicone gel. With the X Series IGBT modules, the materials of the aluminum wire on the chip and under-the-chip solder and the bonding method have been optimized. This has made it possible to improve the ΔT_j power cycle capability so that it is about twice that of the V Series IGBT modules ($T_{jmax}=175^{\circ}\text{C}$, $\Delta T_j=50^{\circ}\text{C}$). The problem with the conventional silicone gel is the susceptibility to hardening in an environment of 175°C . The gel tends to be torn and this degrades the insulation performance. The silicone gel developed has had its composition revised

to reduce hardening in an environment of 175°C and ensure long-term insulation performance. These new technologies have achieved $T_{jop}=175^{\circ}\text{C}$ with the X Series IGBT modules and even higher reliability has been realized.

Launch time

Gradual provision of samples starting in August 2015

Gradual mass production starting in April* 2016

* The schedule differs in individual module types.

Product Inquiries

Sales Department I, Semiconductor Division, Sales Group, Fuji Electric Co., Ltd.

Tel: +81 (3) 5435-7152



Integration of the Future

Fuji Electric's power semiconductors densely containing our unique power electronics technology and possibility of application. We have been improving these key devices to have a high withstanding voltage, high capacitance, low power loss, and compact & light-weight package. The key devices have vigorously playing active parts in the clean energy field including photovoltaic and wind power generation, the energy conservation field, demanded in the industry and the home, and the traffic field including hybrid and electric vehicles. Moreover, we have been developing the next generation power semiconductors of higher performance using new material SiC. Fuji Electric will continue to renovate energy technologies and contribute to realize a safe, secure and sustainable society.



Fuji Electric's power semiconductors

Overseas Subsidiaries

* Non-consolidated subsidiaries

America

Fuji Electric Corp. of America

Sales of electrical machinery and equipment, semiconductor devices, drive control equipment, and devices

Tel +1-732-560-9410

URL <http://www.americas.fujielectric.com/>

Fuji Electric Brazil-Equipamentos de Energia Ltda *

Sales of inverters, semiconductors, and power distribution

Tel +55-11-2283-5991

URL <http://www.americas.fujielectric.com/portugues>

Asia

Fuji Electric Asia Pacific Pte. Ltd.

Sales of electrical distribution and control equipment, drive control equipment, and semiconductor devices

Tel +65-6533-0014

URL <http://www.sg.fujielectric.com/>

Fuji SMBE Pte. Ltd. *

Manufacture, sales, and services relating to low-voltage power distribution board (switchgear, control equipment)

Tel +65-6756-0988

URL <http://smbe.fujielectric.com/>

Fuji Electric (Thailand) Co., Ltd. *

Sales and engineering of electric substation equipment, control panels, and other electric equipment

Tel +66-2-210-0615

Fuji Electric Manufacturing (Thailand) Co., Ltd.

Manufacture and sales of inverters (LV/MV), power systems (UPS, PCS, switching power supply systems), electric substation equipment (GIS) and vending machines

Tel +66-2-5292178

Fuji Tusco Co., Ltd. *

Manufacture and sales of and provision of maintenance services for transformers

Tel +66-2324-0100

URL <http://www.ftu.fujielectric.com/>

Fuji Electric Vietnam Co., Ltd. *

Sales of electrical distribution and control equipment and drive control equipment

Tel +84-4-3935-1593

Fuji Furukawa E&C (Vietnam) Co., Ltd. *

Engineering and construction of mechanics and electrical works

Tel +84-4-3755-5067

PT. Fuji Electric Indonesia *

Sales of inverters, servos, UPS, tools, and other component products

Tel +62 21 398-43211

URL <http://www.id.fujielectric.com/>

Fuji Electric India Pvt. Ltd. *

Sales of drive control equipment and semiconductor devices

Tel +91-22-4010 4870

URL <http://www.fujielectric.co.in>

Fuji Electric Philippines, Inc.

Manufacture of semiconductor devices

Tel +63-2-844-6183

Fuji Electric Semiconductor (Malaysia) Sdn. Bhd.

Manufacture of semiconductor devices

Tel +60-4-494-5800

URL <http://www.fujielectric.com.my/>

Fuji Electric (Malaysia) Sdn. Bhd.

Manufacture of magnetic disk and aluminum substrate for magnetic disk

Tel +60-4-403-1111

URL <http://www.fujielectric.com.my/>

Fuji Furukawa E&C (Malaysia) Sdn. Bhd. *

Engineering and construction of mechanics and electrical works

Tel +60-3-4297-5322

Fuji Electric Taiwan Co., Ltd.

Sales of semiconductor devices, electrical distribution and control equipment, and drive control equipment

Tel +886-2-2511-1820

Fuji Electric Korea Co., Ltd.

Sales of power distribution and control equipment, drive control equipment, rotators, high-voltage inverters, electronic control panels, medium and large-sized UPS, and measurement equipment

Tel +82-2-780-5011

URL <http://www.fujielectric.co.kr/>

Fuji Electric Co., Ltd. (Middle East Branch Office)

Promotion of electrical products for the electrical utilities and the industrial plants

Tel +973-17 564 569

Fuji Electric Co., Ltd. (Myanmar Branch Office)

Providing research, feasibility studies, Liaison services

Tel +95-1-382714

Representative office of Fujielectric Co., Ltd. (Cambodia)

Providing research, feasibility studies, Liaison services

Tel +855-(0)23-964-070

Europe

Fuji Electric Europe GmbH

Sales of electrical/electronic machinery and components

Tel +49-69-6690290

URL <http://www.fujielectric-europe.com/>

Fuji Electric France S.A.S

Manufacture and sales of measurement and control devices

Tel +33-4-73-98-26-98

URL <http://www.fujielectric.fr/>

China

Fuji Electric (China) Co., Ltd.

Sales of locally manufactured or imported products in China, and export of locally manufactured products

Tel +86-21-5496-1177

URL <http://www.fujielectric.com.cn/>

Shanghai Fuji Electric Switchgear Co., Ltd.

Manufacture and sales of switching equipment, monitoring control appliances, and related facilities and products

Tel +86-21-5718-1234

URL <http://www.fujielectric.com.cn/sfswgr/>

Shanghai Fuji Electric Transformer Co., Ltd.

Manufacture and sales of molded case transformers

Tel +86-21-5718-7705

URL <http://www.fujielectric.com.cn/sfswgr/>

Wuxi Fuji Electric FA Co., Ltd.

Manufacture and sales of low/high-voltage inverters, temperature controllers, gas analyzers, and UPS

Tel +86-510-8815-2088

Fuji Electric (Changshu) Co., Ltd.

Manufacture and sales of electromagnetic contactors and thermal relays

Tel +86-512-5284-5642

URL <http://www.fujielectric.com.cn/csfe/>

Fuji Electric (Zhuhai) Co., Ltd.

Manufacture and sales of industrial electric heating devices

Tel +86-756-7267-861

<http://www.fujielectric.com.cn/fez/>

Fuji Electric (Shenzhen) Co., Ltd.

Manufacture and sales of photoconductors, semiconductor devices and currency handling equipment

Tel +86-755-2734-2910

URL <http://www.sz.fujielectric.com.cn/>

Fuji Electric Dalian Co., Ltd.

Manufacture of low-voltage circuit breakers

Tel +86-411-8762-2000

Fuji Electric Motor (Dalian) Co., Ltd.

Manufacture of industrial motors

Tel +86-411-8763-6555

Dailan Fuji Bingshan Vending Machine Co., Ltd.

Development, manufacture, sales, servicing, overhauling, and installation of vending machines, and related consulting

Tel +86-411-8754-5798

Fuji Electric (Hangzhou) Software Co., Ltd.

Development of vending machine-related control software and development of management software

Tel +86-571-8821-1661

URL <http://www.fujielectric.com.cn/fhs/cn/>

Zhejiang Innovation Fuji Technology Co., Ltd. *

Design, development, and services pertaining to software

Tel +86-571-8827-0011

URL <http://www.fujielectric.com.cn/sif/>

Fuji Electric FA (Asia) Co., Ltd.

Sales of electrical distribution and control equipments

Tel +852-2311-8282

URL <http://www.fea.hk/>

Fuji Electric Hong Kong Co., Ltd.

Sales of semiconductor devices and photoconductors

Tel +852-2664-8699

URL <http://www.sz.fujielectric.com.cn/hkeng/company/index.htm>

Hoei Hong Kong Co., Ltd.

Sales of electrical/electronic components

Tel +852-2369-8186

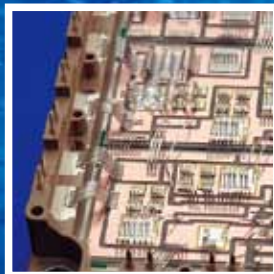
URL <http://www.hoei.com.hk/>

Innovating Energy Technology

Through our pursuit of innovation in electric and thermal energy technology, we develop products that maximize energy efficiency and lead to a responsible and sustainable society.



Corrosion Resistant, Material, and Hot Water Utilization Technology
Geothermal Power Plants



Device Technology
Power Devices (IGBT)



Power Electronics Technology
Power Conditioning Systems (PCS)
for Megasolar Plants



Power Electronics Technology
Inverters



Power Electronics Technology
Uninterruptible Power Supply
Systems (UPS)



Heat Exchange and Refrigerant Control Technology
Hybrid Heat Pump
Vending Machines

F Fuji Electric